N° d'ordre: 06-2016 Année 2016

Université Claude Bernard Lyon 1
Laboratoire d'automatique et
genie des procédés (LAGEP)

Ecole doctorale: EEA

Volvo Trucks
Group Trucks Technology
Advanced Technology and Research

Université de Liège
Faculté des sciences appliquées
Systèmes énergétiques

Ecole doctorale: mécanique et aérospatiale

THESE EN COTUTELLE

en vue de l'obtention des grades de

DOCTEUR DE L'UNIVERSITE DE LYON

ET

DOCTEUR EN SCIENCES DE L'INGENIEUR DE L'UNIVERSITE DE LIEGE

soutenue publiquement le 18 01 2016

par

Mr Vincent GRELET

Rankine cycle based waste heat recovery system applied to heavy duty vehicles: topological optimization and model based control

devant le jury composé de

Mr	Roberto CIPOLLONE,	Examinateur, Professeur des Universités, Université de L'Aquila
Mr	Pascal DUFOUR,	Directeur de thèse, Maître de Conférences, Université Lyon 1
Mr	Pierre DUYSINX,	Président du Jury, Professeur des Universités, Université de Liège
Mr	Vincent LEMORT,	Directeur de thèse, Chargé de cours, Université de Liège
Mr	Sorin OLARU,	Examinateur, Professeur des Universités, SUPELEC Paris
Mr	Nicolas PETIT,	Rapporteur, Professeur des Ecoles des Mines, MINES ParisTech
Mme	Madiha NADRI WOLF,	Co-directeur de thèse, Maître de Conférences, Université Lyon 1
Mr	Franck WILLEMS,	Rapporteur, Professeur Associé, TU Eindhoven

et en présence de

Mr Thomas REICHE, Membre invité, Encadrant VOLVO GTT, Lyon

UNIVERSITE CLAUDE BERNARD - LYON 1

Président de l'Université	**M. François-Noël GILLY**
Vice-président du Conseil d'Administration	M. le Professeur Hamda BEN HADID
Vice-président du Conseil des Etudes et de la Vie Universitaire	M. le Professeur Philippe LALLE
Vice-président du Conseil Scientifique	M. le Professeur Germain GILLET
Directeur Général des Services	M. Alain HELLEU

COMPOSANTES SANTE

Faculté de Médecine Lyon Est – Claude Bernard	Directeur : M. le Professeur J. ETIENNE
Faculté de Médecine et de Maïeutique Lyon Sud – Charles Mérieux	Directeur : Mme la Professeure C. BURILLON
Faculté d'Odontologie	Directeur : M. le Professeur D. BOURGEOIS
Institut des Sciences Pharmaceutiques et Biologiques	Directeur : Mme la Professeure C. VINCIGUERRA
Institut des Sciences et Techniques de la Réadaptation	Directeur : M. le Professeur Y. MATILLON
Département de formation et Centre de Recherche en Biologie Humaine	Directeur : Mme. la Professeure A-M. SCHOTT

COMPOSANTES ET DEPARTEMENTS DE SCIENCES ET TECHNOLOGIE

Faculté des Sciences et Technologies	Directeur : M. F. DE MARCHI
Département Biologie	Directeur : M. le Professeur F. FLEURY
Département Chimie Biochimie	Directeur : Mme Caroline FELIX
Département GEP	Directeur : M. Hassan HAMMOURI
Département Informatique	Directeur : M. le Professeur S. AKKOUCHE
Département Mathématiques	Directeur : M. le Professeur Georges TOMANOV
Département Mécanique	Directeur : M. le Professeur H. BEN HADID
Département Physique	Directeur : M. Jean-Claude PLENET
UFR Sciences et Techniques des Activités Physiques et Sportives	Directeur : M. Y.VANPOULLE
Observatoire des Sciences de l'Univers de Lyon	Directeur : M. B. GUIDERDONI
Polytech Lyon	Directeur : M. P. FOURNIER
Ecole Supérieure de Chimie Physique Electronique	Directeur : M. G. PIGNAULT
Institut Universitaire de Technologie de Lyon 1	Directeur : M. le Professeur C. VITON
Ecole Supérieure du Professorat et de l'Education	Directeur : M. le Professeur A. MOUGNIOTTE
Institut de Science Financière et d'Assurances	Directeur : M. N. LEBOISNE

Abstract

The constant evolution of oil prices and the more and more stringent automotive emission standards force the original engine manufacturers to search for innovative solutions in order to reduce oil consumption. As an important part of the energy contained in the primary carrier (the fuel) is lost to the ambient through heat, it seems convenient to recover a part of this thermal energy and to turn it into fuel consumption reduction. Thermodynamic bottoming cycle such as the Rankine cycle could be used to meet this objective. Its popular use throughout the world for electricity generation makes it a natural candidate for on-board implementation in vehicles. However, a certain number of hurdles are still present before the system can be efficiently applied to heavy-duty trucks.
In the last thirty years, numerous studies heave been carried out to evaluate the real potential of that kind of system on a vehicle but nothing has yet been commercialized. The heat sources to recover from, the constraints relative to the on-board application and the long and frequent transient behavior of the vehicle mean both the system architecture and its control strategy need to be optimized. The system optimization leads to a choice in terms of working fluid, heat sources and sinks, and components sizing in order to maximize power recovery and hence the fuel saving. The control plays a major role by using the capability of such a system to ensure an efficient and safe operation and limiting the interactions with the other vehicle sub-systems.
In this thesis, a system design methodology is introduced to optimize the system architecture using complete model-based vehicle simulation. The constraints relative to the mobile application are taken into consideration to evaluate the potential of such a system. Model-based control strategies for on controlled variable, namely the superheat level, are developed. Constrained by the implementation platform, different control frameworks ranging from PID to model predictive controllers or observer based controllers are developed to fit into a normal automotive electronic control unit. Most of these novel strategies were experimentally validated on a test rig developed during the thesis.

Keywords

Waste heat recovery, Rankine cycle, Heavy duty truck, automotive, heat exchanger, thermal transfer, modeling, process control, multi models, adaptive control, model predictive control, observer.

Résumé

L'évolution croissante du prix des carburants ainsi que les normes antipollution de plus en plus drastiques obligent les fabricants de véhicules commerciaux à développer des solutions innovantes pour réduire la consommation de carburant. Dans cet objectif, comme une grande partie de l'énergie contenue dans le carburant est directement relâchée à l'ambient sous forme de chaleur, celle-ci peut être valorisée et transformée via un cycle thermodynamique secondaire. Dans ce cadre, l'importante utilisation du cycle de Rankine à travers le monde en font un candidat naturel pour une implémentation dans un véhicule. Mais contrairement à une utilisation stationnaire, de nombreux obstacles se dressent pour une intégration totale dans un poids lourd.
De nombreuses études ont été menées ces trente dernières années afin de déterminer le potentiel réel d'un tel système une fois embarqué à bord d'un véhicule. Les nombreuses sources de chaleur valorisables, les contraintes inhérentes à l'application embarquée ou encore les forts régimes transitoires induits par l'utilisation du camion doivent mener à une optimisation à la fois de l'architecture du système ainsi que de son système de contrôle. L'optimisation du système mène à un choix en terme de sources chaudes et froides, de topologie, de fluide de travail ainsi que de dimensionnement des composants afin de maximiser les performances. Le système de contrôle joue lui un rôle primordial afin de tirer un bénéfice maximum d'un tel système connaissant ses limites physiques ainsi que d'assurer une utilisation efficace.
Dans cette thèse, une méthodologie de conception d'un système de valorisation des rejets thermiques est proposée. En se basant sur des simulations du véhicule complet basées sur un modèle détaillé, les thématiques de la sélection du fluide de travail, des sources chaudes et froides ainsi que l'optimisation des composants et du cycle sont approchées. Par la suite, le problème de contrôle en ligne de la surchauffe à la sortie de l'évaporateur est formalisé. En tenant compte des contraintes numériques d'implémentation, différentes stratégies de commande sont mises en place, allant du contrôleur PID à des structures plus avancées telle que la commande prédictive par modèle ou une loi de commande basée sur un observateur. La plupart de ces stratégies sont validées expérimentalement sur un banc d'essai mis en place durant la thèse.

Mots-Clés

Valorisation de chaleur résiduelle, cycle de Rankine, véhicule commercial, automobile, échangeur de chaleur, transfert thermique, modélisation, contrôle des procédés, approche multi modèles, commande adaptative, commande prédictive par modèle, observateur.

Scientific and technical production issued from the thesis

1 article in international journal with review committee

- Grelet, V., Reiche, T., Lemort, V., Nadri, M., Dufour, P. Transient performance evaluation of waste heat recovery Rankine cycle based system for heavy-duty trucks. <In *Applied Energy*, 2016, 165(1), pp. 878–892

5 international conferences with review committee and proceedings

- Grelet, V., Dufour, P., Nadri, M., Lemort, V., Reiche, T. Explicit multi model predictive control of a waste heat Rankine based system for heavy-duty trucks. In *54^{th} IEEE Conference on Decision and Control (CDC)*,pp 179-184, 2015
- Grelet, V., Dufour, P., Nadri, M., Lemort, V., Reiche, T. Model based control for waste heat recovery rankine cycle system in heavy-duty trucks. In *3^{rd} ASME International Seminar on ORC Power Systems (ORC)*, pp. 1203-1212, 2015
- Grelet, V., Lemort, V., Nadri, M., Dufour, P., Reiche, T. Waste heat recovery rankine cycle based system modeling for heavy-duty trucks fuel saving assessment. In *ASME 3^{rd} International Seminar on ORC Power Systems (ORC)*, pp. 1193-1202, 2015
- Grelet, V., Dufour, P., Nadri, M., Reiche, T., Lemort, V. Modeling and control of waste heat recovery Rankine based systems for heavy-duty trucks. In *IFAC International Symposium on Advanced Control of Chemical Processes (ADCHEM)*, pp. 569-574, 2015
- Grelet, V., Reiche, T., Guillaume, L., Lemort, V. Optimal waste heat recovery Rankine based for heavy-duty applications. In *35^{th} FISITA world automotive congress*, 2014

1 international workshop

- Reiche, T., Grelet, V. Waste heat recovery Rankine cycle based system development at Volvo trucks. *In 1^{st} Automotive Consortium on Organic Rankine Cycle (ACORC)*, 2015

Software

- Waste heat recovery Rankine cycle based system dynamic simulation platform. *Volvo trucks internal use*. 20000 source lines of code.
- Rankine cycle heat recovery generic experimental test setup control unit: Software and HMI. *Volvo trucks internal use*. 35000 source lines of code.

Nomenclature

Acronyms

A/C Air conditioning

$ACRC$ Air conditioning and refrigeration center

CAC Charge air cooler

CFC Chlorofluorocarbon

CFD Computational fluid dynamics

CO_2 Carbon dioxide

CV Controlled variable

DOE Department of energy

$EATS$ Exhaust after treatment system

ECU Electronic control unit

EGR Exhaust gas recirculation

$FOPTD$ First order plus time delay

$GADSL$ Global automotive declarable substance list

$GVWR$ Gross vehicle weight rating

GWP Global warming potential

$HCFC$ Hydrochlorofluorocarbon

HD Heavy duty

HEX Heat exchanger

IAE Integrated absolute error

ICE Internal combustion engine

LQR Linear quadratic regulator

LTI Linear time invariant

$MMPC$ Multi model predictive controller

MPC Model predictive controller

$MPID$ Multi model based proportional integral derivative

MV Manipulated variable

$NFPA$ National fire protection agency

NOP Net output power

NOx Nitrogen oxide

NTU Number of transfer unit

ODP Ozone depletion potential

OEM Original engine manufacturer

$OMPC$ Observer based model predictive controller

$OPID$ Observer based proportional integral derivative

ORC Organic Rankine cycle

PC Performance criterion

PID Proportional integral derivative

$PRBS$ Pseudo random binary sequence

$SISO$ Single input single output

$SOPTD$ Second order plus time delay

$SOPTDLD$ Second order plus time delay with lead

SP Set point

TV Total variation

$WHRS$ Waste heat recovery system

WTO World trade organization

Greek letters

α Heat transfer coefficient $(W/m^2/K)$

δ_{cutoff} Cut off probability $(-)$

ϵ Error $(-)$

η Efficiency $(-)$

γ Specific heat ratio $(-)$

γ_p Prediction horizon tuning parameters $(-)$

λ Heat conductivity $(W/m/K)$

μ Dynamic viscosity $(Pa.s)$

Ω Torque $(N.m)$

ω Angular velocity (rad/s)

ϕ Compressibiliy factor $(-)$

ϕ_{ls}^2 Friedel two phase pressure drop multiplier $(-)$

ψ Void fraction $(-)$

ρ Density (kg/m^3)

σ Surface tension (N/m)

τ Time constant (s)
θ Observer tuning parameter $(-)$
θ_C SIMC tuning parameter $(-)$
ε Heat exchanger efficiency $(-)$
φ Critical pressure ratio $(-)$

Latin letters

$\dot{m}$ Mass flow (kg/s)
$\dot{Q}$ Heat flow rate (W)
$\dot{q}$ Linear heat flow rate (W/m)
$\dot{V}$ Volume flow rate (L/s)
$\dot{W}$ Power (W)
A Area (m^2)
a_c Time delay fraction $(-)$
c Developed weighting scheme absolute weight $(-)$
C_c Cubic capacity (m^3)
C_d Discharge coefficient $(-)$
c_p Specific heat $(J/kg/K)$
C_{fan} Fan power parameter (m^5)
c_{us} Isentropic velocity $(-)$
E Energy (J)
e Modeling error $(-)$
Ex Exergy (W)
F Two phase multiplier $(-)$
f Friction coefficient $(-)$
Fr Froude number $(-)$
G Static gain $(-)$
g Gravity constant (m/s^2)
G_{ratio} Gear ratio $(-)$
h Enthalpy (J/kg)
J cost function $(-)$
K Bayesian weighting scheme convergence vector $(-)$
K_p Proportional gain $(-)$
K_{eq} Equivalent throat diameter (m^2)
L Lag (s)
l Length (m)
LHV Low heating value (J/kg)
m Mass (kg)
N Rotational speed (rpm)
Nu Nusselt number $(-)$
P Pressure (Pa)
p Probability $(-)$
Pe Perimeter (m)
PP Pinch point (K)
q Quality $(-)$
R Radius (m)
r Ideal gas constant $(J/kg/K)$
R^2 Agreement coefficient $(-)$
Re Reynolds number $(-)$
S Section (m^2)
s Entropy $(J/kg/K)$
S_{nb} Chen boiling suppression factor $(-)$
Sr Speed ratio $(-)$
Sr Vehicle to ram air speed ratio $(-)$
T Temperature (K)
t Time (s)
T_d Derivative time $(-)$
T_i Integral time $(-)$
U Internal energy (J)
u Input $(-)$
V Volume (m^3)
v Speed (m/s)
w Driving cycle weight $(-)$
w Weight $(-)$
w_u Control move penalty $(-)$
We Weber number $(-)$
x State $(-)$
X_{tt} Martinelli-Lockart parameter $(-)$
y Output $(-)$
z Spatial direction (m)

Subscripts

2Φ Two phase state
air Air
amb Ambient
bay Bayesian
$brake$ Brake
C Cold
CAC Charge air cooler
$conv$ Convection
$coolpack$ Cooling package
$Coolant$ Coolant
$cooler$ Cooler
$cross$ Cross section
$cycle$ Cycle
dev Developed

eff	Effective
egr	EGR gas
$EgrB$	EGR boiler
$elec$	Electrical
eng	Engine
$evap$	Evaporator
exh	Exhaust gas
$ExhB$	Exhaust boiler
exp	Expander
ext	External wall
f	Working fluid
fan	Cooling fan
$filt$	Filter
FZ	Forster and Zuber
g	Gas
H	Hot
$heat$	Heat source
in	Input
int	Internal wall
is	Isentropic
k	Current time
kin	Kinetic
liq	Liquid state
max	Maximum
min	Minimum
NC	Novikov and Chambadal
out	Output
p	Process
pot	Potential
$pump$	Pump
rec	Recovery
sat	Saturated
$shaft$	Shaft
$tank$	Tank
th	Theoretical
v	Valve
vap	Vapor state
$vehicle$	Vehicle
vol	Volumetric
w	Heat exchanger wall

List of Figures

1 Waste heat recovery versus hybridization Stanton (2013) 7

1.1 Temperature-entropy diagram of the ideal Rankine cycle 10
1.2 Sankey diagram of fuel utilization on a Euro 5 engine 14

2.1 Working fluid pump model validation 31
2.2 Temperature estimation error for the EGR boiler 31
2.3 Temperature estimation error for the exhaust boiler 32
2.4 Experimental Inputs: Gas Side 33
2.5 Experimental Inputs: Working fluid Side 33
2.6 EGR and Exhaust Temperature 34
2.7 Working Fluid Temperature 34
2.8 Inlet pressure model prediction at 100krpm 36
2.9 Inlet pressure model prediction at 120krpm 36
2.10 Inlet pressure model prediction at 145krpm 37
2.11 Turbine shaft power model prediction at 100krpm 37
2.12 Turbine shaft power model prediction at 120krpm 38
2.13 Turbine shaft power model prediction at 145krpm 38

3.1 Wet (a) and dry (b) fluids T-s diagrams 40
3.2 Performance map of Acetone at two condensing temperatures 41
3.3 Number of occurrences of each fluid in top five [2] for different boundary conditions . 43
3.4 Exhaust only system schematic 43
3.5 EGR only system schematic 44
3.6 Exhaust and EGR in parallel system schematic 45
3.7 Exhaust and EGR in series system schematic 45
3.8 Cooling configuration 1 (a) and 2 (b) 46
3.9 Fuel energy distribution over classical driving cycle 47
3.10 Driving cycle profile examples 48
3.11 Steady state PC assessment for acetone 50
3.12 Steady state PC assessment for cyclopentane 50
3.13 Steady state PC assessment for ethanol 51
3.14 Steady state PC assessment for water 51
3.15 Mechanical power produced and consumed on driving cycle 2 (a) and 7 (b) 52
3.16 Heat flow rates recovered and rejected on driving cycle 2 (a) and 7 (b) 52
3.17 PC for cooling configuration 1 over dynamic driving cycles 53
3.18 PC for cooling configuration 2 over dynamic driving cycles 53
3.19 PC for optimal sizing of the components 55

4.1 Heat transfer coefficient profiles EGR (a) and exhaust (b) boilers 59
4.2 Temperature (a) and density (b) model validation 60
4.3 Detailed-reduced model comparison: gas (a) and fluid (b) model inputs 61

4.4 Detailed-reduced model comparison: EGR (a) and exhaust (b) model outputs 61
4.5 Experimental validation: gas (a) and fluid (b) model inputs 62
4.6 Working fluid temperature experimental validation: EGR (a) and exhaust (b) boiler outlet 62
4.7 Gases temperature experimental validation: EGR (a) and exhaust (b) boiler outlet . 63
4.8 FOPTD model validation based on the reference model 64
4.9 Open loop comparison of multi-model approach 67
4.10 FOPTD model experimental validation in open loop 68
4.11 Multi model approach experimental validation with $N = 4$ 69
4.12 Multi model approach experimental validation with $N = 8$ 69
4.13 Multi model approach experimental validation with $N = 12$ 70

5.1 Model predictive controller diagram 74
5.2 Engine wasted heat map 75
5.3 FOPTD model parameters 75
5.4 Gain scheduled PID block diagram 76
5.5 Experimental input disturbances for all controller evaluation 77
5.6 Gain scheduled PID: tracking error and manipulated variable 78
5.7 Gain scheduled PID controller parameters versus time 79
5.8 MPID block diagram 80
5.9 MPID: tracking error and manipulated variable 81
5.10 MPID controller parameters 81
5.11 Engine speed and torque over Boras Landvetter Boras cycle 82
5.12 Engine wasted heat over Boras Landvetter Boras cycle 83
5.13 MPID over BLB driving cycle using Bayesian and developed weighting scheme: experimental tracking error 83
5.14 MPID over BLB driving cycle using Bayesian and developed weighting scheme: experimental manipulated variable 84
5.15 Nonlinear controller block diagram 85
5.16 Nonlinear controller: tracking error and manipulated variable 86
5.17 Nonlinear controller: IAE with model uncertainties 86
5.18 MMPC block diagram 89
5.19 MMPC simulation results on benchmark process: controlled variable 90
5.20 MMPC simulation results on benchmark process: manipulated variable 91
5.21 MMPC simulation results on Rankine process: tracking error and manipulated variable 92
5.22 Engine speed and torque variation 92
5.23 MMPC: experimental tracking error and manipulated variable 93
5.24 MMPC: experimental validation of the working fluid temperature estimation at the expansion machine inlet 94
5.25 Different implemented controller comparison: IAE 94

6.1 Observer block diagram 98
6.2 Observer validation: comparison between temperature measured, observed and estimated by means of the multi-model approach 100
6.3 Observer validation: comparison between FOPTD model parameters estimated via the observer (G_{obs},τ_{obs},L_{obs}) and the multi-model approach (G_{mm},τ_{mm},L_{mm}) 101
6.4 OPID block diagram 101
6.5 OMPC block diagram 103

A.1 Working fluid pump 116

B.1 Steady state experimental tests: working fluid superheat at expansion machine inlet 117
B.2 Steady state experimental tests: working fluid mass flow rate 118

B.3 Steady state experimental tests: working fluid temperature at expansion machine inlet 118
B.4 Steady state experimental tests: heat flow rate ratio over the tailpipe evaporator . . 119

List of Tables

1.1 First and second law analysis 15
1.2 Carnot efficiencies for different heat sources and sinks 17
1.3 Triangular cycle efficiencies for different heat sources and sinks 18

2.1 0D model parameters 22
2.2 Evaporator models steady state validation 35
2.3 Evaporator models dynamic validation 35

3.1 Working fluid selection 0D model inputs 41
3.2 Steady state evaluation: Driving conditions and weight for 13 engine operating points 48
3.3 Dynamic evaluation: Driving conditions and weight for the 7 phases 48

4.1 Weighting schemes tuning parameters values 68

5.1 PID tuning method comparison 77
5.2 MPID: tuning parameters values 80
5.3 MMPC: input sequence definition. 88
5.4 Case study parameters (Dougherty and Cooper (2003)) 90

6.1 OMPC: input sequence definition. 102

Acknowledgements

This cotutelle PhD thesis is a collaboration between :

- Laboratoire d'Automatique et de Génie des Procédés (LAGEP) UMR 5007 CNRS-UCBL1, 43 boulevard du 11 Novembre, 69100 Villeurbanne, France [1]
- LABOTHAP, University of Liege, Campus du Sart Tilman Bat. B49, B4000 Liege, Belgium [2]
- Volvo Trucks Global Trucks Technology Advanced Technology and Research, 1 av Henri Germain 69800 Saint Priest, France [3]

The French ministry of higher education and research for the financial support of this CIFRE PhD thesis 2012/549 is also acknowledged.

[1] www-lagep.univ-lyon1.fr
[2] www.labothap.ulg.ac.be
[3] www.volvo.com

Personal acknowledgments

I would firstly like to give special thanks to my supervisors: Vincent Lemort from the University of Liege, Pascal Dufour and Madiha Nadri from the University of Lyon and Thomas Reiche from Volvo Trucks for their daily support, their trust and all the time they have generously given me during the last three years. I would like to say them how important their contributions have been and how much I have appreciated their availability and advices. The four of them have contributed to improving this work through their guidance, their complementarity and their great human qualities.
Then I would like to acknowledge the two reviewers Nicolas Petit and Franck Willems for the time they have devoted to reviewing this work and the precious advice they have given. Finally, I would like to express my gratitude to all the members of the jury: Roberto Cippolone, Pierre Duysinx and Sorin Olaru.
I would like to thank all the people I have the opportunity to work with and especially Nicolas R., Nicolas E., Per, Marc, Jean Marc, Denis, Ubaldo and John who have been present, professional, enthusiastic and who have encouraged me to continue to pursue even greater goals. I also have a thought for all the people not cited but who are contributing to the development of Rankine cycle based exhaust recovery systems at Volvo.
I would also like to thank Ludovic from the University of Liege for the fruitful discussions we have had together and his extensive expertise in the system.
I would like to give special thanks to all my friends who have supported me during the last three years in the good times but also during the time of doubt and for all the good moments we have spent together.
Last but not least, I would like to thank my family who have supported me throughout my whole life and in all the choices I have made so far.

Résumé en langue Française

Depuis les premiers développements fait dans le domaine des moteurs à combustion interne, les ingénieurs ont dû faire face aux différentes pertes inhérentes à cette technologie. Aux cours des années, les moteurs ont ainsi pu atteindre des rendements totaux de l'ordre de 48% dans les moteurs poids lourds actuels. Cependant il semble que la limite technologique soit atteinte aujourd'hui et qu'il faille recourir à de nouveaux systèmes pour dépasser les 50% de rendement.
Au cours des dernières années l'augmentation des cours du pétrole combinée à des réglementations de plus en plus strictes concernant les polluants émis par les véhicules ont obligés les fabricants à travailler sur des solutions innovantes. Dans le monde du véhicule particulier, l'hybridation qui consiste à assister le moteur thermique classique par un moteur électrique est aujourd'hui très en vogue et permet des gains en consommations substantiels. Dans le domaine du véhicule poids lourds cette même technologie perd tout son sens par le poids additionnel qu'elle constitue. En effet, la puissance nécessaire dans un véhicule commercial reviendrait à installer des batteries de plusieurs tonnes ce qui se ferait au détriment du but premier de ce type de véhicule (le transport de marchandises). Dans ce cadre, il a fallu développer des axes de travail permettant de réduire la consommation tout en permettant à l'utilisateur final de conserver la charge utile de ce type de véhicule.
En y regardant de plus près il est facile de déterminer des axes logiques de travail afin d'accomplir ces objectifs. Si l'aérodynamique du véhicule est un axe de travail important, la valorisation des rejets thermiques du moteur à combustion interne pourrait en théorie permettre des gains en consommation de plus de 10%. En effet, une grande partie de l'énergie chimique contenue dans le carburant est dissipée sous forme de chaleur à l'environnement à travers le circuit de refroidissement ou encore les gaz d'échappements.
Si de nombreuses technologies ont étés à l'étude durant ces dernières décennies, la valorisation des rejets thermiques par l'ajout d'un cycle thermodynamique secondaire basée sur le cycle de Rankine semble être au jour d'aujourd'hui la solution préférentielle dans l'industrie du véhicule commercial. Il s'agit ici d'utiliser la chaleur résiduelle contenue dans les nombreuses sources de déperditions du véhicule afin de vaporiser un fluide secondaire sous pression. Une fois vaporisé, celui-ci, se détend à travers une machine d'expansion qui convertit la perte de pression et d'enthalpie en travail mécanique sur son arbre. L'apparente simplicité et la large diffusion dans les applications stationnaires de cette technologie en ont fait un des systèmes les plus étudiés ces dernières années chez les constructeurs.
Si la plupart des études faites au cours des dix dernières années se sont attachées au développement et à l'amélioration des composants du système on ne trouve que peu de développements fait afin d'optimiser ce système et ce sous contraintes d'intégration. En effet, la plupart des systèmes aujourd'hui embarqués dans des véhicules n'ont été développé que dans un soucis de maximisation de leur propre performance sans prêter attention à leur impact sur le véhicule. Les nombreuses interactions induites par l'introduction de cette technologie ne permettent pas tout le temps de justifier la mise en place du dit système. En effet, en prenant l'exemple du poids on peut s'apercevoir que si le système implique une plus grande perte de charge utile que la réduction de consommation associée il devient vite inutile aux yeux de l'utilisateur final.
Les différentes contraintes à prendre en compte obligent les développeurs à tabuler sur des économies plus raisonnables (de l'ordre de 3 à 5 % d'économie de carburant) mais en prenant en compte, cette

fois, les pénalités induites par le système.
Pour cela, il est important de passer par une étape de modèlisation du système ainsi que de l'environnement cible qui permettra de prédire fidélement ses performances. Différents modèles doivent donc être développé répondant chacun à un besoin spécifique. Si un modèle 0D permettra de simuler les performances du système en régime stationnaire, un modèle 1D plus détaillé est nécessaire afin d'évaluer de façon précise l'impact du système sur cycles routiers dynamiques. Le premier type de modélisation permettra donc de réduire le champs des possibilités grâce à des temps de calcul bien plus faible. Il permettra par exemple de simuler un grand nombre de fluide de travail sur un grand nombre de conditions afin de déterminer le fluide de travail le plus approprié à l'application cible. Le modèle détaillé dynamique servira une fois calibré et couplé à une plateforme de simulation du véhicle à déterminer les performances réelles du systèmes ainsi qu'à établir des lois de commandes. Cela permettra aussi à établir les paramètres d'influence sur les performance et les possibles limitations du système de valorisation des rejets thermaique par cycle de Rankine. La modélisation réprésente aujourd'hui une étape nécessaire dans l'introduction d'un nouveau produit afin de réduire les coûts de développement.
Une fois l'architecture du système définie, le seul levier permettant d'améliorer son efficacité et son fonctionnement se situe aux niveau des lois de commandes untilisées par celui-ci. Il a été montrée dans la passée qu'une grandeur importante permettant à la fois d'assurer un fonctionnement efficicace et sûr était la surchauffe du fluide de travail en sortie d'évaporateur. En effet, une régulation précise permet de maintenir la production de travail sur l'arbre de l'expanseur et d'éviter une usure prématurée de ce dernier. Une fois identifiée la variable à manipuler, dans notre cas le débit de fluide de travail à travers l'évaporateur, et la variable à contrôller, ici donc la surchauffe du fluide de travail en entrée de machine de détente il faut s'atteler au dévellopement des lois de contrôle permettant de répondre à notre objectif premier, à savoir la réduction des déviations de la variable de contrôle autour de sa consigne.
Une des majeures problématiques introduites par l'application étudiée ici réside dans l'implémentation de telles stratégies avancées dans les unités électroniques de contrôle utilisées (ECU) dans l'automobile. Ces ECU ne possèdant pas de grandes puissances de calcul il est important d'en tenir compte lors du développement des lois de contrôle commande utilisées par la suite sur le système. Dans ce cadre, une attention toute particulière a été apporté ici à la réduction des modèles non linéaires utilisées pour représenter le comportement dynamiques des échangeurs de chaleur. Afin d'utiliser le moins de capacité de calcul possible une approche multi modèle basée sur des modèles linéaire du premier ordre a été introduite. Cette approche s'est révélée convaincante et possède une certaine flexibilité qui lui permet d'être à la base de nombreuses stratégies des plus simples comme le contrôlleur proportionnel dérivé intégral ou PID, au plus avancé comme la commande prédictive par modèle ou MPC. Cette dernière une fois implémentée s'est montée très performante mais nécessite d'être approfondie car la robustesse d'une telle méthode reste encore à prouver.
Une approche consisterait non plus à définir une banque de modèle hors ligne mais à utiliser un observateur qui identifierai en ligne et à chaque pas de temps les paramètres du modèle linéaire utilisé par la suite dans le contrôlleur. Cette technique étant coûteuse en terme de capacité de calcul n'a pu être validé qu'hors ligne car ne répondant pas aux contraintes d'intégration. Cependant elle ouvre des perspectives intéressantes vers des lois de contrôle autonome où l'effort de calibration serait transféré sur l'effort de calcul.
Si la limite technologique d'un tel système est aujourd'hui presque atteinte il reste de grand progrès à faire sur les lois de contrôle l'accompagnant. Les lois de commande rapprochée proposé dans ce travail contribue à améliorer le fonctionnement et la fiabilité du système. Cependant, il n'est question ici que de commande bas niveau ou rapproché et il meriterait de se pencher vers l'adaptation des consignes au cours du temps afin d'optimiser le fonctionnement du système et de minimiser son impact sur le véhicule. Il faudrait s'atarder aussi sur les contraintes d'implémentation qui limitent l'introduction des lois de commande avancées dans l'automobile. Avec l'augmentation de la capacité de calcul des ECU, de tous nouveaux champs de développement s'ouvrent et la possibilité d'implémenter des stratégies telles que celle basée sur l'observation en ligne devient bien réelle.

Contents

Abstract **v**

Scientific and technical production issued from the thesis **vii**

Nomenclature **xi**

List of figures **xiv**

List of tables **xv**

Acknowledgements **xvi**

Personnal acknowledgements **xvii**

Résumé en langue Française **1**

Contents **5**

Global introduction **6**

1 Rankine based waste heat recovery for heavy duty trucks **9**
1.1 Waste heat recovery: something new, something old 9
1.2 Rankine cycle based recovery systems 10
1.2.1 Rankine process 10
1.2.2 Implementation in vehicles 13
1.2.3 System potential and main limitations 17

2 Rankine system modeling **21**
2.1 Steady state model 21
2.2 Dynamic simulation platform 23
2.2.1 Tank 23
2.2.2 Working fluid pump 23
2.2.3 Compressible flow valves 23
2.2.4 Kinetic expansion machine 24
2.2.5 Evaporators 24
2.2.6 Condenser 29
2.2.7 Cooling module 29
2.3 1D model validation 30
2.3.1 Working fluid pump 30
2.3.2 Evaporators 30
2.3.3 Turbine expander 35

3 Optimization of a Rankine cycle based recovery system for heavy-duty trucks 39
3.1 Working fluid selection . . . 39
3.1.1 Case study . . . 40
3.2 Rankine architecture optimization . . . 42
3.2.1 Rankine layouts . . . 42
3.2.2 Cooling system . . . 44
3.2.3 Performance criterion . . . 46
3.2.4 Duty cycles . . . 47
3.2.5 Steady state performance evaluation . . . 49
3.2.6 Dynamic performance evaluation of ethanol based ORC . . . 49
3.2.7 Components optimization . . . 54

4 Control oriented modeling 56
4.1 Nonlinear model reduction . . . 56
4.1.1 Governing equations . . . 57
4.1.2 Heat transfer . . . 58
4.1.3 Working fluid properties . . . 59
4.1.4 Spatial discretization . . . 60
4.1.5 Simulation results . . . 60
4.1.6 Experimental results . . . 61
4.1.7 Analysis . . . 62
4.2 Multi linear model . . . 62
4.2.1 Model structure selection and validation . . . 63
4.2.2 The piecewise linear approach . . . 64
4.2.3 Simulation results . . . 67
4.2.4 Experimental results . . . 67

5 Rankine system control strategies 71
5.1 Rankine control system: challenges and opportunities . . . 71
5.2 State of the art automotive controller . . . 72
5.3 Gain scheduled PID . . . 74
5.3.1 PID settings comparison . . . 76
5.3.2 Duty cycle and simulation model environment . . . 77
5.3.3 Simulation results . . . 78
5.4 Multi-model based PID strategy . . . 79
5.4.1 Online PID controller parameters calculation . . . 79
5.4.2 Simulation results . . . 80
5.4.3 Experimental results . . . 82
5.5 Nonlinear controller . . . 84
5.5.1 Controller structure . . . 84
5.5.2 Simulation results . . . 85
5.6 Multi-model predictive controller . . . 87
5.6.1 Controller structure . . . 87
5.6.2 Simulation results . . . 89
5.6.3 Experimental results . . . 91
5.7 Controller comparison . . . 93

6 Observer based control strategy 96
6.1 Model design . . . 96
6.1.1 Linear model approximation with the half rule method . . . 96
6.1.2 Considered model structure . . . 97
6.2 Observer design . . . 98

6.2.1 Observability 99
6.2.2 Observer structure 99
6.3 Experimental validation 99
6.4 Observer based PID 100
6.5 Observer based model predictive controller 102

Global conclusion **105**

Appendix **115**

A Test rig **116**

B Experimental test **117**

C MMPC: β_i expression **120**

D OMPC: $\hat{\beta}_i$ expression **121**

Global introduction

Context

Road transport represents a non negligible part of the overall freight transport around the world. Globally, in 2007 the World Trade Organization calculated that road freight transport's global share of inland freight transport (measured in tons kilometers) was 36% , compared with 43% for rail freight, 16% for pipelines and 5% for inland waterways ((IRU)) . Heavy-duty trucks represent the most common solution for road freight transport since they present the greatest flexibility compared to other solutions and are the only ones able to provide a door-to-door service. All these trucks are equipped with an internal combustion engine (ICE) powered with diesel fuel, regardless of their specific application (distribution, long haul, construction, etc). The increase in oil prices during recent years coupled with increasingly stringent pollutant standards have forced the manufacturers to develop energy efficient vehicles (Sims et al. (2014)). In the coming years, these conventional power trains could reach 45 % fuel efficiency (Franke et al. (2014); Suresh et al. (2013)). In addition, smart thermal management (Sermeno et al. (2014)) can lead to an increase in efficiency but not above 50 % when classical ICE architectures are used. Recent developments have shown interesting results from two stroke piston engines (Redon et al. (2014); Regner et al. (2013)) and new combustion modes (Manente et al. (2010)) but regardless of the technology employed theoretical engine efficiency does not exceed 60 %. Hybridization, which relies on the combination of conventional internal combustion with an electric propulsion system, is already today a viable solution for some applications such as city buses or utility trucks (Stanton (2013)). In these applications, for the sake of commonality or features, manufacturers usually mount a larger engine compared to the real needs, while hybridization makes it possible to downsize the combustion engine and optimize overall performance. In Katrašnik (2007), optimal configuration is discussed depending on the driving cycle. It shows that the optimal level of hybridization is dependent on many parameters such as the vehicle load, the components or the storage capacity. Although hybridization is a hot topic for truck manufacturers, few fully electric vehicles have been released to date. Conversely, for long haul applications, the engine is sized properly. For European and North American long haul trucks the time spent on a nominal load point represents 30-50% of the total mission time and there is as yet no justification for even a minimal level of hybridization. Indeed, current battery technologies do not offer reasonable mileage. Most commercial vehicle and engine manufacturers are therefore investigating waste heat recovery systems (WHRS) for long haul truck applications. Figure 1 shows a survey done by the manufacturer Cummins demonstrating the importance of the application when it comes to hybridization. A lot of attention has also been paid to the aerodynamics of the vehicles since drag reduction could be a major contributor to fuel savings (Mammetti et al. (2013); Bachman et al. (2014)). By coupling these improvements with some advanced driving strategies (Dávila and Nombela (2011)), interesting fuel savings can be obtained. Since 2010, the US Department Of Energy (DOE) has been funding the Supertruck program which aims to develop and demonstrate a 50% improvement in freight efficiency (TA Engineering INC. (2012)). Four companies were at that time selected to participate in this program: Cummins, Detroit Diesel, Navistar and Volvo. In 2015, the first press release communicated impressive results

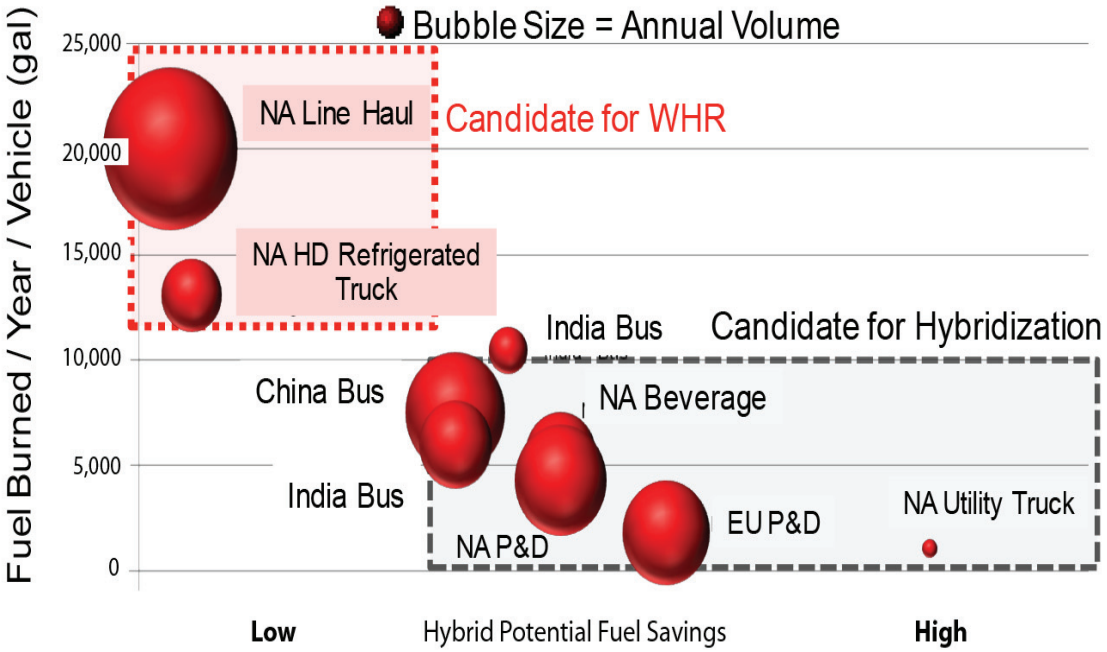


Figure 1 – Waste heat recovery versus hybridization Stanton (2013)

(Daimler Trucks North America (2015)) with fuel consumption of less than 20 liters per $100km$ announced (compared to 30 $L/100km$ for conventional trucks). In every of those demonstrators, waste heat recovery systems were used and contributed significantly to the reduction in fuel consumption.

PhD Thesis contributions

This thesis is a comprehensive study of Rankine cycle based waste heat recovery systems applied to heavy-duty vehicles. The following points are addressed:

- System modeling by means of static 0D and dynamic 1D models.
- System optimization under integration constraints.
- Control oriented modeling by means of physical reduced order model and multi linear model approach.
- Control strategies development subject to implementation constraints.

Manuscript contents

The manuscript is organized in three main parts.

1. The first part is composed of chapter 1 which intends to explain the current status in terms of waste heat recovery systems for mobile applications. The Rankine cycle based heat recovery systems are introduced through a brief history of the different systems used in the internal combustion engine to recover the thermal energy lost to the ambient. The former system is then defined in more detail and the main quantities defining the cycle are introduced. The

Rankine cycle being a thermodynamic cycle operating between a heat source and a heat sink and producing power, indications are given about the main sources and sink available on a vehicle. This chapter also contains a discussion concerning the generated power usage. Finally, the potential and the main limitations of such a device are adressed.

2. The second part of this thesis is devoted to the system modeling and optimization.
   Chapter 2 explains the different simulation tools developed during this PhD thesis where two different approaches were used. Firstly, a 0D model used for potential evaluation and fluid selection is proposed. Then a dynamic simulation model of the whole Rankine cycle recovery system is introduced and validated against experimental data.
   In chapter 3 an approach to the optimization of the system for a heavy-duty trucks application is developed. A complete methodology for the design of a waste heat recovery Rankine cycle based system applied to heavy-duty long haul trucks is developed and the performance of different system configurations is simulated over steady state operating points and dynamic driving cycles. Component optimization is also proposed to increase the overall gain induced by the system.

3. The last part deals with the development of control strategies.
   Chapter 4 proposes a simpler model adapted to the controller synthesis. Two different approaches are developed, one based on a reduced order physical model and another on a multi linear model approach where a new weighting scheme is developed. Both methods are experimentally validated and discussed.
   Chapter 5 explains the closed loop superheat model based control strategies developed for this application : gain scheduled PID, multi model based PID, nonlinear controller and multi model based predictive control. Implementation constraints and calibration effort are the main focus of the development done in this part. Experimental validation is carried out for the new strategies developed.
   Chapter 6 is dedicated to controller developments based on an observer synthesis that aims to replace the previously presented offline identification used for the online control by an online identification of the controller parameters.

Chapter 1

Rankine based waste heat recovery for heavy duty trucks

Abstract. *This chapter sets out the state of the art of heat recovery devices. The principle of the system studied is explained and key quantities are given. The main heat sources and sinks are discussed when the problem of the energy usage is tackled. Finally, the potential performance and main obstacles to implementing a Rankine cycle based heat recovery system in long haul heavy duty trucks are set out.*

1.1 Waste heat recovery: something new, something old

Since the beginning of internal combustion engine development, engineers have been dealng with the problem of losses in the exhaust gases. The gases exiting the combustion chamber are hot and pressurized. Recovering part of the energy contained in those gases could improve ICE efficiency (Johnson et al. (2010)).
In the seventies, the turbocharger, which was the first recovery system introduced into a vehicle, started to be widely used in the automotive industry (Ronan and Abernathy (1979)). Its operation is pretty simple and well adapted to diesel engines. It is composed of two parts: a turbine expanding the pressurized gases and turning the expansion work into mechanical work. This turbine is mechanically linked to a compressor which increases the pressure of fresh air entering into the combustion chamber. Its introduction allowed manufacturers to reduce engine size, pollutant emissions and fuel consumption in recent decades.
Recently, new technologies such as turbocompounding, thermoelectric generators and thermodynamic bottoming cycles have been developed by engine makers (Saidur et al. (2012)).
Turbocompounding has attracted a lot of interest in the automotive industry and especially for commercial vehicles during the last decade (Aghaali and Ångström (2015)). When aircraft were propelled with piston engines (i.e. between the thirties and the fifties), the manufacturers established first turbocompound as fuel saving technology. It was well adapted due to the long hours of operation at constant load and the high expansion ratios at low ambient pressure obtained at cruising altitude. Later, with the mass introduction of turbines as aircraft propellers, the technology became obsolete but found applications in maritime engines. Since then, the technology has been fitted on ship and modern vessel engines and can achieve total efficiency of over 50 % (Hiereth et al. (2007)). Road vehicle manufacturers first became interested in the technology back

in the eighties (Thompson et al. (2009)). In 1991, Scania became the first original equipment manufacturer (OEM) to commercialize a turbocompounded engine. Since, more and more commercial vehicles have been released with a turbocompound and various configurations have been developed (Aghaali and Ångström (2015)).
Heat recovery systems are also strategic for OEMs (Saidur et al. (2012)). Thermoelectric generators (TEGs) are one promising technology mainly due to their apparent simplicity. TEG are based on the Seebeck effect and the properties of some materials which when they are subjected to a temperature difference at the joints, produce a potential difference in the joint circuit. This is called the thermo-current and thermo-electromotive force. Even if the phenomenon is well known, there is ongoing intensive research into the material properties to find the most suitable materials for commercial vehicles and passenger cars (LeBlanc (2014); He et al. (2015)).
Waste heat recovery systems based on thermodynamic bottoming cycles have attracted a lot of interest over the last ten years. In Reiche (2010), various bottoming cycles are analyzed and compared from a first thermodynamic principle point of view. Between the Rankine, Brayton and Ericsson cycles, heat recovery devices based on the Rankine cycle have proved to be the best adapted system for the long haul truck application.

1.2 Rankine cycle based recovery systems

An efficient way to recover the low grade waste heat from the internal combustion engine is the Rankine cycle (Stobart and Weerasinghe (2006); Armstead and Miers (2014)). It uses the same principle as most of heat engines found in power generation plants and makes it possible to convert heat into mechanical work. Different to the classical Rankine cycle which uses water as its working fluid, the organic Rankine cycle (ORC) uses carbon based media.

1.2.1 Rankine process

The Rankine cycle was discovered by William John Macquorn Rankine based on the Carnot cycle. Instead of the two isothermal transformations, the ideal Rankine cycle is composed of two isobaric and two isentropic state changes.

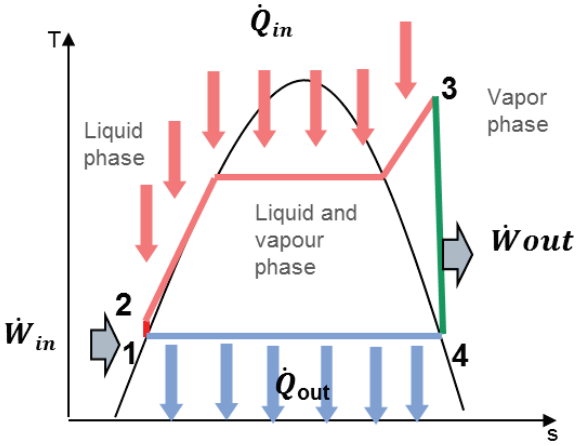


Figure 1.1 – Temperature-entropy diagram of the ideal Rankine cycle

- The pressure of the fluid in liquid state is increased by the pump work up to the evaporating pressure ($1 \rightarrow 2$) consuming power $\dot{W}_{f_{in}}$.
- The pressurized working fluid is pre-heated, vaporized and superheated ($2 \rightarrow 3$) by recovering heat transfer rate $\dot{Q}_{f_{in}}$ from the heat source.
- The superheated vapor expands from evaporating pressure to condensing pressure ($3c \rightarrow 4$) in an expansion device creating mechanical power on the expander shaft $\dot{W}_{f_{out}}$.
- The expanded vapor condenses ($4 \rightarrow 1$) through a condenser (linked to the heat sink) releasing heat flow rate $\dot{Q}_{f_{out}}$.

Ideally the Rankine cycle operates closely to the Carnot cycle due to the isothermal phase change occurring during the evaporation and condensation process. In reality, the Rankine cycle used in waste heat recovery system differs from the ideal Rankine cycle due to the irreversibilities in the different components. The main sources of irreversibility are:

- Losses during compression and expansion due to friction, leakages, etc.
- Pressure drops in the heat exchangers and piping due to friction.
- Heat losses to the ambient due to non adiabatic components.
- Irreversibilities due to finite temperature differences in heat exchangers.

A classical representation of the Rankine cycle is shown in its associated temperature entropy (T-s) diagram shown in Figure 1.1. This is practical since it gives a rough estimation of the cycle efficiency. The highest efficiency is obtained when the cycle looks like a rectangle on the T-s diagram. Indeed, the more rectangular, the closer it is to the Carnot cycle. In reality, net output power maximization is preferred which is not always in line with efficiency maximization.

1.2.1.1 Important quantities

Each component of the Rankine cycle based system can be seen as a control volume (or "open-system"). The first law of thermodynamics applied to these control volumes can be written as:

$$\dot{W}_f + \dot{Q}_f + \dot{m}_{f_{in}} h_{f_{in}} - \dot{m}_{f_{out}} h_{f_{out}} = \frac{dE}{dt}, \tag{1.1}$$

where $\dot{W}$ being the rate of work transfer from or to the system, $\dot{Q}_f$ the rate of heat transfer from or to the system, $\dot{m}_{f_{in}} h_{f_{in}}$ the enthalpy flow rate entering into the system, $\dot{m}_{f_{out}} h_{f_{out}}$ the enthalpy flow rate leaving into the system and $\frac{dE}{dt}$ the rate of change in total energy of the system The latter is the sum of the internal, kinetic and potential energies

$$E = U + E_{kin} + E_{pot}, \tag{1.2}$$

In steady-flow regime, the fluid flows steadily through the different components of the WHRS. In a steady-state process, the total energy content of each component seen as control volumes remains constant. Hence the rate of variation of total energy in 1.1 is equal to zero and the latter equation reduces (if we neglect the kinetic and potential energies of the fluid flows entering and leaving the systems) to:

$$\dot{W}_f + \dot{Q}_f = \dot{m}_{f_{out}} h_{f_{out}} - \dot{m}_{f_{in}} h_{f_{in}}. \tag{1.3}$$

By applying this principle to the four different components which make up the Rankine cycle based heat recovery device, it becomes:

- Pump: the evolution of the fluid through the pump is assumed to be adiabatic (i.e. no heat is exchanged with the surroundings) therefore $\dot{Q}_{f_{pump}} = 0$:

$$\dot{W}_{f_{in}} = \dot{m}_f \left(h_{f_2} - h_{f_1}\right) \tag{1.4}$$

- Evaporator: as no moving parts are present in the evaporator there is no mechanical power exchanged

$$\dot{Q}_{f_{in}} = \dot{m}_f \left(h_{f_3} - h_{f_2}\right) \tag{1.5}$$

- Expander: as for the pumping process, the transformation is considered adiabatic

$$\dot{W}_{f_{out}} = \dot{m}_f \left(h_{f_4} - h_{f_3}\right) \tag{1.6}$$

- Condenser: condenser works in a similar way to the evaporator therefore:

$$\dot{Q}_{f_{out}} = \dot{m}_f \left(h_{f_1} - h_{f_4}\right) \tag{1.7}$$

To characterize the Rankine cycle the following efficiencies are defined:

- Pump: in a real cycle the pumping process is not isentropic. An isentropic efficiency equal to the ratio of enthalpy difference in case of an isentropic transformation on the actual enthalpy difference.

$$\eta_{is,pump} = \frac{h_{f_{2,is}} - h_{f_1}}{h_{f_2} - h_{f_1}}, \tag{1.8}$$

  where $h_{f_{2,is}}$ represents the enthalpy at the pump outlet in case of an isentropic transformation. To calculate the real pump power needed, the mechanical efficiency has to be taken into account:

$$\eta_{m,pump} = \frac{\dot{W}_{f_{in}}}{\dot{W}_{shaft,pump}} = \frac{\dot{m}_f \left(h_{f_2} - h_{f_1}\right)\ 30}{N_{pump}\ \pi\ \Omega_{shaft,pump}}, \tag{1.9}$$

  where $\Omega_{shaft,pump}$ represents the torque needed to drive the pump and the fluid mass flow rate is defined by:

$$\dot{m}_f = \rho_f\ C_c\ \frac{N_{pump}}{60}\ \eta_{vol,pump}. \tag{1.10}$$

  In addition, if an electric motor drives the pump the electrical efficiency should be defined:

$$\eta_{elec,pump} = \frac{\dot{W}_{shaft,pump}}{\dot{W}_{elec,pump}}. \tag{1.11}$$

- Expander: as for the pumping process the expansion does not take place at iso entropy. The isentropic efficiency is then defined as:

$$\eta_{is,exp} = \frac{h_{f_3} - h_{f_4}}{h_{f_3} - h_{f_{4,is}}}, \tag{1.12}$$

  where $h_{4,is}$ represents the working fluid enthalpy at the expansion machine outlet for an isentropic expansion. Similarly to the pump, mechanical efficiency, taking friction into account, is defined:

$$\eta_{m,exp} = \frac{\dot{W}_{shaft,exp}}{|\dot{W}_{f_{out}}|} = \frac{N_{exp}\ \frac{\pi}{30}\ \Omega_{exp}}{\dot{m}_f \left(h_{f_3} - h_{f_4}\right)}. \tag{1.13}$$

  If an electric generator is coupled to the expander, the mechanical to electrical conversion is taken into account by the electrical efficiency:

$$\eta_{elec,exp} = \frac{\dot{W}_{elec,exp}}{\dot{W}_{shaft,exp}}. \tag{1.14}$$

- Evaporator: a recovery efficiency can be defined as the ratio of the heat flow rate recovered by the working fluid to the heat flow rate given by the heat source:

$$\eta_{rec,evap} = \frac{\dot{Q}_{f_{in}}}{\dot{Q}_H} = \frac{\dot{m}_f \, (h_{f_3} - h_{f_2})}{\dot{m}_H \; c_{p_H} \; \Delta T_H}. \tag{1.15}$$

  The latter can be turned into theoretical efficiency taking into account the ambient temperature:

$$\eta_{rec,evap,th} = \frac{\dot{Q}_{f_{in}}}{\dot{Q}_{H,T_{amb}}} = \frac{\dot{m}_f \, (h_{f_3} - h_2)}{\dot{m}_H \; c_{p_H} \; (T_H - T_{amb})}. \tag{1.16}$$

  where $\dot{Q}_{H,T_{amb}}$ represents the total heat available in the heat source.

- Rankine cycle based power unit: the WHRS is mainly characterized by two quantities: the net conversion efficiency and the waste heat recovery efficiency. The first is the ratio of usable power on the heat flow rate recovered by the working fluid. Considering that both expander and pump are linked to the internal combustion engine:

$$\eta_{cycle} = \frac{\dot{W}_{shaft,exp} - \dot{W}_{shaft,pump}}{\dot{Q}_{f_{in}}}. \tag{1.17}$$

  The waste heat recovery efficiency corresponds to the ratio of usable power to the total available energy:

$$\eta_{whr} = \frac{\dot{W}_{shaft,exp} - \dot{W}_{shaft,pump}}{\dot{Q}_{H,T_{amb}}}. \tag{1.18}$$

  The net conversion efficiency is used when it comes to Rankine cycle based system efficiency whereas the second value gives an indication of the amount of heat from the heat source that has not been transferred to the working fluid and therefore an indication of evaporator efficiency.

1.2.2 Implementation in vehicles

Rankine cycle based WHR systems consist of using a Rankine cycle to recover waste heat from the internal combustion engine. Nowadays vehicles are powered with reciprocating internal combustion engines where engine efficiency and fuel consumption are increasingly prioritized in the evaluation of the vehicle's overall performance.
In the early seventies, during the first oil crisis, the first developments were made in the field of Rankine bottoming cycle. The most advanced project was certainly the ThermoElectron project reported in Patel and Doyle (1976) and Doyle and Kramer (1979), where a prototype was built and tested on road over the course of a year. A Mack 676 diesel engine was compounded with an ORC, recovering heat from the exhaust gases. Road tests have demonstrated an improvement of up to 15 % in fuel efficiency and a drop in noxious emissions equal to the gain in efficiency. As oil prices returned to their pre-crisis level after 1980, fuel efficiency became less important for truck manufacturers. As a consequence, the need for such technology was null and the program was canceled.
No further work is reported until the early nineties, where the Iraqi invasion of Koweit created a rapid rise in petrol prices. Some companies started to investigate the Rankine cycle again as a solution to reduce fuel consumption. The most interesting project during this timeframe is the work reported in Oomori (1993) applying the Rankine cycle to a passenger car. The engine acted as a boiler and the traditional engine cooling system was turned into an evaporative cooling system. This was done in order to simplify the Rankine system and remove the needs of an external evaporator. Results indicate a fuel saving of 3% under normal operating conditions.
Until the beginning of 21st century, no major research and development activities were reported.

Since then, all major actors of the automotive industry have demonstrated an interest in this technology: AVL (Teng et al. (2007a)), Honda (Ibaraki et al. (2007)), BMW (Freymann et al. (2008)), Volvo trucks (Espinosa (2011)), Cummins (Dickson et al. (2014)) and many others. Several demonstrators are today running around the globe and proving that the technology could lead to significant benefits in fuel consumption. Despite those numerous advanced engineering projects, the viability of such a system for mass production has not yet been demonstrated.

1.2.2.1 Heat sources

In a vehicle, the number of heat sources is limited. As can be seen in Figure 1.2 the main heat carriers are the cooling system (including exhaust gas recirculation cooling), the exhaust gases and the charge air cooling. By doing a simple energy balance on the engine, the following relationship can be written:

$$\dot{m}_{fuel} LHV + \dot{m}_{air} h_{air} \approx \dot{W}_{brake} + \dot{Q}_{coolant_{eng}} + \dot{Q}_{coolant_{EGR}} + \dot{Q}_{CAC} + \dot{Q}_{exh}, \tag{1.19}$$

where on the right-hand side of the equation 1.19, $\dot{W}_{brake}$ is the engine power and the four last terms represent recoverable waste heat. Those contributions can be calculated as follows:

$$\dot{Q}_{coolant_{eng}} = \dot{m}_{coolant_{in,eng}}\, c_{p_{coolant}} \left(T_{coolant_{out,eng}} - T_{coolant_{in,eng}}\right). \tag{1.20}$$

$$\dot{Q}_{coolant_{EGR}} = \dot{m}_{egr_{in,cooler}}\, c_{p_{egr}} \left(T_{egr_{in,cooler}} - T_{egr_{out,cooler}}\right). \tag{1.21}$$

$$\dot{Q}_{CAC} = \dot{m}_{air_{in,CAC}}\, c_{p_{air}} \left(T_{air_{in,CAC}} - T_{air_{out,CAC}}\right). \tag{1.22}$$

$$\dot{Q}_{exh} = \dot{m}_{exh}\, c_{p_{exh}} \left(T_{exh} - T_{amb}\right). \tag{1.23}$$

This first law analysis sometimes gives a misleading evaluation of energy usage because it does not

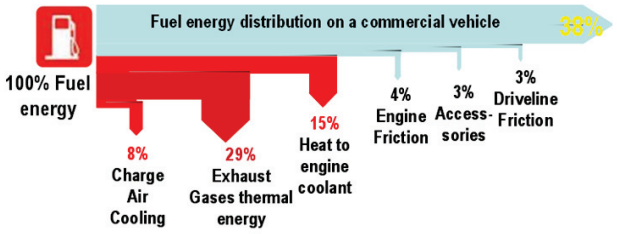


Figure 1.2 – Sankey diagram of fuel utilization on a Euro 5 engine

reflect how much work can be produced and the associated effort. To this end, an exergy (or second law analysis) must be conducted. The exergy of a system is defined as the maximum work possible to bring the system into equilibrium considering its heat sink. Ambient is a common sink for energy processes in practical energy utilization. As the energy store in the ambient can not be turned into useful work, it should be defined as unavailable energy. The difference between the energy and the exergy content coming from the irreversibilities due to the increase in entropy (claimed by the second law of thermodynamics) and the loss of exergy (also called anergy) is proportional to the degree of irreversibility in a process. For heat, the exergy is defined as the amount of power generated by a Carnot cycle operating between the considered heat sources and the ambient:

$$\dot{E}x_{\dot{Q}} = \left(1 - \frac{T_0}{T_H}\right) \dot{Q}_H \tag{1.24}$$

However, in Rankine cycle based power production devices, the heat source is cooled down during the heat exchange process so the maximization of Carnot efficiency and transferred heat flow rate do not go hand in hand (Schuster et al. (2010)). On the other hand, the temperature increase of

the heat sink is not very high due to its presence in a very large quantity.
Those two phenomena have to be taken into account when determining the exergy of a Rankine cycle based system. To this end, the mean temperature of the heat transferred is used which results in the model of a triangular (or trilateral) cycle. The exergy defined by 1.24 now becomes:

$$\dot{E}x_{\dot{Q}} = \frac{T_H - T_0}{T_H + T_0}\dot{Q}_H \tag{1.25}$$

Considering a cruise point on a heavy-duty long haul truck and conducting a first and second law analysis led to the results presented in Table 1.1. It clearly shows that the most interesting sources of all those present on a vehicle are the exhaust stream. A similar conclusion is presented by Teng et al. (2007a). Although this analysis leads to the choice of the exhaust stream as the only heat source, a more practical consideration often pushes the system designer to select the EGR as the heat source. Indeed, as exhaust gas recirculation is cooled down by the cooling system, the use of EGR as heat source does not increase the load on the cooling package which has been seen as one of the main limitations (Edwards et al. (2012)) of the implementation of this kind of recovery system.

Heat source	T_H	$\dot{Q}_H$	$\dot{E}x_{\dot{Q}}$
	℃	kW	kW
Charge air cooler	95	15	1.6
EGR cooler	454	15.9	6.7
Cooling (engine + oil)	90	89.5	8.8
Exhaust	312	51.2	16.6

Table 1.1 – First and second law analysis

1.2.2.2 Heat sink

The Rankine cycle, by nature, needs a heat sink to operate. On a vehicle the only heat sink available is the ram air created by the vehicle movement. The ram air is used by the cooling package as secondary fluid for the different heat exchangers which make up the latter. The vehicle cooling module is usually composed of the air conditioning (A/C) condenser, the charge air cooler, the main engine radiator and the cooling fan. Those components typically consume the whole space between the vehicle grill and the engine and adding a new heat exchanger, either a direct condenser or a heat exchanger dedicated to an indirect condenser, is challenging. In addition to space constraints, the need for additional cooling capacity could limit the heat recovery and the related fuel saving. During operation, an insufficient cooling capacity can limit the amount of heat entering into the system by throttling a portion of the heat source or cause the cooling fan to engage which is an energy guzzler. Truck cooling systems are designed to provide sufficient cooling power to the engine under most restrictive conditions (i.e. low vehicle speed at maximum engine load with ambient temperature of 40 ℃) and the fan should be able to extract the heat coming from the different heat exchangers mentioned above.
Several studies have dealt with condenser or additional radiator locations. In Dickson et al. (2014), a direct condenser is used in front of the cooling package where the cooling module is composed of high capacity, high effectiveness large area heat exchangers. This results in an increase in the overall cooling package air pressure drop, which reduces the ram air effect. In Espinosa (2011), it is shown that only a fraction of the ram air actually passes through the cooling package. With a low pressure drop, the ratio between the air velocity inside the heat exchangers and the vehicle speed is more or less constant and within the range of 25%. In Edwards et al. (2012), the engine

coolant is used to feed an indirect condenser in addition to smart thermal management. It has been shown that this configuration does not lead to excessive cooling fan power consumption due to the WHRS. Other arrangements can be found, where additional radiators are placed either in the cooling module (Kardos and Klingberg (2013)) or an alternative location. An internal study (Holmqvist (2006)) has been conducted to search for additional radiator locations on heavy-duty vehicles. The roof and sun visor have been tested and can increase the cooling capacity of the truck. Those locations, also, have the advantage of not impacting the charge air and engine cooling since they are not located in the engine environment. However, installation at these locations is tricky due to the tilting mechanism present on cab over engine vehicles.
All in all, the heat sink and its temperature level significantly affect the system design and performance. The cooling limitation seems to be a major barrier to vehicle implementation and should be addressed with new cooling and thermal management systems.

1.2.2.3 Energy usage

The use of produced power can be considered as an important area for development since it represents one of the main interfaces between the driveline and the Rankine system. One can distinguish two major paths: electrical power production via a generator and mechanical coupling to directly re-inject the produced torque into the engine driveline.
Electrical production could be valuable in terms of control and power optimization since it makes it possible to control the expansion machine speed and then, if a volumetric expander is used, the evaporative pressure. In any case, the machine speed control makes it possible to control the amount of energy produced in order to adapt it to the vehicle electrical consumption. The main issue is how to correctly predict the latter. On-board electrical consumption is today too low to absorb the production of a Rankine cycle which could be in the range of 2 to 10 kW depending on the engine operating point. This recovery method is usually paired with accessory electrification. In Espinosa (2011), the electrification of water, fuel and steering pumps increases the electrical requirement to 4.5 kW in peak conditions, which does not correspond to Rankine production. In haulage, electrical consumption is around 1.5 kW, which is lower than Rankine production at full capacity. Some of the entering heat needs to be bypassed or the electricity generated must be wasted in a resistive load. In Horst et al. (2014), the fuel saving is calculated taking into account the on-board network electric power demand for a light duty vehicle. At baseline, the fuel saving potential is around 2.3 % whereas an increase in electrical consumption of 50 % could lead to a fuel saving of up to 4 %. A more flexible solution would be to mount an electrical motor directly on the engine or vehicle driveline. This makes it possible to use the electricity whatever the electrical demand of the on-board network or to use batteries to store the electricity produced by the WHRS. However, the last s two solutions both increase the cost and complexity of the system.
Recovering mechanical energy seems to be the safest and simplest solution for a WHRS. However, this solution means there is a certain loss of freedom in the control strategy. With impulse kinetic turbines (which are usually used for this type of application (Kunte and Seume (2013)), this freedom is lost in any case, since machine speed is not linked to supply pressure and one more input disturbance has to be taken into account when design the control software. With this solution, despite the efficient mechanical transmission, that can be higher than 95 %, a major obstacle appears. Indeed, the transmission ratio has to be carefully designed to avoid under- or over-speed of the machine. For a kinetic expander, this requires very low machine efficiency (that is optimal around a very narrow range and then drops rapidly), whereas with a volumetric expander, this could lead to too low or high pressure and low machine efficiency due to over and under expansion phenomena. However, on a long haul truck the engine runs most of the time at its design speed and mechanical torque reinjection seems best adapted, regardless of the expansion machine technology.

1.2.3 System potential and main limitations

As mentioned in section 1.2.2, waste heat recovery systems based on the Rankine cycle are a promising technology to reduce the fuel consumption and to comply with future standards in terms of pollutant emissions. However, it is difficult nowadays, to put an exact number on the system's potential. Depending on the considered level of integration (Horst et al. (2014)), test cycle (Edwards et al. (2012)) or system and limitations (Grelet et al. (2014)), the fuel savings go from 1.5 to 7%. Due to the recovery system's complex interactions with the vehicle, the optimization of the system architecture and control strategy still need to be addressed.

1.2.3.1 Theoretical efficiency

Among all the limitations in such a system, the second law of thermodynamics fundamentally limits the thermal efficiency of all heat engines. Even when considering an ideal, frictionless engine, recovering heat between a heat source at temperature T_H and a heat sink at temperature T_C, not all the heat can be converted into work. This limit is called the Carnot efficiency and represents the efficiency of the ideal, reversible Carnot cycle. It is the fundamental limitation of all systems converting heat into work regardless of the thermodynamic cycle applied. This efficiency is defined by:

$$\eta_{Carnot} = 1 - \frac{T_C}{T_H}, \tag{1.26}$$

where the heat source and sink temperature are on an absolute scale such as the Rankine or the Kelvin scale. Assuming 3 different heat sinks: ambient, low temperature cooling cycle and engine cooling system, the Carnot efficiencies presented in Table 1.2 are calculated as:

		Ambient	Low temperature cooling	Engine cooling
		$T_C = 25$ °C	$T_C = 60$ °C	$T_C = 90$ °C
Charge air	$T_H = 95$ °C	19%	10%	1%
EGR cooler	$T_H = 454$ °C	59%	54%	50%
Cooling	$T_H = 90$ °C	18%	8%	N/A[1]
Exhaust	$T_H = 312$ °C	49%	43%	38%

Table 1.2 – Carnot efficiencies for different heat sources and sinks

It can easily be concluded, that the higher the temperature the higher the limit. However, the Carnot efficiency should be considered carefully since it represents the maximum amount of work that can be produced given the heat source and sink using reversible transformations. As introduced in section 1.2.2.1, in a Rankine cycle based heat recovery system the heat source undergoes a temperature drop during the heat exchange process whereas the heat sink is heated to a temperature close to its initial state. The advantage of a trilateral cycle is that it represents the studied system in a more realistic way:

$$\eta_{tri} = \frac{T_H - T_0}{T_H + T_0} \tag{1.27}$$

For a given heat source, the ideal triangular process would be able to transfer the heat at an infinitesimal temperature difference, i.e. starting from the condensing temperature which is considered equal to the cold source temperature T_0 the final temperature after the heating process is the hot source temperature T_H. It is obvious that this process is impossible in reality but it serves as a benchmark for all other processes. Table 1.3 shows the triangular cycle efficiency for different heat sources and sinks.
Although this indicator looks more realistic, it still supposes that the working fluid is at the heat

		Ambient	Low temperature coolant	Engine coolant
		$T_C = 25$ ℃	$T_C = 60$ ℃	$T_C = 90$ ℃
Charge air	$T_H = 95$ ℃	10.5%	5%	0.7%
EGR cooler	$T_H = 454$ ℃	41.8%	37.2%	33.4%
Cooling	$T_H = 90$ ℃	9.8%	4.3%	N/A
Exhaust	$T_H = 312$ ℃	32.5%	27.4%	23.4%

Table 1.3 – Triangular cycle efficiencies for different heat sources and sinks

source and sink temperature after the heat transfer processes. In reality, heat exchangers used in Rankine processes are not perfect and present a pinch point, meaning the working fluid never reaches the source or sink temperature. It can be concluded that the lower the pinch point the higher the efficiency, but this is only true for large heat exchangers which are often incompatible with vehicle installation.

1.2.3.2 Subsystem interactions

Vehicle operation is influenced by the introduction of a WHRS.
The first cited interaction is the cooling capacity of the truck. To a certain extent, as the device shares the same cooling circuit (i.e. ram air effect), it is easy to understand that this impacts the truck's operation. In Dickson et al. (2014) a direct condenser in front of the cooling package is used. This has a direct influence on the the charge air temperature and consequently on engine performance. This can be compensated for, and some original engine manufacturers have used indirect charge air cooling, giving the same temperature levels as in this configuration.
Another well-quantified impact is the weight penalty. in Europe, the gross vehicle weight rating (GVWR) is limited to 44 tons including the trailer. An increase in vehicle weight means a decrease in payload since the GVWR is limited. The recovery device must be as light as possible which counters the objective of maximizing recovery.
As previously introduced, EGR could be an interesting heat source since it presents the higher grade of energy (see Table 1.1) with the advantage of not impacting the cooling margin since classical EGR coolers already use the engine coolant circuit. However, as EGR systems are part of the pollutant reduction system this function should not be adversely impacted by the WHRS. By diluting the fresh air with a fraction of the exhaust gases, the amount of O_2 in the combustion chamber is reduced and the combustion temperature lower. This results in a drop in NO_x emissions. This system is commonly used in the heavy-duty industry but it needs to be cooled down before mixing up with the fresh air coming from the CAC. By using it as heat source, a trade off needs to be found between EGR cooling and Rankine cycle performance, in order to avoid negatively impacting engine emissions and performance. In practice, the EGR's primary function should never be derated to the detriment of the heat recovery system.
Another regularly cited impact is the exhaust back pressure (Horst et al. (2014)) increase due to the exhaust evaporator. This influences the turbocharger performance and the gas exchange in the cylinder process and results in a negative impact on fuel consumption. In Espinosa (2011), engine simulations are carried out to find the impact of the increase in exhaust back pressure. The author found a negative impact on fuel consumption (around 1% for 50 mbar) but a positive impact on NO_x emissions. This is due to a higher EGR rate resulting in lower nitrogen oxide production. In reality, this number would appear to be an over estimate and the current evaporators do not create a bigger drop pressure in the exhaust stream than this 50 mbar (Flik and Pantow (2009)).
Control strategies play an important role in limiting the impact of the heat recovery device on the engine and vehicle and maximizing power production, and their design is an important step towards successful integration of such a system.

1.2.3.3 Control strategy

There is an increasing focus on the role of control systems in maximizing performance and ensuring the safe operation of systems. Despite the vital importance of this topic, it remains under explored. In the past, experimental studies such as Ibaraki et al. (2007) or Park et al. (2011) have shown that controllability of Rankine cycle based heat recovery systems for mobile applications is no trivial matter. The long and frequent transient behavior of the heat sources and sinks, coupled with the numerous system interactions and limitations make the control algorithm of prime importance.
As a starting point, the literature on air conditioning is a good basis since it is more extensive and the vapor compression cycle used in refrigeration is the opposite of the Rankine cycle. Several publications can be cited, namely *air conditioning and refrigeration center (ACRC) of the university of Illinois* (Rasmussen et al. (2002); Rasmussen (2006); Elliott and Rasmussen (2008); Rasmussen and Alleyne (2010)) where the control problem of this kind of system has been well addressed and different levels of complexity, ranging from decentralized proportional-integral (PI) to model predictive framework, are used to improve system performance.
For stationary ORCs, the control problem is well documented and a lot of research work has been carried out in this field. Quoilin et al. (2011) proposes a simulation and optimal control strategy for a small scale waste heat recovery device in large scale operating conditions (start, stop, part load). The simulation results are presented and show that the superheat could be maintained over time with a transient heat source. In Hou et al. (2011) a decentralized controller is used to track the working fluid temperature after the evaporator. An optimizer feeds the PI controller with optimal set point. This structure makes it possible to integrate other indicators, including economic ones, in the set point generation to optimize the Rankine cycle operation. In Zhang et al. (2012a) a multivariable linear quadratic regulator (LQR) is designed and validated around one operating point, which is suitable for stationary power plants but not for a mobile application. Finally, more advanced controllers, such as model predictive controllers are presented in Zhang et al. (2012b). This framework is practical since it makes it possible to handle multivariable constrained problems.
In the field of mobile applications, few papers deal with control strategy development and even fewer with experimental validation. Stobart et al. (2007) highlighted the influence of the components and the system architecture on the controllability. They have shown that some control variables are better suited (namely the pressure) to enhancing system performance. In Willems et al. (2012), an optimal control strategy is developed for the entire powertrain in order to maximize the NO_x CO_2 trade-off. A global approach is developed but the WHRS model used in this study is relatively simple and does not reflect the real behavior of the system. Luong and Tsao (2014a) present a linear quadratic regulator for a system recovering heat from the exhaust and EGR in parallel. Simulations show that the LQR controller coupled to an additional actuator outperforms the classical PI structure. The experimental validation of different controller structures is presented in Peralez (2015). It has been shown that using an inverted non-linear model as feedforward and a conservative PI as feedback leads to a very low deviation of the controlled variable around its set point (around of +/- 3°C). This last strategy coupled to a state feedback (Peralez (2015)) gives even better results when evaporating pressure and superheating are controlled. Last but not least, the use of MPC is poorly reported. Feru et al. (2014) reported the development of linear and non-linear MPC and their performance over a world harmonized transient cycle but no experimental validation is proposed.
Beyond the control problem, the integration constraints of advanced algorithms are rarely explored. Indeed, automotive electronic control units are not as powerful as current laptops and this constraint should be taken into account when designing control strategies for automotive waste heat recovery devices.

Conclusion. *In this chapter, the current status of waste heat recovery systems applied to heavy-duty long haul trucks is presented. Rankine cycle based heat recovery systems are introduced and the main barreirs to their implementation into a vehicle are addressed. It is shown that although the principle is well known and used for electricity generation, integrating a thermodynamic bottoming cycle into a truck remains challenging. The heat sources and sinks identified need to be selected based on a number of parameters and cannot be performed only based on performance. Two types of power recovery are in competition: electric and mechanical. While electricity generation offers greater flexibility it costs much more and implies mild hybridization. Mechanical power recovery by means of a direct coupling between the expander and the driveline is simpler but creates more control effort. In recent years, controller development has been increasingly addressed but few studies have reported experimental validation.*
The optimization of Rankine cycle based heat recovery devices and their successful integration will require the development of different simulation models used for different purposes, ranging from working fluid selection to performance evaluation.

Chapter 2

Rankine system modeling

Abstract. *This second chapter aims to present the models developed in this thesis. Two different approaches have been used, each targeting a specific usage. A 0D model, use for concept assessment and working fluid selection and a 1D simulation platform for concept optimization and dynamic performance evaluation are presented. The latter is then validating by means of a comparison with experimental data.*

2.1 Steady state model

As a first step, a 0D model of a Rankine cycle using one heat source has been developed. It does not intend to represent real system performance but allows for a comparative study of a number of working fluids. It helps to select the suitable working fluids for the studied application as either the source or the sink grade or quality can be varied. This model is based on the enthalpy changes in the Rankine process and is able to perform either a subcritical or supercritical cycle, which avoids the vaporization process and leads to a smaller system and a better heat recovery process (Karellas et al. (2012)). Several studies use this methodology to design and optimize a waste heat recovery Rankine cycle based system. The assumptions made are verified as long as the heat transfer between the system components and the ambient and the pressure losses are neglected. The 0D model used is

given by the system of equations (2.1):

$$\begin{cases} P_{cond} &= P_{sat}(T_{cond}) \\ P_{f_{in,pump}} &= P_{cond} \\ T_{f_{in,pump}} &= T_{sat}(P_{f_{in,pump}}) - \Delta T_{subcooling} \\ h_{f_{in,pump}} &= h(T_{f_{in,pump}}, P_{f_{in,pump}}) \\ s_{f_{in,pump}} &= s(h_{f_{in,pump}}, P_{f_{in,pump}}) \\ P_{f_{out,pump}} &= P_{evap} \\ h_{f_{out,pump}} &= h_{f_{in,pump}} + \frac{(h_{f_{out,pump,is}} - h_{f_{in,pump}})}{\eta_{is,pump}} \\ T_{f_{out,pump}} &= T(h_{f_{out,pump}}, P_{f_{out,pump}}) \\ s_{f_{out,pump}} &= s(h_{f_{out,pump}}, P_{f_{out,pump}}) \\ P_{f_{out,boiler}} &= P_{f_{out,pump}} \\ h_{f_{out,boiler}} &= h_{f_{out,pump}} + \frac{\dot{Q}_{gas}}{\dot{m}_f} \\ T_{f_{out,boiler}} &= T(h_{f_{out,boiler}}, P_{f_{out,boiler}}) \\ s_{f_{out,boiler}} &= s(h_{f_{out,boiler}}, P_{f_{out,boiler}}) \\ P_{f_{out,exp}} &= P_{cond}, \\ h_{f_{out,exp}} &= h_{f_{out,boiler}} + (h_{f_{out,boiler}} - h_{f_{out,exp,is}})\eta_{is,exp}, \\ s_{f_{out,exp}} &= s(h_{f_{out,exp}}, P_{f_{out,exp}}) \\ P_{f_{out,cond}} &= P_{f_{out,exp}} \\ T_{f_{out,cond}} &= T_{sat}(P_{f_{out,cond}}) - \Delta T_{subcooling} \\ h_{f_{out,cond}} &= h(T_{f_{out,cond}}, P_{f_{out,cond}}) \\ s_{f_{out,cond}} &= s(h_{f_{out,cond}}, P_{f_{out,cond}}). \end{cases} \tag{2.1}$$

where

$$\begin{cases} h_{f_{out,pump,is}} &= h^{'}(P_{f_{out,pump}}, s_{f_{in,pump}}) \\ \dot{Q}_{gas} &= \dot{m}_{gas} c_{p_{gas}} * (T{gas}_{in,boiler} - T{gas}_{out,boiler}) \\ h_{f_{out,exp,is}} &= h^{'}(P_{f_{out,exp}}, s_{f_{out,boiler}}) \\ h_{f_{out,exp}} &\geq h^{''}(q_{f_{out,exp,min}}, P_{f_{out,exp}}). \end{cases} \tag{2.2}$$

Table 2.1 shows an example of the model parameters. Those parameters are chosen according to the usual performance of current components. In addition, a routine verifies that the pinch point

Model parameters	Variable in (2.1)	unit	value
Pump isentropic efficiency	$\eta_{is,pump}$	%	65
Expander isentropic efficiency	$\eta_{is,exp}$	%	70
Maximum evaporating pressure	P_{evap}	bar	40
Minimum condensing pressure	P_{cond}	bar	1
Maximum pressure ratio	$\frac{P_{evap}}{P_{cond}}$	-	40:1
Pinch points HEX	PP	K	10
Pressure ratio among HEX	$\frac{P_{f_{out,boiler}}}{P_{f_{out,pump}}}$	-	1
Minimum quality after expansion	$q_{f_{out,exp,min}}$	-	0.9

Table 2.1 – 0D model parameters

(PP) is respected during the evaporation process. This iterative routine calculates the pinch point at 5 different points along the temperature decrease of the heat source and checks whether the pinch point is higher than specified in the model parameters. If the temperature difference between the working fluid and the heat source/sink is lower than the specified pinch point at one of those five points, the temperature is recalculated at this position. The routine iterates until the pinch point criterion is respected at the five specified temperature points.

The Refprop database Eric. W. Lemmon (2013) is used to compute the following quantity: h, s, T, P_{sat} and T_{sat}. The input variables for the model (2.1) are the gas mass flow rate and temperature (denoted by $\dot{m}_{gas}$ and $T_{gas_{in,boiler}}$) entering the system and the condensing temperature (T_{cond}). Outputs of the model are the power produced by the expansion $\dot{W}_{exp}$, the power consumed by the compression $\dot{W}_{pump}$ and the net output power NOP which are defined as:

$$\left\{ \begin{array}{rcl} NOP & = & \dot{W}_{exp} - \dot{W}_{pump} \\ \dot{W}_{exp} & = & \dot{m}_f * (h_{f_{in,exp}} - h_{f_{out,exp}}) \\ \dot{W}_{pump} & = & \dot{m}_f * (h_{f_{in,pump}} - h_{f_{out,pump}}). \end{array} \right. \tag{2.3}$$

The model 2.1 is not dynamic and is only used for generic evaluations. A dynamic 1D model is therefore developed to evaluate the system performance in more realistic dynamic driving conditions.

2.2 Dynamic simulation platform

2.2.1 Tank

The reservoir is modeled by a fixed volume, which can be either vented to the atmosphere or remain hermetic (depending on the condensing pressure) in order to avoid sub atmospheric conditions. The mass and energy conservation equations are:

$$\left\{ \begin{array}{rcl} \dot{m}_{f_{in,tank}} - \dot{m}_{f_{out,tank}} & = & \frac{\partial m_{f_{tank}}}{\partial t} \\ \dot{m}_{f_{in,tank}} h_{f_{in,tank}} - \dot{m}_{f_{out,tank}} h_{f_{out,tank}} & = & m_{f_{tank}} \frac{\partial h_{f_{tank}}}{\partial t}. \end{array} \right. \tag{2.4}$$

2.2.2 Working fluid pump

The working fluid pump is simply represented by a fixed displacement and isentropic efficiency.

$$\dot{m}_{f_{out,pump}} = \rho_{f_{in,pump}} \frac{N_{pump}}{60} C_{c_{pump}} \eta_{pump_{vol}}, \tag{2.5}$$

where the volumetric efficiency is a function of the outlet pressure and pump speed:

$$\eta_{pump_{vol}} = N_{pump} \left(a + b \frac{P_{out,pump}}{N_{pump}} + \frac{c}{N_{pump}} \right), \tag{2.6}$$

with a,b and c constant parameters identified with experimental data. The outlet enthalpy is calculated as shown in the equation for $h_{f_{out,pump}}$ in the 0D model (2.1).

2.2.3 Compressible flow valves

The fluid flow $\dot{m}$ through the valve is modeled using a compressible valve equation of the form:

$$\dot{m}_{f_{in,v}} = C_{d_v} S_{eff_v} \sqrt{\rho_{f_{in,v}} P_{f_{in,v}} \phi}, \tag{2.7}$$

where the compressibility coefficient ϕ is defined as:

$$\phi = \frac{2\gamma_f}{\gamma_f - 1}(\varphi^{\frac{2}{\gamma_f}} - \varphi^{\frac{\gamma_f+1}{\gamma_f}}), \tag{2.8}$$

with

$$\varphi = \begin{cases} \frac{P_{f_{out,v}}}{P_{f_{in,v}}} & \text{if } \frac{P_{f_{out,v}}}{P_{f_{in,v}}} > \frac{2}{\gamma_f+1}^{\frac{\gamma_f}{\gamma_f-1}} \\ \frac{2}{\gamma_f+1}^{\frac{\gamma_f}{\gamma_f-1}} & \text{if } \frac{P_{f_{out,v}}}{P_{f_{in,v}}} \leq \frac{2}{\gamma_f+1}^{\frac{\gamma_f}{\gamma_f-1}}, \end{cases} \tag{2.9}$$

where γ_f is the ratio of the specific heats of the working fluid and depends on the temperature and the pressure. Equation (2.9) defines the parameter φ whether as the existing pressure ratio for subsonic flow or as critical pressure ratio for supersonic flow conditions.

2.2.4 Kinetic expansion machine

Several studies have been carried out in order to choose the correct expansion machine for Rankine cycle based recovery systems (Wang et al. (2011)). In most of those where vehicle installation is considered, turbine expanders are preferred for their compactness and their high level of performance (Espinosa (2011)) while the major advantage of volumetric expanders such as piston machines is the volume ratio (Latz et al. (2013)). However, a recent study (Kunte and Seume (2013)) has shown turbines with expansion pressure ratio higher than 40:1 on a single stage as having good performance at a tolerable speed for a vehicle installation.
Similarly to Vaja (2009), the semi-empirical formulation of the Stodola equation is applied to link the mass flow rate going through the kinetic expander to the pressure drop

$$\dot{m}_{f_{exp}} = K_{eq}\sqrt{\rho_{f_{in,exp}} P_{f_{in,exp}}\left(1 - \frac{P_{f_{in,exp}}}{P_{f_{out,exp}}}^{-2}\right)}, \tag{2.10}$$

where K_{eq} integrates the equivalent inlet nozzle cross section and the discharge coefficient and is calculated from turbine performance at nominal condition. It should be noted that this relation is also valid when choked flow occurs at high pressure ratios. Conversely, in a volumetric expansion machine (Espinosa (2011)), there is a relationship between the rotational speed and the mass flow entering the machine. The isentropic efficiency model is based on the turbine cinematic ratio according to:

$$\eta_{exp_{is}} = \eta_{exp_{is_{max}}}\left(\frac{2c_{us}}{c_{us_{max}}} - \frac{c_{us}}{c_{us_{max}}}^2\right), \tag{2.11}$$

where c_{us} corresponds to the isentropic exit velocity and is equal to.

$$c_{us} = \frac{u}{c_s} = \frac{\omega_{exp} R_{exp}}{2\sqrt{h_{f_{in,exp}} - h_{f_{in,exp_{is}}}}}. \tag{2.12}$$

The model parameters, namely the maximum isentropic efficiency $\eta_{exp_{is_{max}}}$ and isentropic exit velocity $c_{us_{max}}$, have to be identified from the turbine efficiency maps provided by the supplier or through experimental testing.

2.2.5 Evaporators

Model assumptions

Several assumptions are made to simplify the problem to the greatest possible extent. These are usually admitted when investigating heat exchanger modeling (Vaja (2009); Feru et al. (2013)):

- The transfer fluid is always considered in single phase, i.e. no condensation in the EGR/exhaust gases is taken into account.
- The conductive heat fluxes are neglected since the predominant phenomenon is the convection.
- All HEX are represented by a straight pipe in a pipe counterflow heat exchanger of length L.
- Fluid properties are considered homogeneous in a volume.
- Pressure dynamics are neglected since they are very fast compared to the relevant dynamics of the heat exchanger.

Governing equations

Boiler models are based on mass and energy conservation principles.

- Working fluid (internal pipe):

$$\begin{cases} A_{cross_f}\frac{\partial \rho_f}{\partial t} + \frac{\partial \dot{m}_f}{\partial z} = 0 \\ A_{cross_f}\frac{\partial \rho_f h_f}{\partial t} + \frac{\partial \dot{m}_f h_f}{\partial z} + \dot{q}_{conv_{f_{int}}} = 0 \\ \dot{q}_{conv_{f_{int}}} = \alpha_f Pe_{exch_f}(T_f - T_{w_{int}}). \end{cases} \tag{2.13}$$

- Internal pipe wall: An energy balance is expressed at the wall between the working fluid and the gas and is expressed as follows:

$$\dot{Q}_{conv_{f_{int}}} + \dot{Q}_{conv_{g_{int}}} = \rho_w c_{p_w} V_{w_{int}} \frac{\partial T_{w_{int}}}{\partial t}. \tag{2.14}$$

- Gas side (external pipe): The energy conservation is then formulated as follows:

$$\rho_g A_{cross_g} c_{p_g} \frac{\partial T_g}{\partial t} + c_{p_g} \dot{m}_g \frac{\partial T_g}{\partial z} + \dot{q}_{conv_{g_{int}}} + \dot{q}_{conv_{g_{ext}}} = 0, \tag{2.15}$$

  where the convection on the external side is used to represent the heat losses to the ambient.

- External pipe wall: As for the internal pipe an energy balance is expressed between the gas and the ambient:

$$\dot{Q}_{conv_{g_{ext}}} + \dot{Q}_{conv_{amb_{ext}}} = \rho_w c_{p_w} V_{w_{ext}} \frac{\partial T_{w_{ext}}}{\partial t}. \tag{2.16}$$

In equation (2.14) and (2.16) the convective heat flow rate ($\dot{Q}_{conv}$) is expressed as:

$$\begin{aligned} \dot{Q}_{conv_{j_k}} &= \alpha_j A_{exch_{j_k}}(T_{w_k} - T_j), \\ \text{where } j &= g, f, amb \\ \text{and } k &= int, ext. \end{aligned} \tag{2.17}$$

Furthermore, to complete the system, one needs boundary and initial conditions. Time-dependent boundary conditions are used at $z = 0$ and $z = L$ ($t > 0$):

$$\dot{m}_f(t,0) = \dot{m}_{f_0}(t), \tag{2.18}$$
$$h_f(t,0) = h_{f_0}(t), \tag{2.19}$$
$$\dot{m}_g(t,L) = \dot{m}_{g_L}(t), \tag{2.20}$$
$$\dot{T}_g(t,L) = T_{g_L}(t). \tag{2.21}$$

The initial conditions for the gas and wall temperatures and working fluid enthalpy are given by ($z \in [0, L]$):

$$\begin{aligned} h_f(0,z) &= h_{f_{init}}(z) && (2.22)\\ T_{w_{int}}(0,z) &= T_{w_{int_{init}}}(z) && (2.23)\\ T_g(0,z) &= T_{g_{init}}(z) && (2.24)\\ T_{w_{ext}}(0,z) &= T_{w_{ext_{init}}}(z). && (2.25) \end{aligned}$$

Heat transfer

To model the convection from the transfer fluid to the pipe walls and from the internal pipe to the working fluid, a heat transfer coefficient (α) is needed. The convection from a boundary to a moving fluid is usually represented by the dimensionless number Nusselt (Nu) which is the ratio of convective to conductive heat transfer.

$$Nu(\alpha) = \frac{\alpha l}{\lambda}, \tag{2.26}$$

where l represents a characteristic length and is, in this case, the hydraulic diameter. Numerous correlations to approach this number can be found in the literature and are usually derived from experiments, see for example Thome (2010).
The transfer or secondary fluid does not undergo any phase change therefore the heat transfer coefficient is only dependent on the flow regime.

$$\begin{cases} Nu = 4.36^{1}, & \text{for laminar flow} \\ Nu = 0.024 Pr^{0.4} Re^{0.8} \frac{D_{ext}}{D_{int}}^{0.59}, & \text{for turbulent flow.} \end{cases} \tag{2.27}$$

For the working or primary fluid both flow regime and phase composition have to be taken into account. Therefore several correlations have been implemented.
In liquid phase, the following relationships are used:

$$\begin{cases} Nu = 4.36, & \text{for laminar flow} \\ Nu = \frac{\frac{f}{8}(Re-1000)Pr}{1+12.7\left(\frac{f}{8}\right)^{\frac{1}{2}}\left(Pr^{\frac{2}{3}}-1\right)}, & \text{for turbulent flow.} \end{cases} \tag{2.28}$$

During the vaporization of a fluid inside a tube, heat exchange is governed by two fundamental mechanisms: nucleate boiling and forced convection. During nucleate boiling, bubbles appear. These grow and separate, destroying the limit layer close to the wall. In forced convection, the major thermal resistance relies on the liquid film covering the wall before it dries. These two phenomena are of varying importance depending on the quality, the pressure or the fluid speed. Here, a superposition model is chosen to take into account these two effects:

$$\alpha_{2\varphi} = \alpha_{FZ} S_{nb} + \alpha_{liq} F, \tag{2.29}$$

where:

- α_{FZ} is the nucleate pool boiling coefficient of Forster and Zuber used to calculate the nucleate heat transfer coefficient
- S_{nb} is the nucleate boiling suppression factor
- α_{liq} is the liquid phase heat transfer coefficient and is calculated according to 2.28

- F is the two phase multiplier increasing the liquid phase heat transfer coefficient due to two phase flow.

The Forster and Zuber nucleate pool boiling coefficient α_{FZ} is:

$$\alpha_{FZ} = 0.00122 \left[\frac{\lambda_{sat,liq}^{0.79} c_{p_{sat,liq}}^{0.45} \rho_{sat,liq}^{0.49}}{\sigma^{0.5} \mu_{sat,liq}^{0.29} \Delta h_{vap}^{0.24} \rho_{sat,vap}^{0.24}} \right] \Delta T_{sat}^{0.24} \Delta P_{sat}^{0.75}, \tag{2.30}$$

where the wall superheat ΔT_{sat} is the temperature difference between the wall and the saturation temperature such that $\Delta T_{sat} = T_w - T_{sat}$, the pressure difference ΔP_{sat} is obtained by differentiation of the fluid saturation pressure at the wall temperature and the actual pressure $\Delta P_{sat} = P_{sat}(T_w) - P$. The thermophysical properties, namely the heat conductivity λ, the specific heat c_p, the density ρ, the surface tension σ, the dynamic viscosity μ and the latent heat of vaporization Δh_{vap} are calculated with the Refprop database version 9.1.
The liquid heat transfer coefficient α_{liq} is calculated in the saturated liquid conditions where the two phase multiplier F is applied:

$$F = \left(\frac{1}{X_{tt}} + 0.213 \right)^{0.736}, \tag{2.31}$$

where the two phase effect on convection is taken into account via the Martinelli parameter X_{tt} defined as:

$$X_{tt} = \left(\frac{1-q}{q} \right)^{0.9} \left(\frac{\rho_{sat,vap}}{\rho_{sat,liq}} \right)^{0.5} \left(\frac{\mu_{sat,vap}}{\mu_{sat,liq}} \right)^{0.1}. \tag{2.32}$$

The Chen boiling suppression factor is then calculated according to:

$$S_{nb} = \frac{1}{1 + 2.53e^{-6} Re_{2\varphi}^{1.17}}. \tag{2.33}$$

This correlation has been chosen since a number of fluids are included in its database including water, a certain number of alcohols and alkanes.

Pressure drop

Pressure drop in both fluids is taken into account in order to simulate the real performance of the system. The pressure drop can be split into three main contributors:

$$\Delta P = \Delta P_{static} + \Delta P_{momentum} + \Delta P_{friction}, \tag{2.34}$$

where the static pressure drop (ΔP_{static}) is a function of the change in static head (i.e. the height), the momentum pressure drop ($\Delta P_{momentum}$) depends on the change in density during phase change and the friction contribution ($\Delta P_{friction}$) is a function of the speed of the fluid and the considered geometry. For heat exchangers of this size, the change in height is considered null and therefore the associated pressure drop contribution ($\Delta P_{static} = 0$).
In single phase, the expression of the linear pressure drop $\Delta P_{friction}$ of a fluid flowing in a pipe of length L is equal to:

$$\Delta P_{friction} = \frac{\rho v^2 L}{2 d_h} f, \tag{2.35}$$

where f is the friction pressure loss coefficient depending on the flow regime. For laminar regime , (i.e. for Reynolds number lower than 2000) the assumption of a Poiseuille flow is made:

$$f = \frac{64}{Re}. \tag{2.36}$$

In turbulent regime, the Blasius relation is used:

$$f = \frac{0.316}{Re^{0.25}}. \tag{2.37}$$

To ensure the continuity and avoid numerical issues, the transition Reynolds number is calculated to ensure the two coefficients are equal:

$$\frac{64}{Re} = \frac{0.316}{Re^{0.25}}, \tag{2.38}$$

which gives a transition Reynolds number of about 1189 instead of 2000.
In two phases, the friction pressure drop contribution has to be calculated differently since it is dependent on the density change during the evaporation process. As for the heat transfer, numerous types of correlations can be found in the literature. These consist of two types:

- Homogeneous phase correlations where the velocities of each phase are assumed to be equal (no phase slip). Consequently, the flow quality is considered to be equal to the local flow quality of the fluid. This is generally assumed for heat exchanger modeling but tends to underestimate the pressure drop.
- Separated phase correlations, where the liquid and vapor phase are artificially separated into two streams each flowing at its own velocity, in its own pipe. The cross sectional areas of the two pipes are proportional to the void fraction. Numerous methods are available for predicting the void fraction, but in each correlation a thermodynamic equilibrium is assumed between the two phases.

Here, the second type has been selected for reasons of accuracy. The pressure drop is then calculated by considering a liquid flowing at the same mass velocity ($G = \frac{\dot{m}}{A}$) as the two phase flow corrected by a term (ϕ_{ls}^2) function of the local quality. According to Thome (2010), the Friedel correlation is one of the most appropriate for the pressure drop during evaporation process. The friction pressure drop contribution is then equal to:

$$\Delta P_{friction} = \Delta P_{friction,liq}\ \phi_{ls,Friedel}^2, \tag{2.39}$$

where $\Delta P_{friction,liq}$ is calculated according to equation 2.35 and the Friedel friction coefficient as:

$$\phi_{ls,Friedel}^2 = E + \frac{3.24\ F\ H}{Fr^{0.045}\ We^{0.035}}, \tag{2.40}$$

with:

$$\begin{aligned} E &= (1-q)^2 + q^2 \frac{\rho_{liq}\ f_{vap}}{\rho_{vap}\ f_{liq}} \\ F &= q^{0.78}\,(1-q)^{0.224} \\ H &= \frac{\rho_{liq}}{\rho_{vap}}^{0.91}\ \frac{\mu_{vap}}{\mu_{liq}}^{0.19}\ \left(1 - \frac{\mu_{vap}}{\mu_{liq}}\right)^{0.7}. \end{aligned} \tag{2.41}$$

Moreover, the Weber (We) and Froude (Fr) number are expressed as:

$$\begin{aligned} We &= \frac{\rho v^2 L}{\sigma} \\ Fr &= \frac{v}{\sqrt{gd}}. \end{aligned} \tag{2.42}$$

In the Webber number, We, the mixture density is $\rho = \frac{1}{\frac{q}{\rho_{vap}} + \frac{1-q}{\rho_{liq}}}$.
The momentum pressure drop contribution, reflecting the change in kinetic energy is for the present case:

$$\Delta P_{momentum} = \dot{m}^2 \left\{ \left[\frac{(1-q)^2}{\rho_{liq}\,(1-\psi)} + \frac{q^2}{\rho_{vap}\psi} \right]_{out} - \left[\frac{(1-q)^2}{\rho_{liq}\,(1-\psi)} + \frac{q^2}{\rho_{vap}\psi} \right]_{in} \right\}. \tag{2.43}$$

Numerous methods can be found to calculate the void fraction (x_i). In Thome (2010), it is recommended to use:

$$\psi = \frac{q}{\rho_{vap}} \left[(1 + 0.12\,(1-q)) \left(\frac{q}{\rho_{vap}} + \frac{1-q}{\rho_{liq}} \right) + \frac{1.18\,(1-q)\,[g\sigma\,(\rho_{liq} - \rho_{vap})]^{0.25}}{\dot{m}^2 \rho_{liq}^{0.5}} \right]^{-1}. \tag{2.44}$$

2.2.6 Condenser

For the condenser, the same modeling methodology as for the evaporator is applied. Only the correlation for heat transfer during condensation changes since the flow pattern for this process is different from the pattern during evaporation.

Heat transfer

When the hot vapor gets in contact with a cold surface, it starts to condense and becomes liquid. This process can be of two kinds:

- Condensation in film where the liquid wets the surface
- Droplet condensation where the surface remains dry

With the fluids used in the organic Rankine cycle, the film condensation is predominant. Usually, a liquid film is created on the wall perimeter and the vapor is in the central core. Along the tube, the vapor velocity decreases which decreases the vapor shear and makes the liquid film thicker at the bottom of the tube. The liquid quantity increases and finally all the vapor is turned to liquid. The correlation proposed by Shah is based on one of the largest data banks of fluids. It ignores the effect of gravity which means it is valid for both horizontal and vertical pipes. It is an intensification model based on the Dittus-Boelter relation:

$$Nu = 0.023 Re_{liq}^{0.8} Pr_{liq}^{0.4} \left[(1-q)^0\,.8 + \frac{3.8\; q^{0.76}\;\; (1-q)^{0.04}}{\frac{P_{sat}}{P_{crit}}^{0.38}} \right]. \tag{2.45}$$

Pressure drop

The pressure drop is calculated in the same way as for the evaporators. As the momentum contribution, denoted by equation 2.43, depends mainly on the quality change between the inlet and the outlet ports of the heat exchanger, it can result in an increase in pressure also called pressure recovery.

2.2.7 Cooling module

2.2.7.1 Heat exchangers

In order to describe the vehicle cooling system, the number of transfer unit (NTU) approach is used. It is commonly adopted when it comes to single phase heat exchanger modeling. For an air cooled radiator the following relations are used:

$$\dot{Q}_{air} = \dot{m}_{air} c_{p_{air}} \varepsilon (T_{coolant_{in}} - T_{air_{in}}). \tag{2.46}$$

For a given geometry, ε can be calculated using correlations based on the heat capacity ratio. By considering parallel flow configuration for the radiators, the effectiveness can be written:

$$\varepsilon = \frac{1 - e^{-NTU\left(1+\frac{(\dot{m}c_p)_{min}}{(\dot{m}c_p)_{max}}\right)}}{1 + \frac{(\dot{m}c_p)_{min}}{(\dot{m}c_p)_{max}}}, \tag{2.47}$$

$$\text{with } NTU = \frac{UA}{(\dot{m}c_p)_{min}}. \tag{2.48}$$

2.2.7.2 Cooling fan

The engine fan is a map-based model delivering a given volume flow rate at a given speed. The fan consumption is calculated according to:

$$\dot{W}_{fan} = C_{fan}\ \rho_{air} N_{eng} G_{ratio} N_{fan}^2, \tag{2.49}$$

where the coefficient C_{fan} is experimentally defined and intends to represent the fan performance and G_{ratio} is the gear ratio between the engine and the fan. Those two parameters are dependent on the fan model and vehicle. The mass flow rate blown by the fan is mapped according to data from the supplier and depends on the fan speed and atmospheric conditions. The air mass flow rate going through the cooling package ($\dot{m}_{air}$) is a combination of the natural air mass flow rate (corresponding to a fraction of the vehicle speed) and the forced mass flow rate (corresponding to the mass flow blown by the fan).

$$\dot{m}_{air} = \rho_{air} A_{cool\ pack} Sr_{air} v_{vehicle} + \dot{m}_{fan}(N_{fan}, \rho_{air}), \tag{2.50}$$

where Sr_{air} is the ratio between the vehicle speed and the air speed in front of the cooling package and is either calculated via CFD or measured in a wind tunnel.

2.3 1D model validation

2.3.1 Working fluid pump

The working fluid pump delivers the mass flow rate as shown by equation 2.5. The volumetric efficiency model parameters are calculated to fit the experimental measurements in the +/-5% range. Figure 2.1 shows the mass flow model validation.

2.3.2 Evaporators

Special attention is paid to the evaporators in order to accurately predict the steady state and dynamic performance of those components (corresponding to the model presented in section 2.2.5).

2.3.2.1 Steady state validation

The comparison is more relevant for the EGR outlet temperature since in most of the measurements the working fluid is in two phase state. During the phase change, the temperature is more or less constant (a small temperature increase is observed for the mixture) and comparison on this criterion

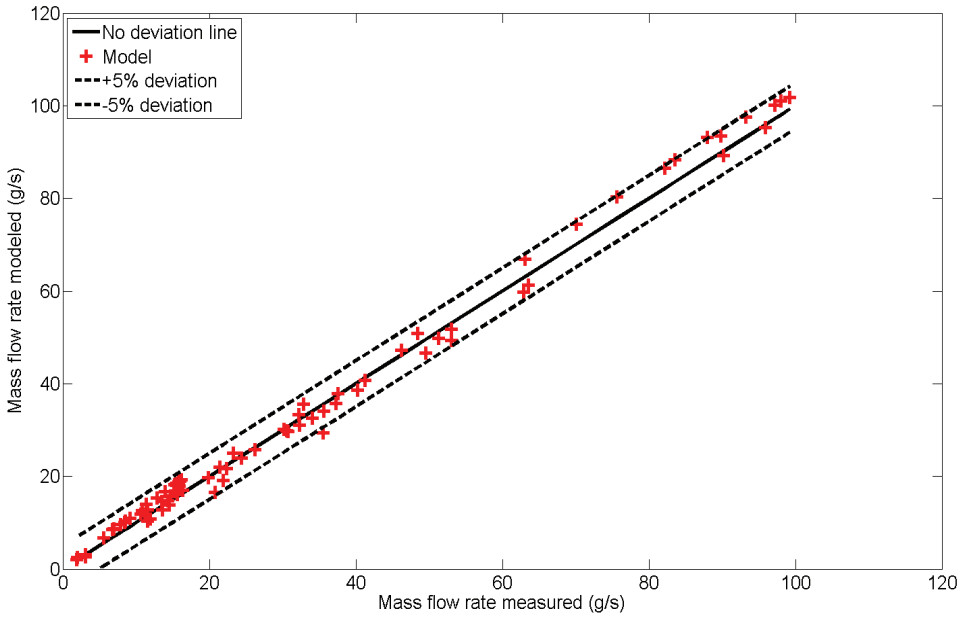


Figure 2.1 – Working fluid pump model validation

is not relevant (major source of error coming from the pressure which is considered constant in both boilers). Figure 2.2 presents the modeling error observed for both fluids: transfer (EGR) and working fluid (water ethanol mixture). The maximum deviation observed on the EGR temperature is 7.6 K and the average error is around 2.6K. Figure 2.3 presents the temperature difference observed

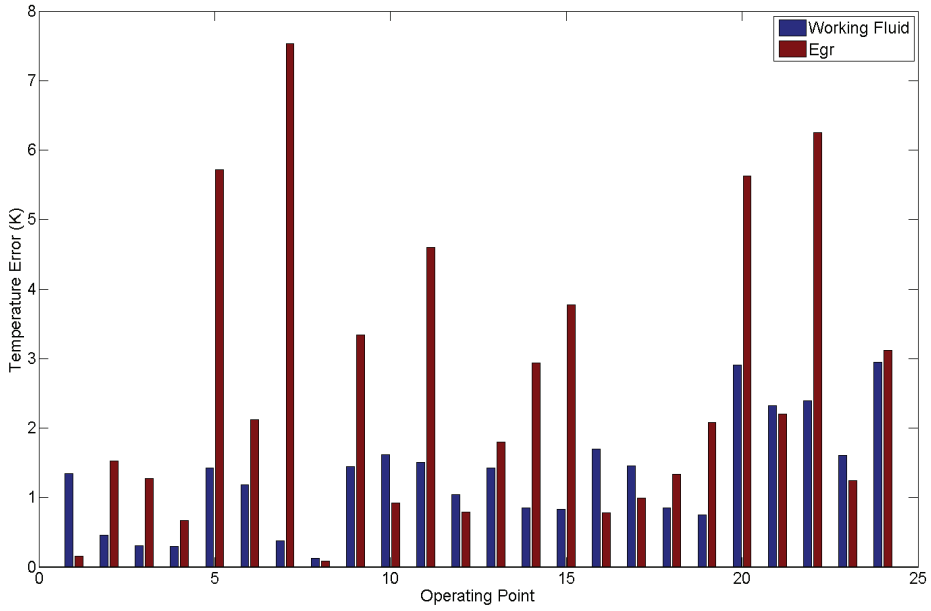


Figure 2.2 – Temperature estimation error for the EGR boiler

between the model and the experiments. Here both temperatures are relevant for comparison since the fluid is fully vaporized at the outlet. On the water ethanol side the maximum error is 9.2K and the mean deviation is around 4K. On the gas side the maximum error observed is 15.5K and the

average difference is about 4.7K. The largest differences are observed on the exhaust which is not so important since accuracy regarding the working fluid is more significant for control purposes. The model predicts well heat exchanger performance in a steady state over the engine map. The main differences come from the non-dependency of the gas specific heat on the air-fuel ratio (i.e. gas composition) and the uniform distribution of heat since the heat exchangers are simply represented by a single pipe. In reality, they are made of several channels and the working fluid is not necessarily homogeneously distributed between all the channels (this is also true for the gas). Last but not least, the heat losses here are represented by a single heat exchange coefficient, but in reality they are influenced by several parameters (external temperature and conditions). Moreover, one important issue has been to ensure reproducibility in the experiment. Indeed, it has been assumed that the fluid distribution between each channel was not homogeneous due to the two phase state of the working fluid. Gravity could cause such a phenomenon by attracting the liquid to the lower channels when vapor is flowing through the upper channels. This phenomenon is observed in Latz et al. (2015) by means of a thermal camera. On top of this, the different control loop actions (engine, Rankine and test cell) could have an influence on the reproducibility of the experiments.

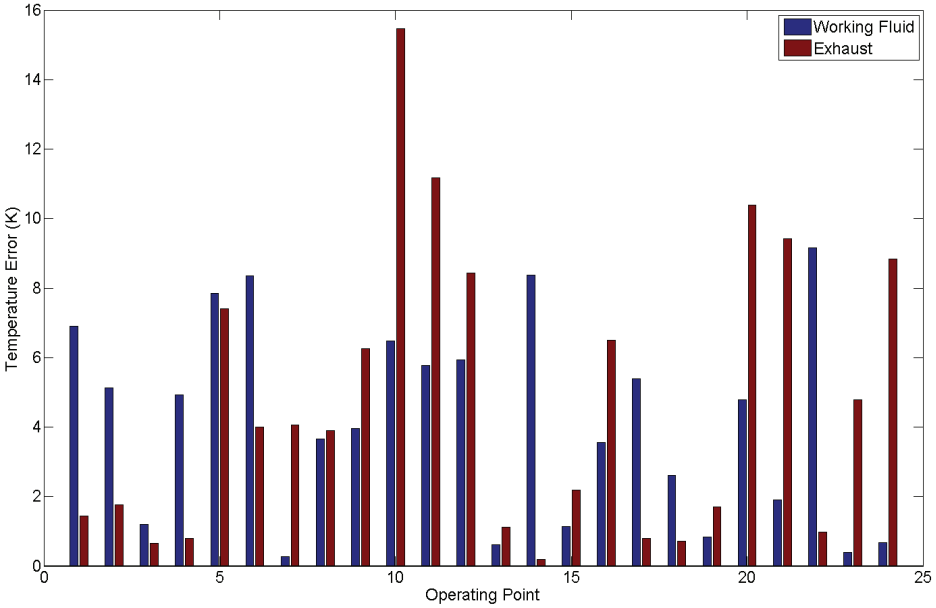


Figure 2.3 – Temperature estimation error for the exhaust boiler

2.3.2.2 Dynamic validation

The model is then compared to dynamic experiments where either working fluid mass flow or EGR and exhaust conditions may vary. At that time, no real transient experiments were performed and the validation was done using a set of simple dynamic tests. An example is shown in Figure 2.4 and 2.5. The latter correspond to the experimental inputs used in the example validation below.
Figures 2.6 and 2.7 show the model predicted temperature versus the measured ones for the gas and working fluid sides, respectively. A large error can be observed at time 0 due to the initial conditions. It was difficult to access certain values in the experimental set-up to correctly set initial conditions in the model (e.g. internal and external wall temperatures). Nevertheless, the dynamic behavior of the complete system is relatively well represented with a maximum deviation of 26 K on the working fluid predicted temperature and 20 K on the gas side. The EGR boiler behavior is

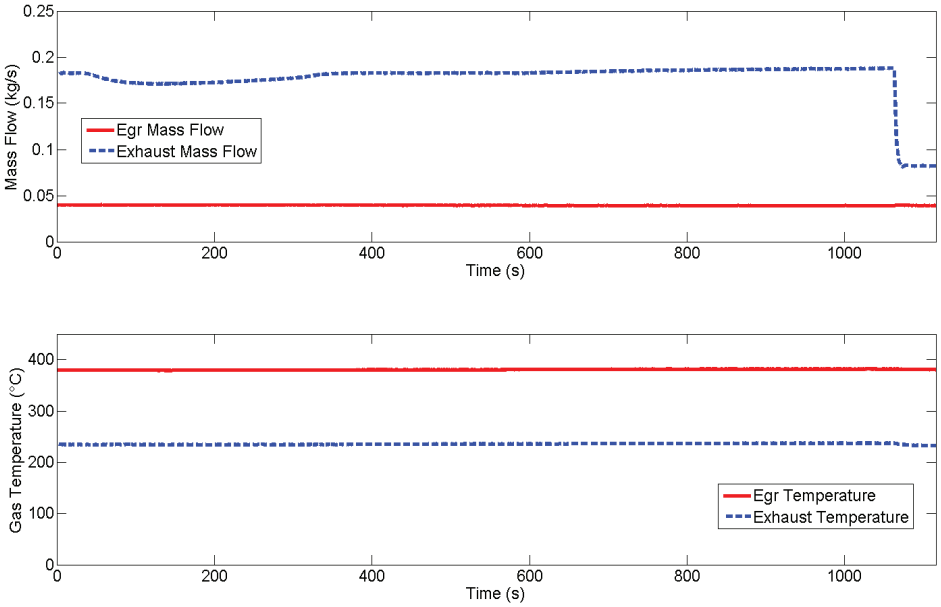


Figure 2.4 – Experimental Inputs: Gas Side

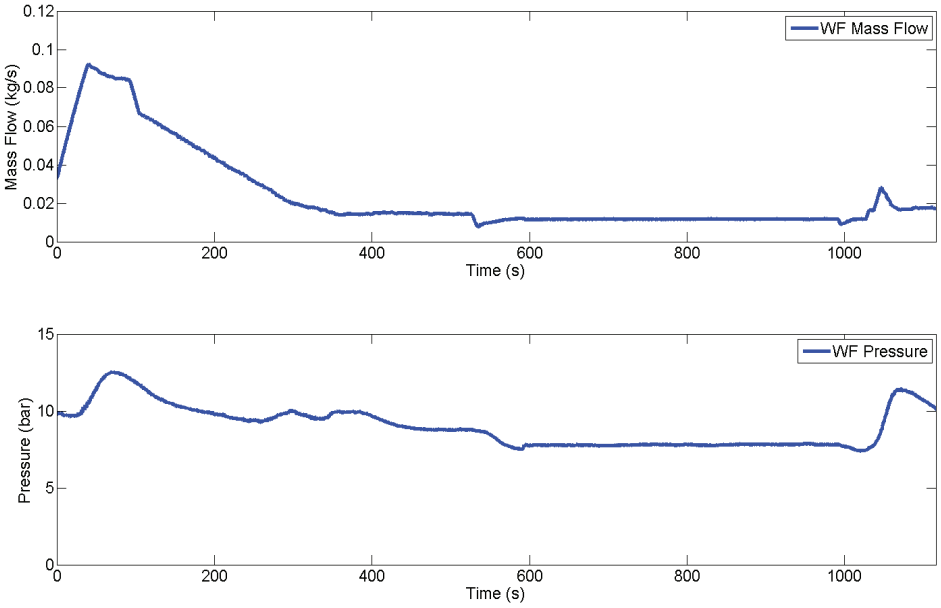


Figure 2.5 – Experimental Inputs: Working fluid Side

better represented due to the simpler geometry. This component has only one core and the simple representation chosen is relatively accurate whereas the exhaust boiler is composed of two cores. However, as the split between each core was not known it has been decided to represent it as a single core heat exchanger.

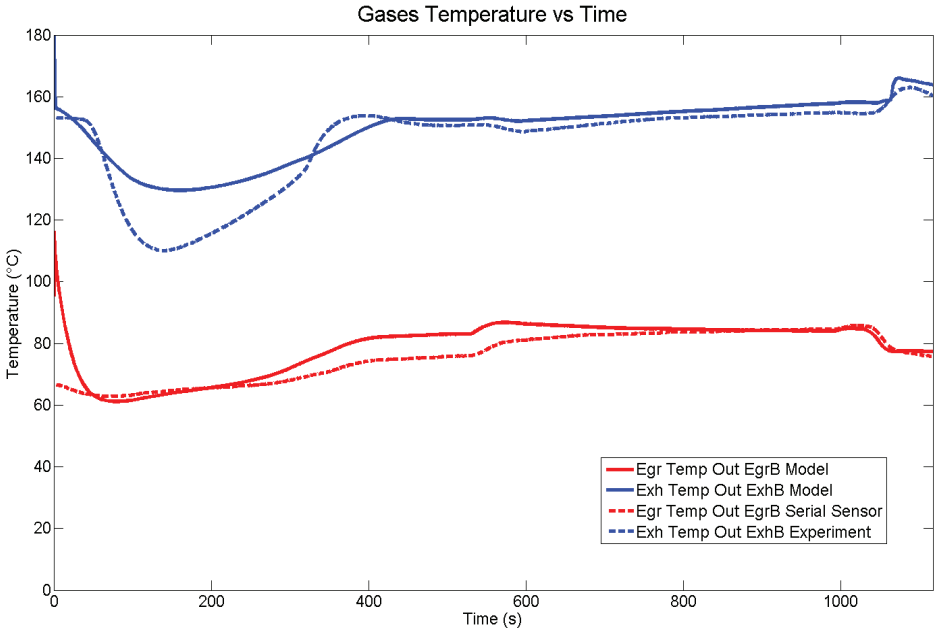


Figure 2.6 – EGR and Exhaust Temperature

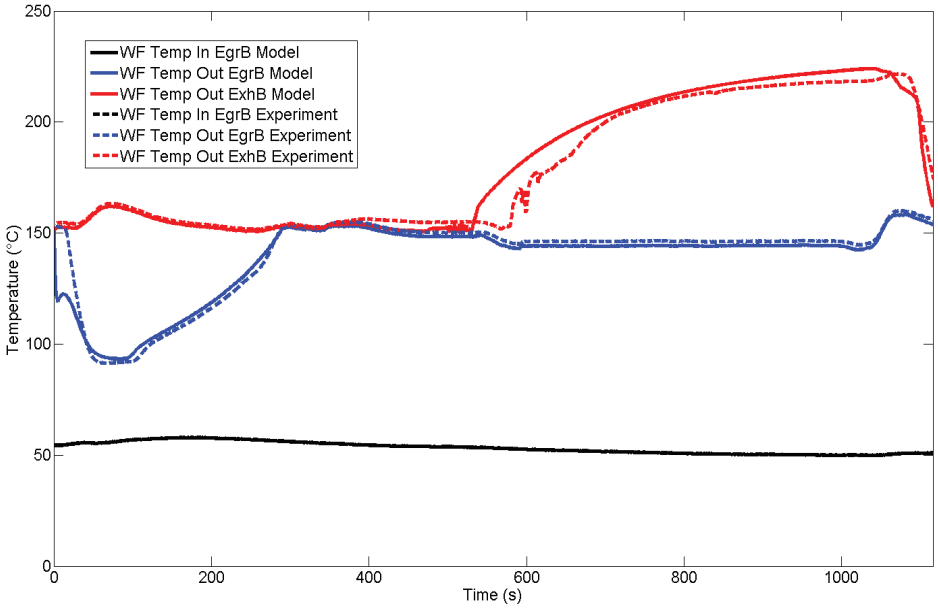


Figure 2.7 – Working Fluid Temperature

2.3.2.3 Evaporators validation summary

Tables 2.2 and 2.3 show respectively steady state and dynamic prediction errors. Note that in both cases the relative error is computed according to the maximum temperature difference between the heat exchanger bounds (usually $T_{g_L} - T_{f_0}$).

	$T_{f_{L_{EGRB}}}$		$T_{f_{L_{ExhB}}}$		$T_{egr_{0_{EGRB}}}$		$T_{exh_{0_{ExhB}}}$	
Error	max	mean	max	mean	max	mean	max	mean
Absolute (K)	2.95	1.30	9.15	4.16	7.54	2.54	15.47	4.71
Relative (%)	0.57	0.29	8.84	3.28	2.34	0.61	8.61	3.40

Table 2.2 – Evaporator models steady state validation

	$T_{f_{L_{EGRB}}}$		$T_{f_{L_{ExhB}}}$		$T_{egr_{0_{EGRB}}}$		$T_{exh_{0_{ExhB}}}$	
Error	max	mean	max	mean	max	mean	max	mean
Absolute (K)	4.5	1.5	25.9	2.3	7.9	2.8	20	4.2
Relative (%)	1.38	0.46	14.37	1.28	2.43	0.86	11.1	2.33

Table 2.3 – Evaporator models dynamic validation

2.3.3 Turbine expander

The turbine expander model presented in section 2.2.4 is fitted according to supplier data. Figures 2.8, 2.9 and 2.10 show the validation of the predicted turbine inlet pressure at three different turbine wheel speeds. The same validation is done for the shaft power calculated using the model and is shown in Figures 2.11, 2.12 and 2.13. In each case, the working fluid mass flow rate and temperature at the turbine inlet and the outlet pressure are imposed and the outputs of the model, namely the inlet pressure and the shaft power, are compared to the supplier data.

Conclusion. *In this chapter, two different Rankine cycle modeling methodologies are presented. Each one intended for a different use. While the first approach is used to quickly assess the potential of such a system using thermodynamic optimization on some steady state operating points, the second represents physical component performance and could be used to establish a dynamic evaluation over a driving cycle. Particular focus has been placed on the evaporators since they are considered of vital importance in the system's behavior. A finite volume approach has been preferred for its simple implementation and integration scheme and its natural ability to handle phase apparition and disappearance.*
Based on these models, the results will be presented in the next chapter where special attention will be paid to the concept optimization using static and dynamic performance evaluation.

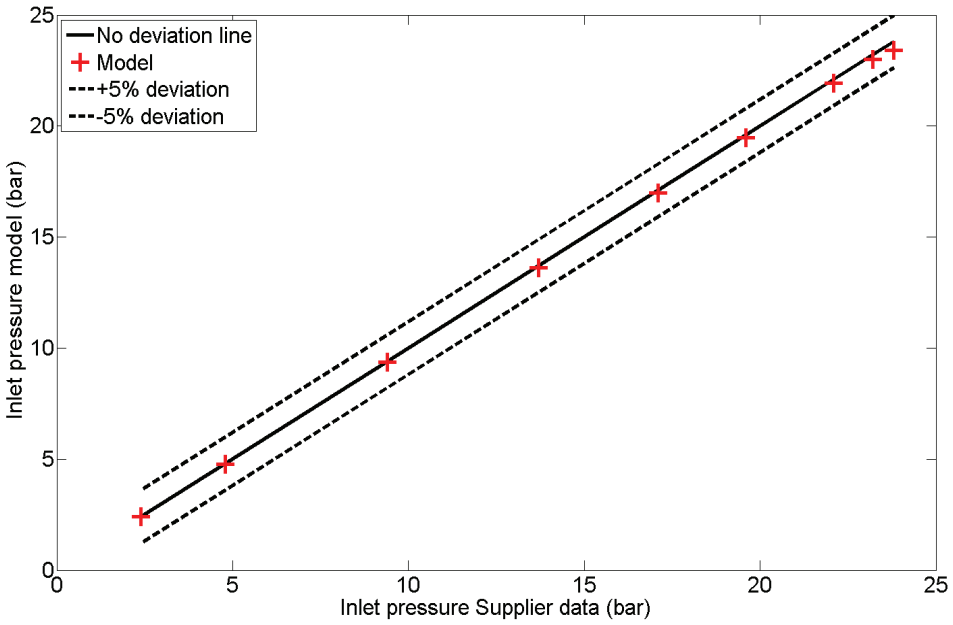


Figure 2.8 – Inlet pressure model prediction at 100krpm

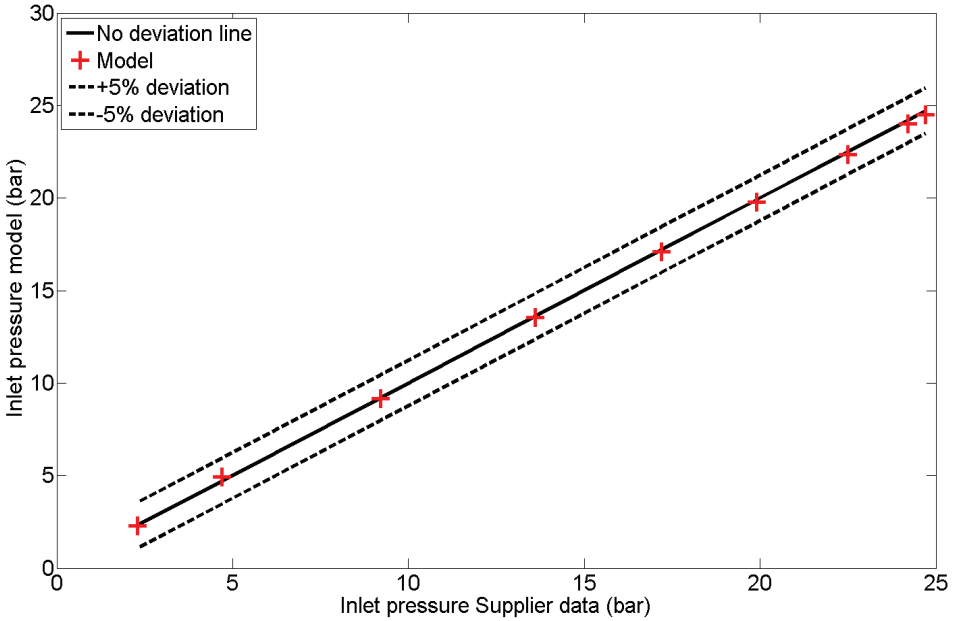


Figure 2.9 – Inlet pressure model prediction at 120krpm

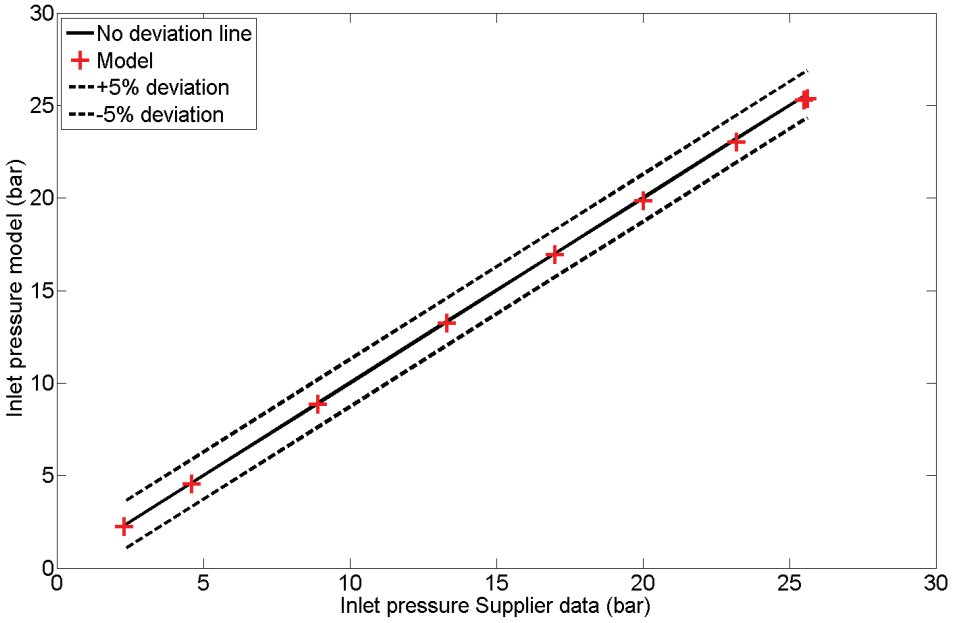


Figure 2.10 – Inlet pressure model prediction at 145krpm

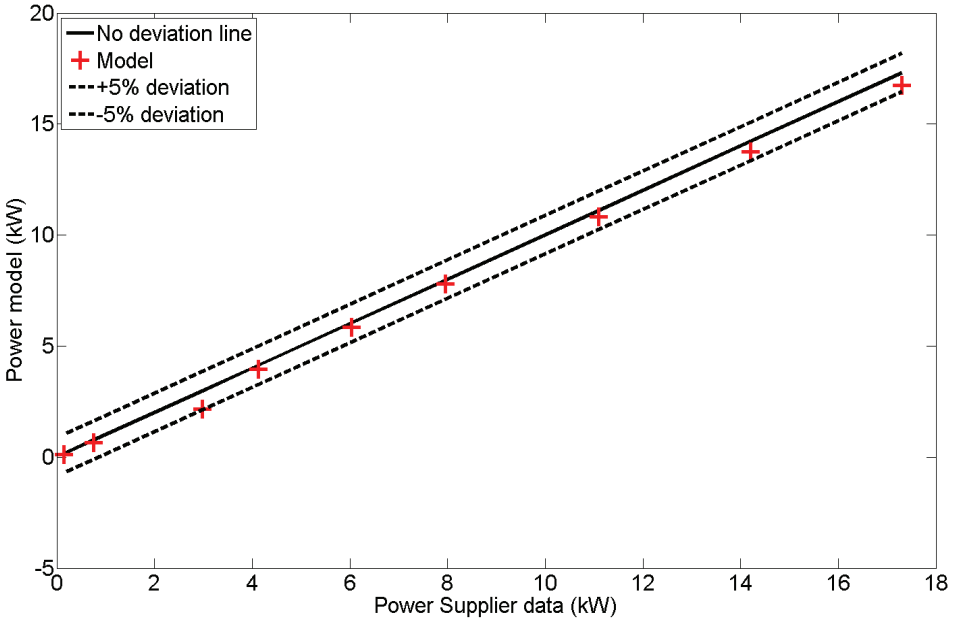


Figure 2.11 – Turbine shaft power model prediction at 100krpm

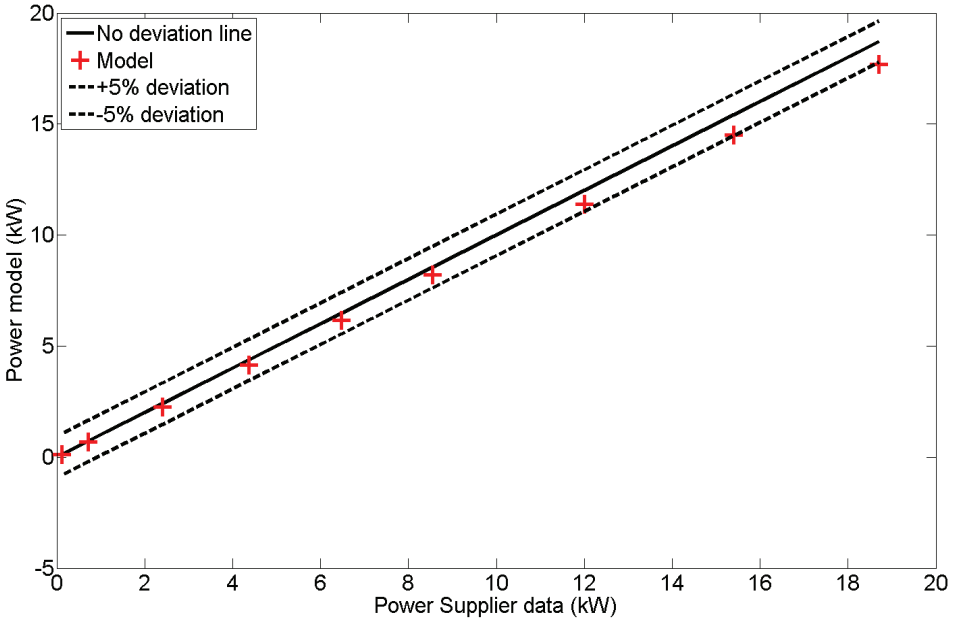


Figure 2.12 – Turbine shaft power model prediction at 120krpm

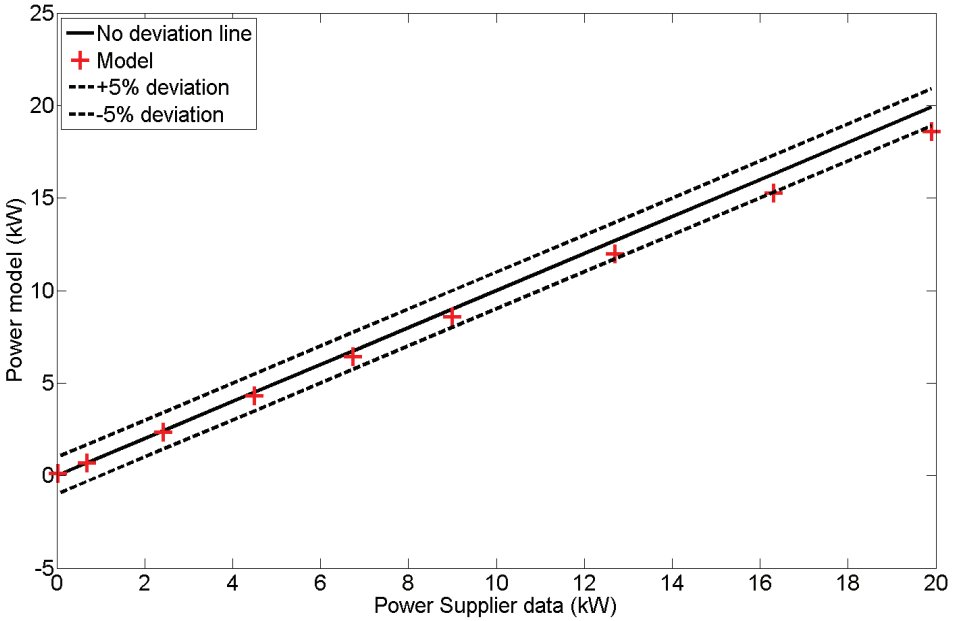


Figure 2.13 – Turbine shaft power model prediction at 145krpm

Chapter 3

Optimization of a Rankine cycle based recovery system for heavy-duty trucks

Abstract. *Chapter 3 shows a case study and a waste heat recovery Rankine cycle based system optimization. The models developed previously are used to maximize the fuel economy induced by the system. Different concepts are evaluated on different referenced driving cycles to select the best one. Optimization on components' level is then proposed to increase the fuel savings.*

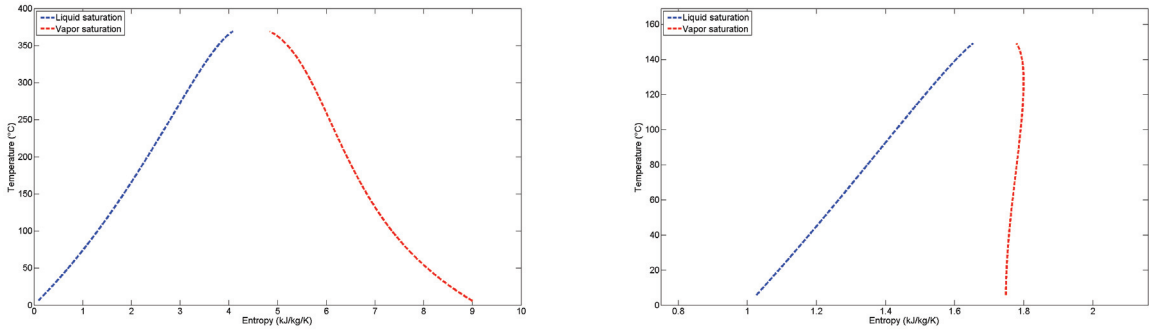
3.1 Working fluid selection

Several aspects have to be taken into account when selecting a working fluid for heat recovery system based on the Rankine cycle for mobile applications. Unlike stationary power plants where the main consideration is the output power or the efficiency, here other aspects have to be considered such as fluid deterioration, environmental aspects or freezing.
Up until now, several studies have tried to identify the ideal fluid for WHRS (Mago et al. (2007); Stijepovic et al. (2012); Papadopoulos et al. (2010)) but no ideal fluid has been found. Recently, new performance indicators have been introduced (Lecompte et al. (2013); Cayer et al. (2010)), where cost and design issues enter into consideration.
Working fluids for Rankine cycle are classified into two categories:

- Wet fluids: the vapor saturation curve in the temperature entropy diagram is defined by a negative slope. By considering a non- or limited superheated state at the end of the heating process, the ideal (isentropic) expansion ends in the dome (two phase state). Those fluids require, then, a higher degree of superheat to keep the vapor state in the expansion process (even though in reality, entropy is created during this process). This constrains the vapor creation by imposing a minimum degree of superheat to start creating mechanical work by means of the expander (this is even more true for a kinetic expander that does not tolerate droplets).

- Dry fluids: conversely, these are characterized by a positive slope of the vapor saturation curve in the T-s diagram. Those fluids, similar to the refrigerants used in air conditioning systems, do not need a high degree of superheat and generally possess a high molecular mass due to their complex structure.

Note that, in some studies (Mago et al. (2007); Teng et al. (2007b)), a third category of fluids is introduced: isentropic fluids. They are characterized by a straight vapor saturation curve in the T-s diagram. Those kind of fluids are, here, integrated in the dry fluids due to their propensity to keep vapor state during ideal expansion. Figure 3.1 shows the temperature entropy diagram of dry and wet fluids (respectively water and R245fa). Even if water is considered as the perfect



(a) (b)

Figure 3.1 – Wet (a) and dry (b) fluids T-s diagrams

fluid for Rankine application and is the reference fluid in electricity generation and cogeneration, it does not suit waste heat recovery of diesel engines (Larnaud (2010)) due to its high latent heat of vaporization and requirement in terms of superheat. Organic fluid is, then, more appropriate (Stijepovic et al. (2012)) to low temperature recovery applications.
Last but not least, the working fluid has a strong impact on the system and components design. This impacts the component's technology choice, the system performance as well as its dynamic behavior. Every one of those aspects needs to be considered when fluid selection study is carried out.

3.1.1 Case study

The steady state model presented in section 2.1 is used to simulate the system operating with a various number of fluids and compare the performance achieved by each fluid. Both evaporating pressure and superheat are optimized to recover as much energy as possible during the expansion process. Model parameters shown in 2.1 are set to represent real components' performance. Model inputs are set to represent the whole engine map in terms of heat sources' flow rates and temperatures. An example of a possible results representation is shown in Figure 3.2. This model helps to compare several fluids at different boundary conditions and to select the suitable fluids for the considered application.
To select the fluids giving the best performance, simulations are carried out on a succession of representative steady state points chosen to represent a classical long haul heavy-duty truck usage.

From an exhaustive fluid list (Eric. W. Lemmon (2013)), fluids that do not respect the following criteria have been removed:

- Chemical class: chlorofluorocarbons (CFCs) have been made illegal by the Montreal Protocol and hydrochlorofluorocarbons (HCFCs) production is planned to be phased out by 2030.
- Presence on the global automotive declarable substance list (GADSL).

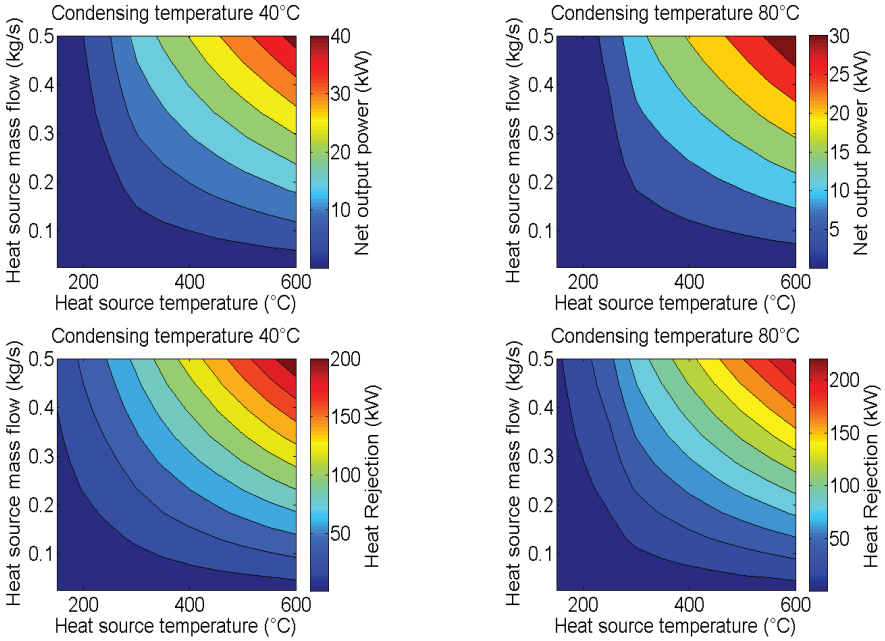


Figure 3.2 – Performance map of Acetone at two condensing temperatures

	Name	EGR mass flow	EGR temperature	EGR heat	Exhaust mass flow	Exhaust temperature	Exhaust heat
	Unit	g/s	$℃$	kW	g/s	$℃$	kW
1		43	280	11.8	69	259	17.4
2		33	374	12.4	156	291	44.8
3		53	668	36.8	304	434	134.3
4		57	543	31.9	238	365	87.4
5		63	329	20.7	150	266	39.0
6		65	450	29.8	227	315	71.1
7		71	525	38.3	271	352	95.7
8		59	674	41.4	369	435	163.4
9		83	624	53.7	393	396	157.5

Table 3.1 – Working fluid selection 0D model inputs

- Chemical properties such as the global warming potential (GWP), the ozone depletion potential (ODP) or the risk phrases (R-phrases).
- Classification according the national fire protection agency (NFPA) 704 classification (ranking above 1 in Health or Instability class)

On top of that, the freezing point has to be below -11 ℃[1] since freezing protection devices, such as the one reported in Ternel et al. (2011), increases the level of complexity and obviously the cost of the system. However, as water is a good reference fluid since it is generally used in power plants Fischer (2011), it has been kept. Hereafter the 9 operating points of Table 3.1 are simulated for two condensing temperatures 60℃ and 90℃, representing two different heat sinks: the first one being a dedicated low temperature circuit, the second one being the classical engine cooling circuit Bredel et al. (2011). Here, each hot stream is simulated separately in order to see the impact of the heat source on the Rankine fluid selection. The simulation matrix contains 9 operating points and 14 selected working fluids. For sake of simplicity, the results presented in Figure 3.3 show the number of occurrences where the fluid is in the top five [2] regarding the NOP.

When analyzing each operating point and configuration separately among the 9x14 simulations, water is giving the best performance for heavily loaded operating points [3]. For low and medium heat load, as gases' temperatures are lower and due to the large enthalpy of vaporization of water and the high level of superheating required, it is not recommended to use it. Acetone, cyclopentane and ethanol show good performance at mid and high load despite the cold sink temperature. Refrigerants such as R1233zd or Novec 649 show good results for heat source temperature under 280 ℃ at the lowest condensing temperature. More exotic fluids such as cis-butene or MM (silicon oil) could be attractive for low and medium engine load respectively at 60℃ condensing temperature for the first one and 90℃ for the second one. These first simulation results limit the number of investigated working fluids to the following ones: acetone, cyclopentane, ethanol and water. Those four fluids represent the highest number of occurrences for the architecture optimization. As these fluids have similar volumetric flows it would be possible to use the same components' characteristics with only some minor changes (e.g. throat diameter for the turbine model and pump displacement).

3.2 Rankine architecture optimization

3.2.1 Rankine layouts

Several studies have been conducted in the field of Rankine cycle based heat recovery systems for mobile applications. A screening of the different heat sources available is reported in Freymann et al. (2008) and shows that the most promising ones are the EGR and the exhaust streams. Only these two heat sources are considered since they demonstrate the higher grade of temperatures among other sources. Therefore four different Rankine layouts are studied:

1. Exhaust recovery where the only heat source is the exhaust gases (shown in Figure 3.4).
2. EGR recovery where only the EGR gases are used as heat source (shown in Figure 3.5). From a thermodynamic perspective, using the highest grade of heat first could be considered as

[1] This temperature corresponds to the freezing temperature of the urea used for selective catalyst reduction

[2] top five means the NOP related to the fluid is ranked in one of the five first position among all simulated fluids

[3] load is defined as the ratio of the actual available heat to the maximum available heat in the considered stream

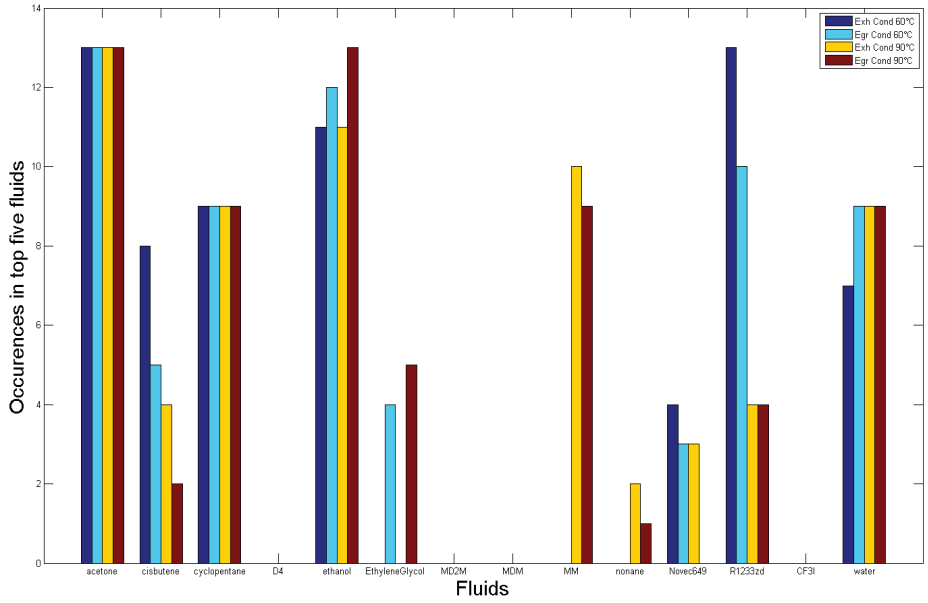


Figure 3.3 – Number of occurrences of each fluid in top five [2] for different boundary conditions

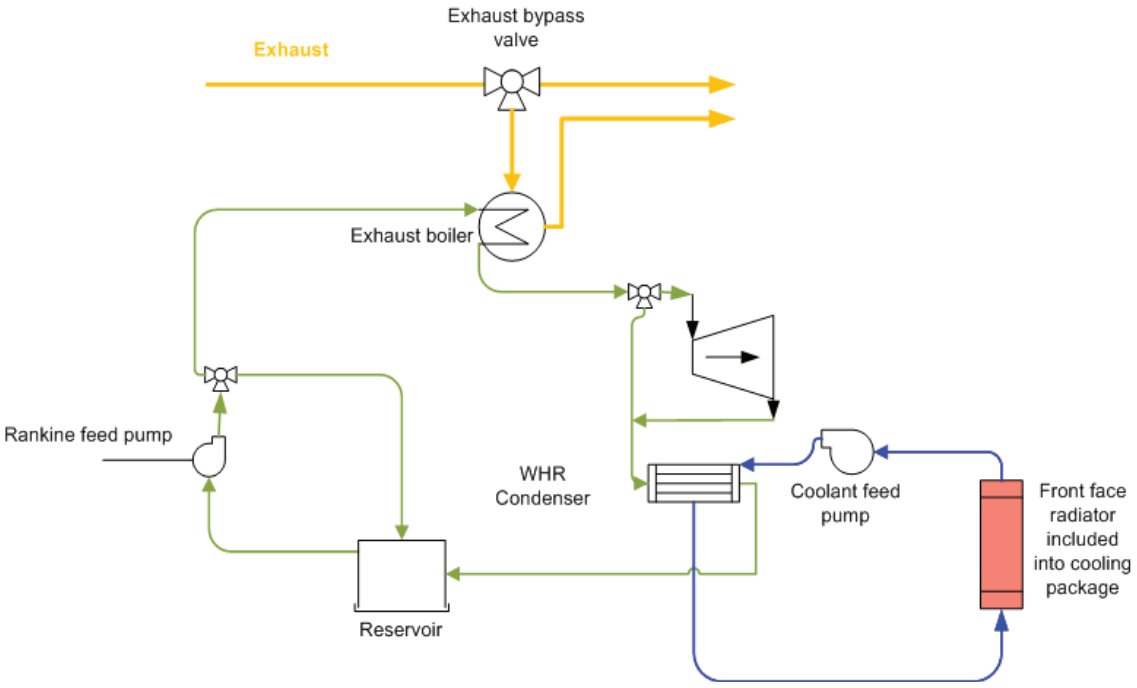


Figure 3.4 – Exhaust only system schematic

nonsense but the EGR's primary function is to decrease the noxious emission of the engine using low temperature combustion gases to dilute the combustion air. Therefore, in order not to degrade the EGR function it has to be cooled in the same way than with an EGR cooler justifying this arrangement where the cold fluid first flows through the EGR boiler and then through the tailpipe evaporator.

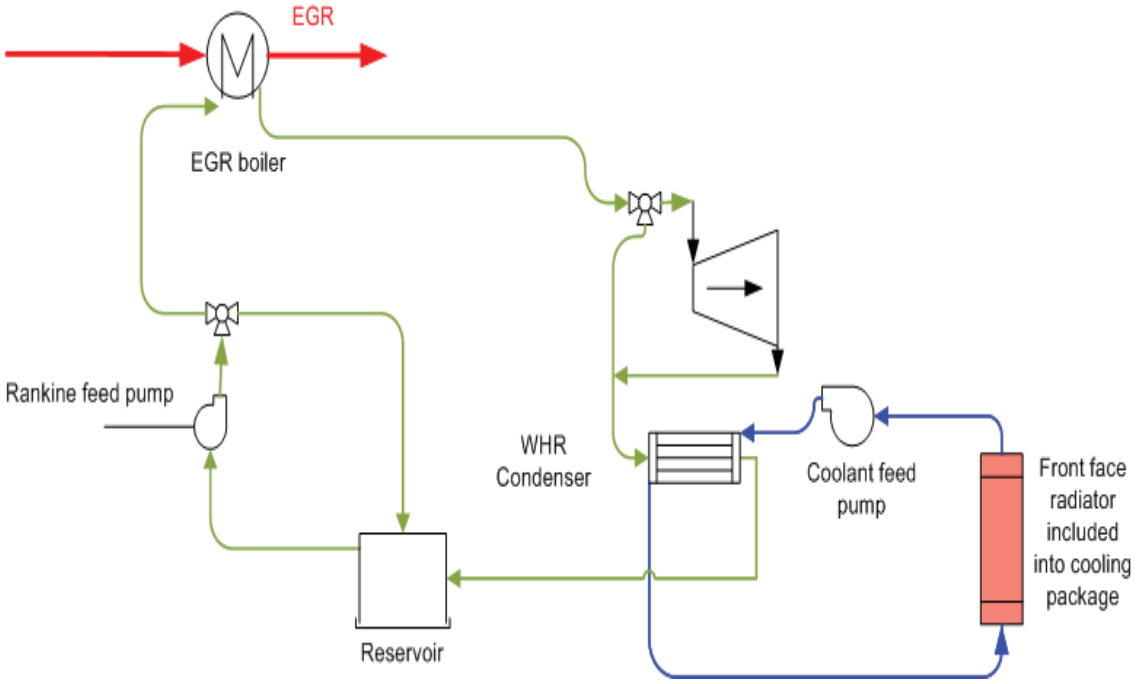


Figure 3.5 – EGR only system schematic

3. Both sources in parallel where the working fluid is split into two streams heated up separately by each source and then mixed before the expander (shown in Figure 3.6).

4. EGR and exhaust in series where the EGR gases are used to preheat the fluid and the exhaust gases to vaporize and superheat (shown in Figure 3.7). Using the EGR as a preheater, instead of a superheater, lowers the EGR gases' temperature after the evaporation process.

3.2.2 Cooling system

The cooling system is the heat sink of the Rankine cycle. The design of this has a strong influence on the waste heat recovery system performance. Over the last years, different studies (Espinosa (2011); Dickson et al. (2014)) have shown the importance of the cooling on the maximization of the system performance. Several cooling module arrangements have been studied in Edwards et al. (2012) and show that an air cooled condenser greatly impacts the charge air cooler efficiency and results into a limitation of the Rankine system due to cooling fan engagement. In order to avoid overly derating engine performance and excessive fan engagement, only water-cooled condenser are considered. It is fed with coolant coming from an air-cooled radiator included into the front face cooling package. Two different layouts are investigated:

- A first one (called in the following Cooling Config 1) which uses a low temperature radiator dedicated to the Rankine condenser and is placed between the charge air cooler (CAC) and the engine radiator.

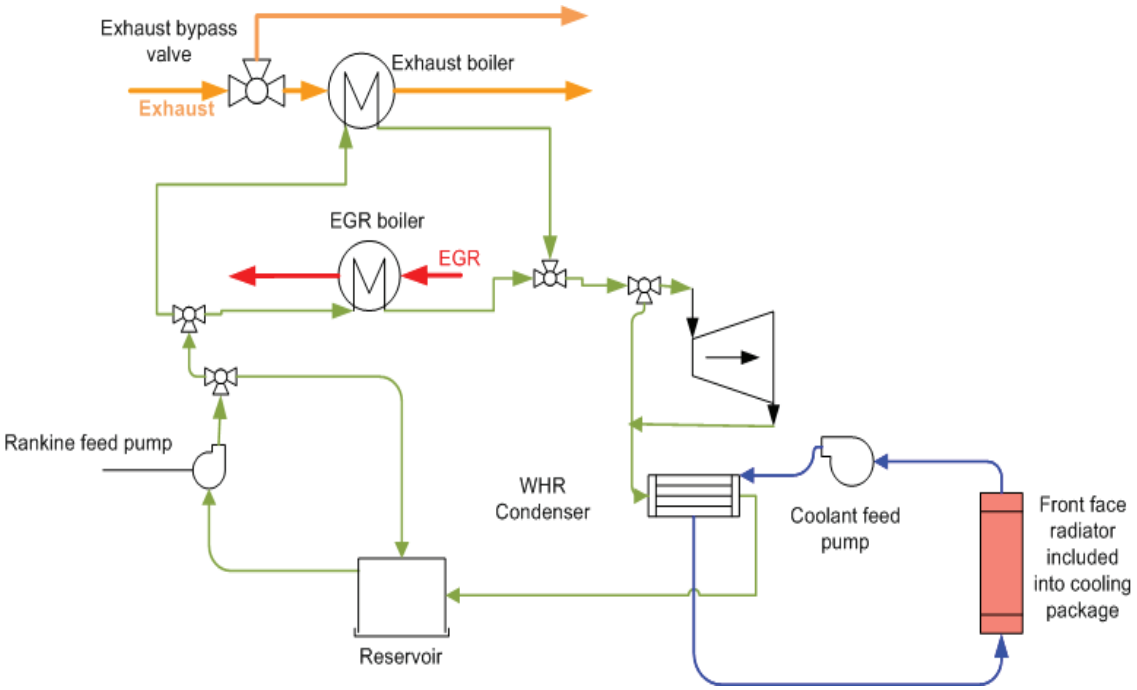


Figure 3.6 – Exhaust and EGR in parallel system schematic

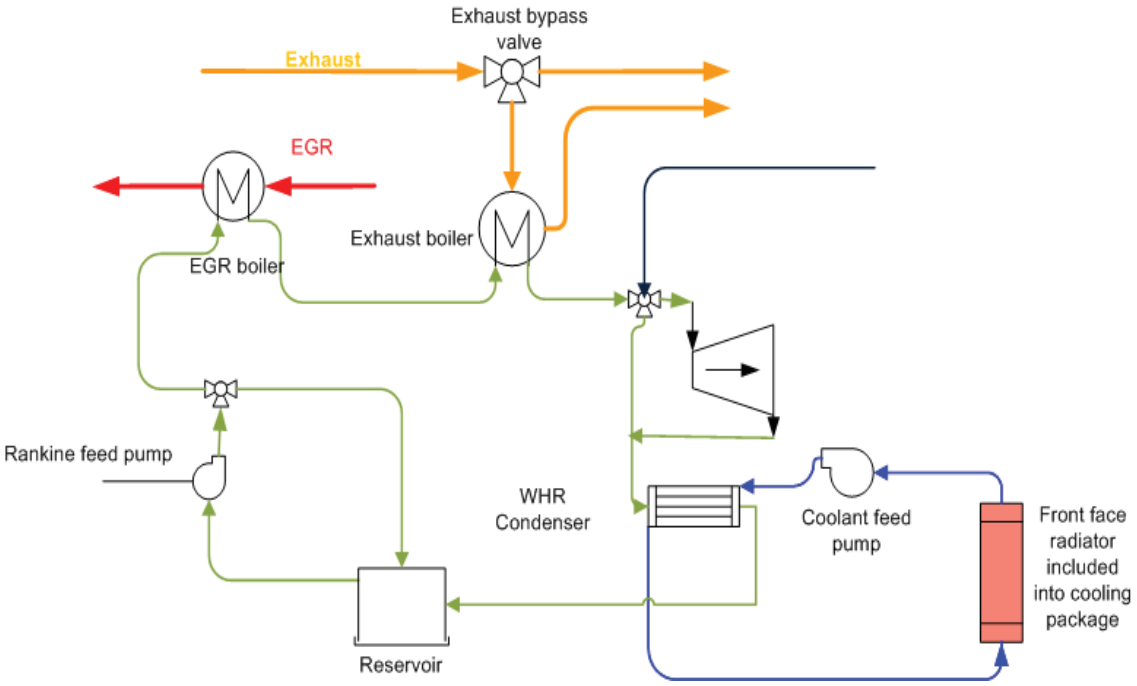
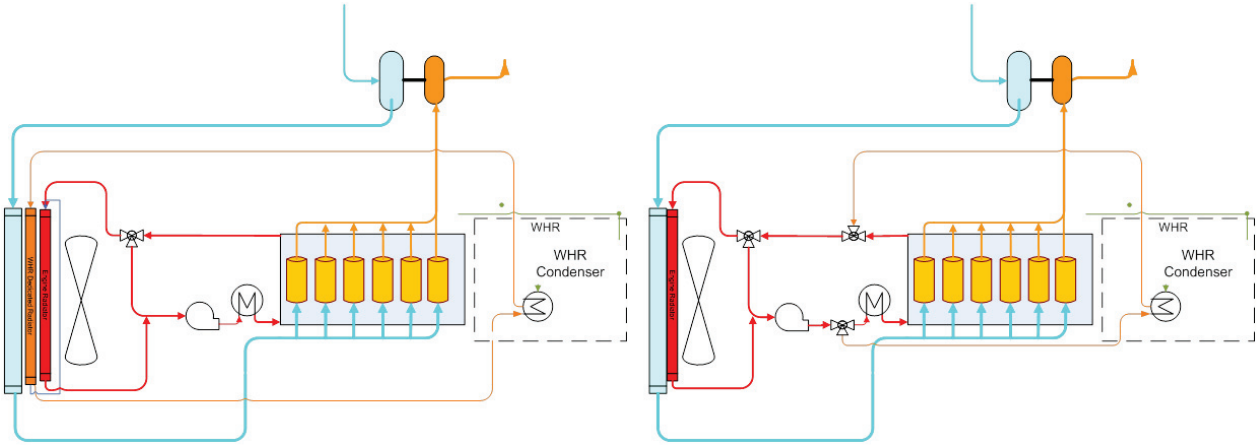


Figure 3.7 – Exhaust and EGR in series system schematic

- A second one (called in the following Cooling Config 2) using the engine coolant as a heat sink for the Rankine cycle. In this case, a derivation of the coolant is made in front of the engine to benefit from the lowest temperature grade.

Both cooling configurations are depicted in Figure 3.8.



(a) (b)

Figure 3.8 – Cooling configuration 1 (a) and 2 (b)

3.2.3 Performance criterion

The criterion used for the performance evaluation under steady state and dynamic driving conditions is the total net reinjected power to the conventional driveline. This is done by taking into account the power producer (WHRS expander) and different power consumer devices (cooling fan, WHRS pump and WHRS coolant pump) and assuming them to be mechanically driven (this is not always true for the pumps but efficiencies are detuned to take into account the mechanical to electrical conversion). A complete vehicle model integrating engine, EATS, transmission, cooling package, WHRS and road environment is used to simulate the total vehicle approach and calculate the power needed to drive the vehicle. The performance criterion (PC) is then calculated as the ratio of this reinjected power to the engine power:

$$PC_i = \int_{t_{init}}^{t_{final}} \frac{\dot{W}_{exp} - \dot{W}_{pump} - \dot{W}_{cool,pump} - \dot{W}_{fan}}{\dot{W}_{eng}}, \tag{3.1}$$

where the engine power ($\dot{W}_{eng}$) takes into account the mechanical auxiliaries consumption mounted on it (high pressure injection pump, air compressor, ...) and the increase in exhaust backpressure (due to the exhaust evaporator). The vehicle gross weight is assumed constant and equal to 36 tons so as to represent the average load on a long haul truck. The performance criterion (PC) over the different steady state operating points or driving cycles is then calculated by summing the weighted PC on each points/cycles:

$$PC = \sum_{i=1}^{k} w_i PC_i, \tag{3.2}$$

where k is the number of considered steady state operating points or dynamic driving cycles.

3.2.4 Duty cycles

Driving conditions act as input disturbances and therefore, their impact on the target performance must be studied with care.

3.2.4.1 Steady state evaluation

Under steady state driving conditions, the performance is evaluated by expressing the weighted average net output power of the 1D model (the NOP, which is the additional power that the engine receives, therefore corresponds to the fuel economy) on 13 engine operating points (summarized in Table 3.2) . These operating points are chosen to represent a classical long haul driving cycle and weighted according to the percentage of fuel power used on each operating point ($\dot{Q}_{fuel} = \dot{m}_{fuel} * LHV_{fuel}$). Figure 3.9 shows the fuel energy usage on the considered driving cycle versus engine torque and speed.

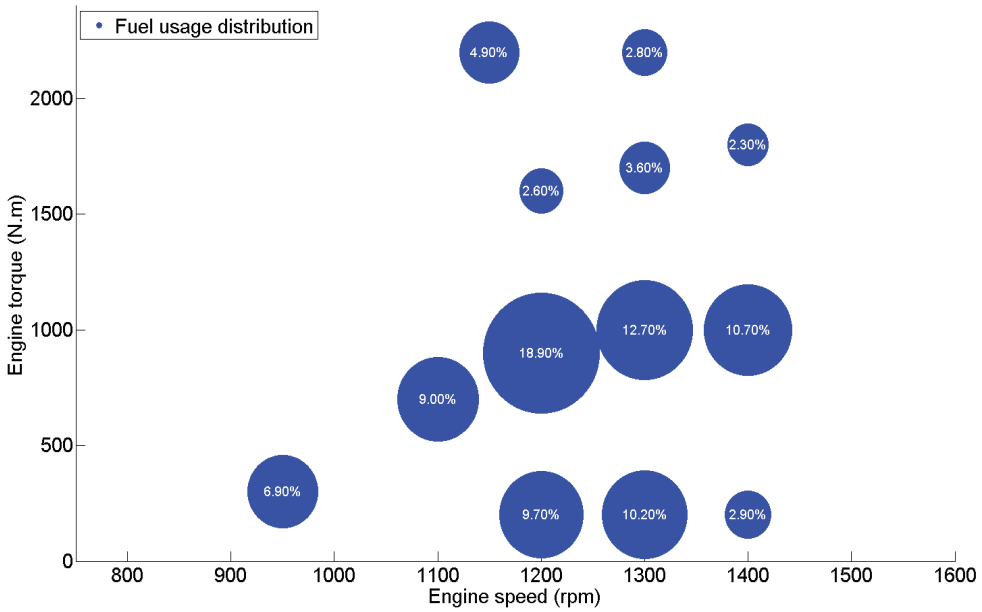


Figure 3.9 – Fuel energy distribution over classical driving cycle

Operating point number 5 is identified as the design point whereas the operating points 3 and 11 are considered critical due to the high engine load and the low vehicle speed.

3.2.4.2 Dynamic evaluation

In order to accurately assess the potential of the WHRS, dynamic driving cycles are also used to complete the study and check whether the performance found with the previous method is correct. This is very important when coming to thermal systems performance estimation since they generally have long response times Stobart et al. (2007). The driving cycle used is split into 7 phases (summarized in Table 3.3), and is supposed to represent all conditions of a long haul truck usage. Each phase is considered as a unique driving cycle of approximately the same metric length (denoted by a number from 1 to 7) and weighted according to their real life importance (for a long haul truck highway is predominant). Figure 3.10 shows the altitude change and the set speed of two driving cycles.

Operating point	Name	Engine speed	Engine load	Vehicle speed	EGR mass flow	EGR temperature	Exhaust mass flow	Exhaust temperature	Weight factor
	Parameter	N_{eng}	-	$v_{vehicle}$	$\dot{m}_{egr}$	T_{egr_0}	$\dot{m}_{exh}$	T_{exh_0}	w_i
	Unit	rpm	$\%$	km/h	g/s	$°C$	g/s	$°C$	$\%$
1		950	25	20	31.5	263.1	78.7	237.9	6.9
2		1100	50	85	38	409.5	119.8	338.2	9.0
3		1150	100	60	59.5	635.0	309.3	443.9	4.9
4		1200	75	85	54.6	544.0	252.4	413.0	2.6
5		1200	25	75	46.1	454.0	154.6	366.4	18.9
6		1200	50	85	56.3	247.5	85.7	212.5	10.5
7		1300	75	30	85.9	631.0	352.7	425.1	2.8
8		1300	100	85	69.4	562.5	290.5	405.5	3.6
9		1300	100	50	58	473.0	183.2	336.2	12.7
10		1300	100	85	59.8	251.0	95.2	216.0	11.2
11		1400	75	45	87.1	581.0	326.8	400.8	2.3
12		1400	25	75	68.9	472.0	198.4	359.6	10.7
13		1400	50	85	62.9	252.5	102.8	217.5	3.9

Table 3.2 – Steady state evaluation: Driving conditions and weight for 13 engine operating points

Driving cycle	1	2	3	4	5	6	7
Road Type	Extra urban	Highway	Highway	Extra urban	Extra urban	Extra urban	Hilly
Vehicle speed	Medium	High	Medium	Low	Medium	High	High
Weight factor w_i $(\%)$	10	10	50	7.5	10	7.5	5

Table 3.3 – Dynamic evaluation: Driving conditions and weight for the 7 phases

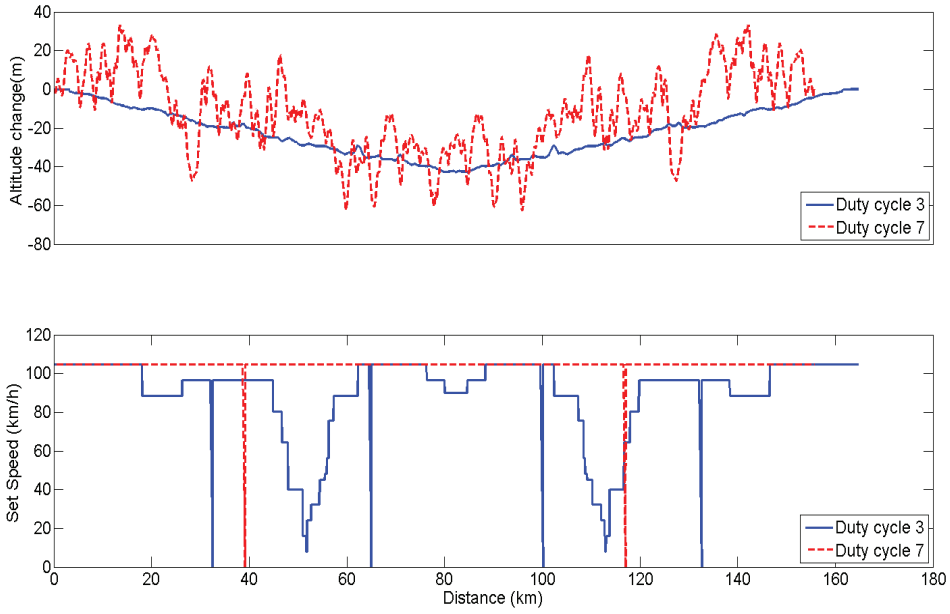


Figure 3.10 – Driving cycle profile examples

3.2.5 Steady state performance evaluation

The performance criterion is then analyzed on the 13 operating points and the 2 cooling architectures (Cooling config 1 and 2) for the previously chosen working fluids. The savings are computed thanks to the weight factors presented in Table 3.2. Figures 3.11, 3.12, 3.13 and 3.14 present the NOP to engine power ratio evaluated for all the layouts. It can be observed that the decrease due to higher condensing temperatures induced by cooling configuration 2 depends on the working fluid assessed. This drop in performance is due to the increase in condensing pressure which affects the overall pressure ratio through the expansion machine and therefore its performance. As water has the higher boiling point of the selected working fluid in 3.1, the impact is lower. However, this effect could be partially balanced by a specific design of the expansion machine in order to have a variable nozzle geometry that keeps the pressure ratio constant when the condensing pressure increases. A similar approach is done in Kunte and Seume (2013) to adapt the nozzle geometry to the mass flow entering in the turbine. In terms of the performance of these components, regardless of the fluid considered, the parallel arrangement of the heat sources gives the best PC since both heat sources are used in a separate way and the heat recovery process is maximized. For all fluids, the hierarchy of architectures is conserved: parallel gives the best PC, followed by the serial layout, then the exhaust only system and finally the EGR only system. However, for organic fluids (i.e. acetone, cyclopentane and ethanol) the difference between series and parallel layout is not as important and the lower number of valves needed by the former could compensate this drop in performance. For water, the big drop in performance due to this arrangement can be explained by the high superheating needed at the kinetic turbine inlet to ensure a fully vapor expansion which tends to reduce the mass flow through the boiler and affect both evaporating pressure and EGR temperature after the boiler. In some cases, the impact on the engine could even be negative since a higher EGR temperature results in higher pollutant emissions. In this configuration, if water is used as working fluid, the EGR temperature should be monitored with attention to the expense of the power production. On the other hand, using organic media as the working fluid mass flow is controlled to obtain a superheated vapor state at the outlet of the tailpipe boiler, the mass flow rate is then higher than in any other configurations. It results in lower EGR temperatures which could be a benefit in terms of engine performance and pollutant emission control (Willems et al. (2012)). Last but not least, with the EGR only solution, even if the weight and installation impact is low (the heaviest component is the EGR evaporator that replaces the traditional EGR cooler), the PC seems too low for a vehicle installation. This obviously needs further analysis whilst also taking into account the cost impact of each solution on the total cost of ownership. As ethanol gave the best performance over the different investigated Rankine architectures, the focus is now done only on this fluid for dynamic evaluation of the waste heat recovery performance.

3.2.6 Dynamic performance evaluation of ethanol based ORC

Dynamic simulations are run to further assess the performance criterion of the WHRS where ethanol is now the only considered working fluid. Rankine cycle based heat recovery systems could have long time constants due to the boiler(s) inertia, mainly contained in the wall capacity. This could help in terms of control by filtering some high transients of the heat sources but reduce the heat transferred to the fluid, since only a fraction of the heat contained in the hot gases is then used instantaneously (Peralez (2015)). The performance criterion is assessed on 7 different driving cycles (see Table 3.3) representative of a long haul truck usage. Each driving cycle is simulated separately starting from ambient conditions that can result in a lower PC due to the long warm up time of the exhaust after treatment system (EATS). Weights (see Table 3.3) are applied to the different driving cycles to calculate the total performance criterion of the WHRS.
An example of the simulated quantities around the driving cycle is shown in figures 3.15 and 3.16

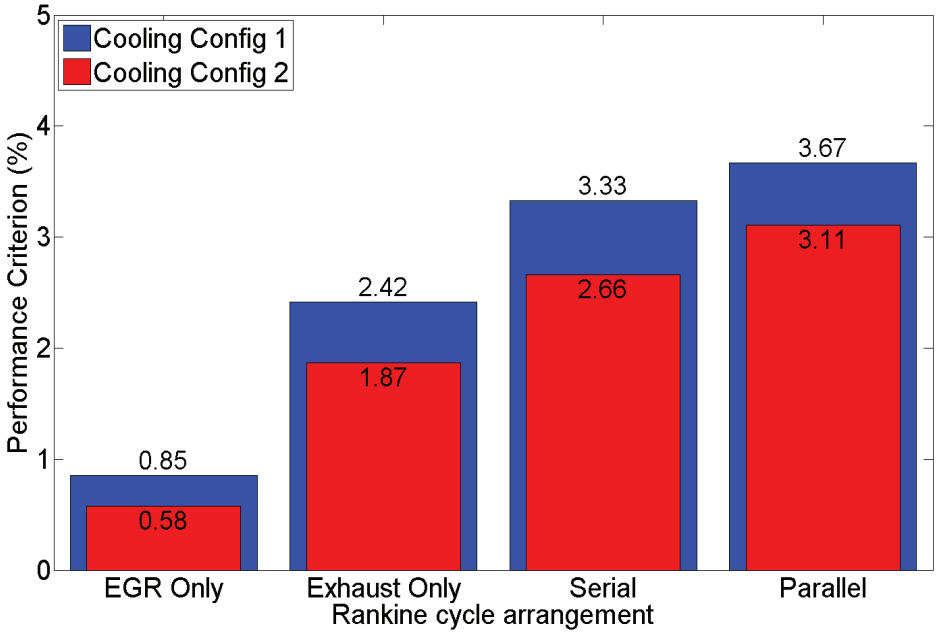


Figure 3.11 – Steady state PC assessment for acetone

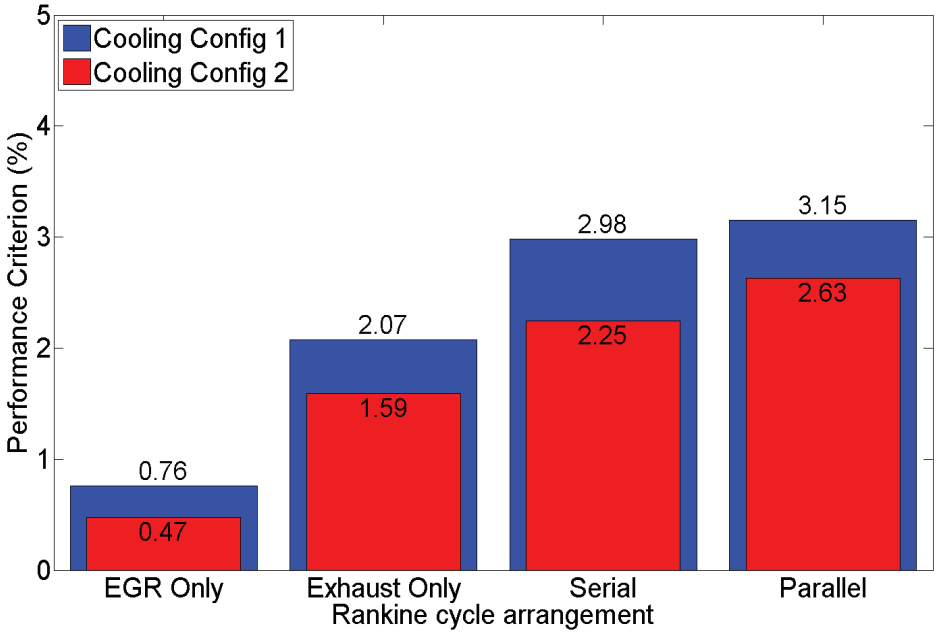


Figure 3.12 – Steady state PC assessment for cyclopentane

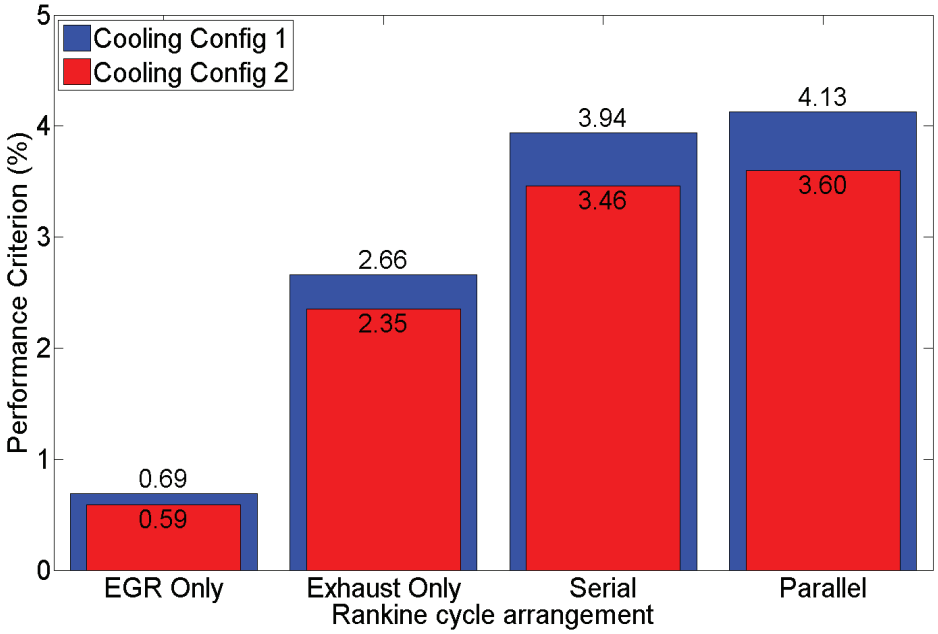


Figure 3.13 – Steady state PC assessment for ethanol

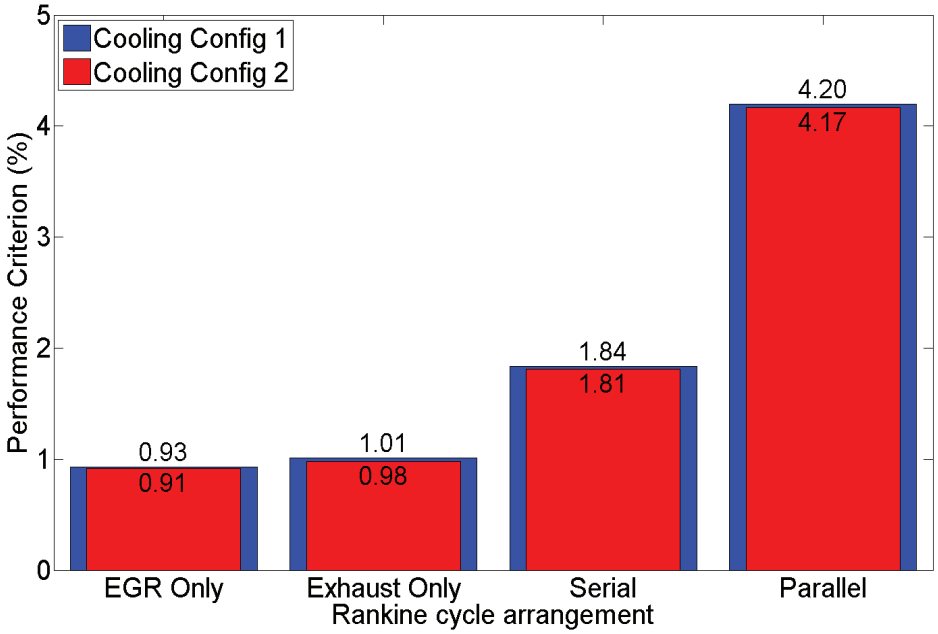
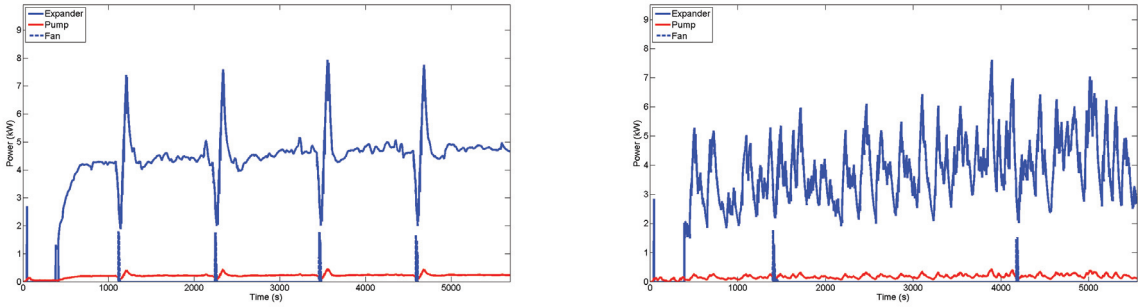


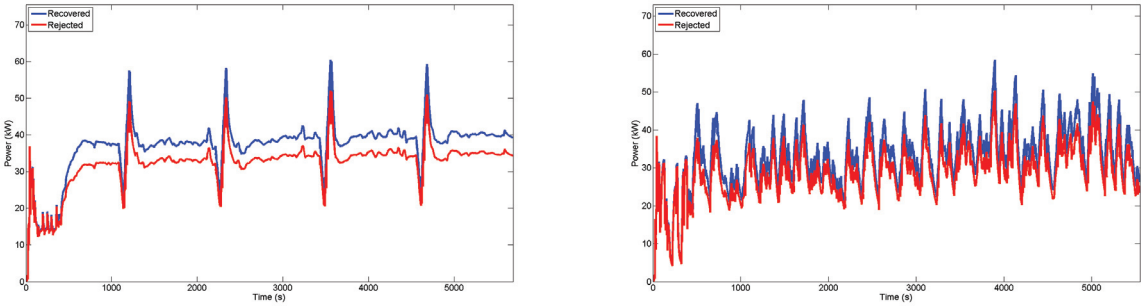
Figure 3.14 – Steady state PC assessment for water

for a system recovering heat from EGR and exhaust in parallel with the first cooling configuration on the road profile number 2 and 7. It can be seen that cooling fan overconsumption due to the heat recovery device is always balanced by the expander generated power (ambient temperature is assumed to be constant during the cycle and equal to 20°C). Figures 3.17 and 3.18 show the *PC*



(a) (b)

Figure 3.15 – Mechanical power produced and consumed on driving cycle 2 (a) and 7 (b)



(a) (b)

Figure 3.16 – Heat flow rates recovered and rejected on driving cycle 2 (a) and 7 (b)

reached by each Rankine configuration respectively for cooling configuration 1 and 2. As shown in 3.2.5, the decrease in performance using cooling configuration 2 rather than cooling configuration 1 is more or less constant and around 11%. This drop is considered important from the performance perspective but acceptable from the integration point of view since it does not require an additional cooler or pump. The main information presented by this study remains the lower fuel savings when simulating the system in dynamic instead of steady state, which can be as big as 50% for the systems using exhaust as a heat source.

- the exhaust after treatment system, which has a very important time constant, causes a big temperature drop during fast highly loaded engine conditions where a lot of heat is supposed to be available.
- the non optimal design of the tailpipe boiler used in the simulation model. Indeed the validation of the model shown in section 2.3 is based on prototypes components that do not represent the optimum in terms of size and transient performance.

[Anyway], similarly to the previous results in steady state, the configuration giving the highest fuel savings remains the EGR and exhaust in parallel with cooling configuration 1 that brings 2.2% savings on the overall weighted driving cycle. In addition to this, it can be seen that the relative performance is kept from arrangement to arrangement (compared to section 3.2.5).

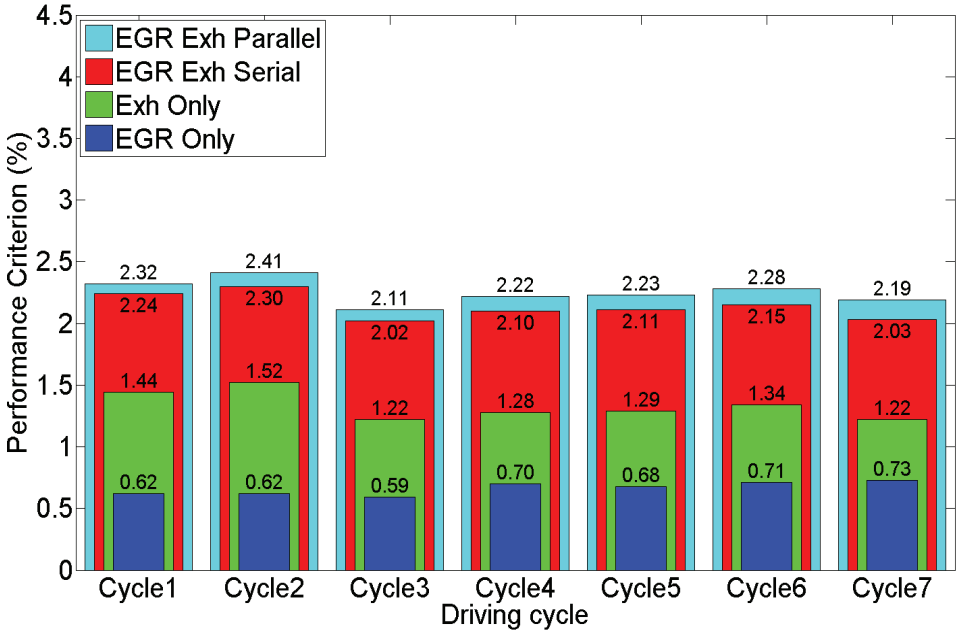


Figure 3.17 – *PC* for cooling configuration 1 over dynamic driving cycles

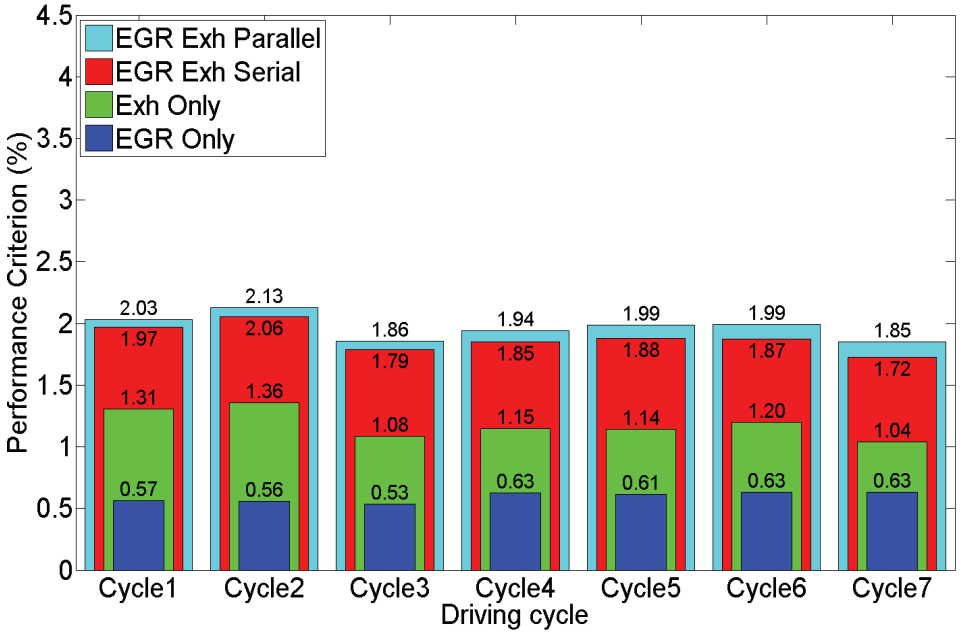


Figure 3.18 – *PC* for cooling configuration 2 over dynamic driving cycles

3.2.7 Components optimization

The low performance figures presented in sections 3.2.5 and 3.2.6 are mainly due to non-optimized components for the considered application. Indeed, the simulation platform has been validated by means of prototypes test. Those prototypes do not represent an optimal in terms of components sizing and/or performance. In order to evaluate what could be the economy brought by an optimized system, the different components constituting the WHRS are redesigned to perfectly match the targeted application. In addition to that, a perfect insulation of these different components is then considered. Optimization has been carried out on boilers and condenser size with respect to the additional volume. The heat exchanger's length is increased since this quantity affects the heat transfer area and the total volume without affecting the cross section area, meaning the heat transfer performance is conserved by keeping the fluids' velocities unchanged. It is obvious that in terms of performance maximization, the longer the evaporator the better. However, some installation constraints are introduced since the weight impact on fuel consumption is not that much for heavy-duty vehicles (the gross vehicle weight is limited to 44 tons in Europe, then the additional vehicle weight decreases the payload and affects the truck's profitability but not its consumption). The exhaust boiler length is limited to the actual muffler size, that is to say roughly 700 mm whereas the EGR evaporator is more constrained since it should fit into the current packaging, which is, today, around 630 mm long. The length of each heat exchanger is then optimized to reach the best ratio heat exchange area on net output power (such that pump and fan consumption are taken into consideration). The same kind of methodology is used in Lecompte et al. (2014), where different optimization objectives are simulated and discussed. Pump and expansion machine performance are increased to reach standards in power plant Rankine cycles, i.e. $\eta_{pump_{is}} = 70\%$ and $\eta_{exp_{is,max}} = 78\%$ (Sun and Li (2011)). Both approaches previously used (steady state and dynamic analysis) are presented in Figure 3.19 with only cooling configuration 1 since it has been shown that it leads to larger savings. Using those components' settings result in higher saving potential, since recovering heat from both EGR and exhaust in parallel leads, now, to a PC equal to 4.11% on the weighted driving cycles (compared to the 2.2% as demonstrated before). It is obvious that the cost should be analyzed carefully and the performance analysis carried out here should be coupled to a return on investment study, where the additional material cost and the decrease in vehicle payload is analyzed. In any case, it is shown here that when conducted optimization for waste heat recovery systems is applied to heavy-duty trucks, dynamic simulation plays an important role and should be carried out, since again a huge gap can be observed between steady state and dynamic PC predictions.

Conclusion. *In this chapter, different concepts of Rankine cycle based heat recovery systems are evaluated by means of numerical simulations. The constraints inherent to a long haul heavy-duty truck implementation are addressed and taken into account which results into lower fuel economy figures than in other studies. Optimization at the concept as well as the components' level is proposed but the cost impact on the overall system is not analyzed. A total vehicle approach is preferred to analyze and include every side effect of the system implementation into the vehicle. Different solutions for the system integration into the cooling package are proposed. It is shown that using a dedicated cooler housed between the CAC and the engine radiator leads to an increase in performance of around 11%. Last but not least, it is shown that performance evaluation on steady state operating points by means of driving cycle reduction tends to overestimate the fuel gain induced by the WHRS. The next chapter will be dedicated to model simplification for controller development.*

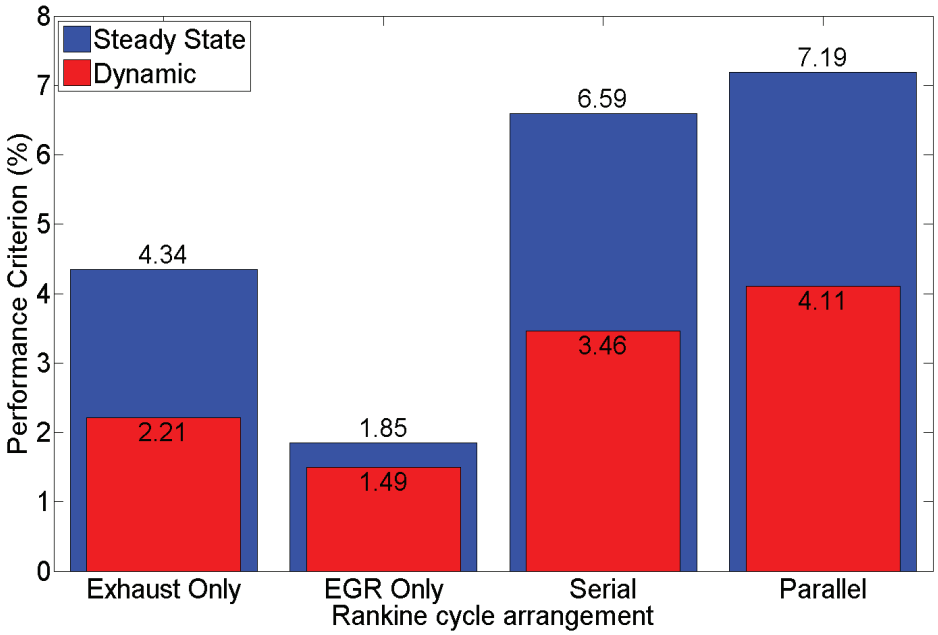


Figure 3.19 – *PC* for optimal sizing of the components

Chapter 4

Control oriented modeling

Abstract. *The use of the model developed at the previous chapter does not fit with controller synthesis. It is therefore needed to adopt other modeling methodologies for further control purpose. Two different approaches are developed in this chapter. The first one aims to reduce the model previously presented in chapter 2 by removing the fastest dynamics while keeping the physical sense and the validity over a wide range of operating conditions. The second approach is based on a linear piecewise model development. It is supposed that the system behaves linearly around one operating point and that a bank of linear time invariant models can represent the system on its operating range.*

4.1 Nonlinear model reduction

The complete Rankine system model developed in chapter 2, even in its simplest configuration, remains quite complex and presents a high order. The resulting differential algebraic system could hardly be used to design a controller. Therefore this nonlinear evaporator model needs to be simplified to make it suitable for controller development. In Luong and Tsao (2014b), this modeling problem is simplified by introducing a linear system by means of linearization around one single operating point from which a model predictive controller can easily be designed from it. In Rasmussen (2006), a linear time invariant controller is designed from a reduced linearized system. Yet, this kind of controller has difficulty achieving the control objective with good performance over a real driving cycle (Tona et al. (2012)), where the heat source can demonstrate fast and frequent transient behavior and the boiler shows strong non-linearity linked to those disturbances. This is outlined by the big differences in linear model parameters when linearizing around two different operating points. In Munch Jensen and Tummescheit (2002), the authors analyze the eigenvalues of the linearized system and discovered that the time scales associated to the different dynamics vary a great deal. This phenomenon motivates the development of a new model separating the slowest and fastest dynamics.
Here, in order to keep the model validity over its entire operating range, it is proposed to reduce the detailed model by:

- Removing the fastest dynamics, i.e. density and pressure. Indeed, the time scales associated to the different dynamics of model state vary considerably (Munch Jensen and Tummescheit (2002); Peralez (2015)).

- Creating a simple model to calculate working fluid properties instead of using thermodynamic database such as Eric. W. Lemmon (2013), permitting to remove external function calls or big maps which increase the computational complexity.
- Using simpler correlations for heat transfer coefficient calculation, allowing to reduce the number of needed properties (such as viscosity and surface tension).

This allows for keeping physical parameters of the evaporator, such as the transfer areas or the volumes and to use the model for controller design. The model developed, hereafter, catches the main dynamics of the evaporator and is adapted for the synthesis of a controller aiming to manage the working fluid temperature exiting the heat exchanger.

4.1.1 Governing equations

Based on the detailed model, developed in section 2.2.5, and assuming that the pressure dynamics is very fast compared to the temperature dynamics, we get:

- Fluid Side (inner pipe): As the continuity equation is neglected ($\frac{\partial \rho}{\partial t} = 0$) only the energy conservation principle is describing the working fluid behavior:

$$A_{cross_f} \frac{\partial \rho_f h_f}{\partial t} + \frac{\partial \dot{m}_f h_f}{\partial z} + \dot{q}_{f_{int}} = 0. \tag{4.1}$$

- Gas side (outer pipe): The same principle describing the gas behavior where enthalpy takes the following form:

$$h_g = c_{p_g}(T_g) T_g. \tag{4.2}$$

  The energy conservation principle is then expressed under the following form:

$$\frac{\partial \dot{m}_g c_{p_g}(T_g) T_g}{\partial z} + \frac{\partial \dot{m}_g c_{p_g}(T_g) T_g}{\partial t} + \dot{q}_{g_{int}} + \dot{q}_{g_{ext}} = 0. \tag{4.3}$$

- Internal pipe wall: An energy balance is expressed at the wall between the two fluids and is written as follows:

$$\dot{q}_{f_{int}} + \dot{q}_{g_{int}} = \frac{\partial m_{w_{int}} c_{w_{int}} T_{w_{int}}}{\partial t}. \tag{4.4}$$

- External pipe wall: Similarly to the internal wall the balance of the entering and leaving heat fluxes is expressed on the external wall:

$$\dot{q}_{g_{ext}} + \dot{q}_{amb_{ext}} = \frac{\partial m_{w_{ext}} c_{w_{ext}} T_{w_{ext}}}{\partial t}. \tag{4.5}$$

In addition to those equations, boundary conditions are needed at $z = 0$ and $z = L$, based on time functions:

$$\begin{array}{rcl} \dot{m}_f(t,0) & = & \dot{m}_{f_0}(t) \\ h_f(t,0) & = & h_{f_0}(t) \\ \dot{m}_g(t,L) & = & \dot{m}_{g_L}(t) \\ T_g(t,L) & = & T_{g_L}(t). \end{array} \tag{4.6}$$

The initial condition for each state is given by:

$$\begin{array}{rcl} \dot{m}_f(0,z) & = & \dot{m}_{f_{init}}(z) \\ h_f(0,z) & = & h_{f_{init}}(z) \\ T_{w_{int}}(0,z) & = & T_{w_{int_{init}}}(z) \\ T_g(0,z) & = & T_{g_{init}}(z) \\ T_{w_{ext}}(0,z) & = & T_{w_{extinit}}(z). \end{array} \tag{4.7}$$

4.1.2 Heat transfer

To model the convection from the transfer fluid to the pipe walls and from the internal pipe to the working fluid a heat transfer coefficient (α) is needed. The convection from a boundary to a moving fluid is usually represented by the dimensionless Nusselt number (Nu), which represents the ratio of convective to conductive heat transfer and is equal to:

$$Nu = \frac{\alpha l}{\lambda}, \tag{4.8}$$

where l represents a characteristic length and is the hydraulic diameter. Numerous correlations to approach this number (α) can be found in the literature Thome (2010) and are usually derived from experiments. Those correlations depend on the flow regime, the number of phases and the geometry studied. In single phase the following correlation is implemented:

$$Nu = CRe^n Pr^m, \tag{4.9}$$

where C is a constant, Re and Pr are dimensionless numbers (respectively Reynolds and Prandtl number). By integrating the Reynolds and Prandtl number definitions in equation (4.9) it becomes:

$$Nu = C\left(\frac{4\dot{m}}{\pi d_h \mu}\right)^n \left(\frac{c_p \mu}{\lambda}\right)^m. \tag{4.10}$$

In the single phase region, the heat conductivity (λ), the viscosity (μ) and the specific heat (c_p) are assumed constant and the following expressions for the heat transfer coefficient are then derived:

$$\begin{array}{rcl} \alpha_{f_{liq}} & = & \alpha_{f_{liq_{ref}}} \dot{m}_{f_{liq}}^n \\ \alpha_{f_{vap}} & = & \alpha_{fvap_{ref}} \dot{m}_{f_{vap}}^n \\ \alpha_g & = & \alpha_{g_{ref}} \dot{m}_{g_{gas}}^n, \end{array} \tag{4.11}$$

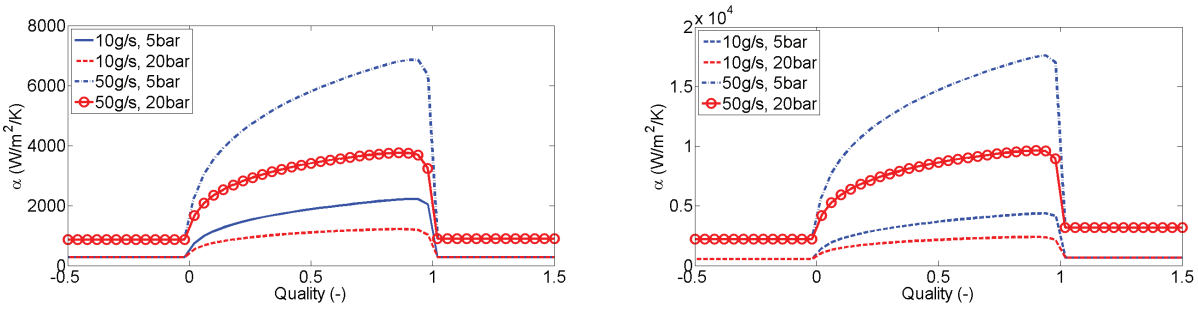
where the constant α_{ref} and the exponent n have to be identified in liquid and vapor region for the working fluid and in single-phase for the gas. In the two-phase region, a similar correlation Horst et al. (2013) is used to enhance the single-phase heat transfer coefficient. This correlation corresponds to a tube arrangement and is practical since it creates continuity between single and two-phase heat transfer coefficients and does not need transport properties such as viscosity or heat conductivity.

$$\begin{aligned} \alpha_{f_{2\phi}} = \alpha_{f_{liq}} \Bigg\{ & (1-q)^{0.01} \left[(1-q) + 1.2 q^{0.4} \left(\frac{\rho_{liq}}{\rho_{vap}}\right)^{0.37} \right]^{-2.2} + \dots \\ & q^{0.01} \left[\frac{\alpha_{liq}}{\alpha_{vap}} \left(1 + 8\,(1-q)^{0.7} \left(\frac{\rho_{liq}}{\rho_{vap}}\right)^{0.67} \right) \right]^{-2} \Bigg\}^{-0.5}, \end{aligned} \tag{4.12}$$

where q is the fluid quality defined as the quantity of vapor present in the two-phase flow:

$$q = \begin{cases} 0 & \text{if } h_f \le h_{sat_{liq}} \\ \frac{h_f - h_{sat_{liq}}}{h_{sat_{vap}} - h_{sat_{liq}}} & \text{if } h_{sat_{liq}} \ge h_f \le h_{sat_{vap}} \\ 1 & \text{if } h_f \ge h_{sat_{vap}}. \end{cases} \tag{4.13}$$

Figure 4.1 shows the working fluid heat transfer coefficient (α) for the EGR (left) and exhaust (right) boilers. For convenience, the quality (q) is not bounded between the interval [0, 1] as shown in equation (4.13). In the two-phase transfers ($q \in [0\ ,\ 1]$), the heat transfer coefficient is much higher than in single-phase (5 to 10 times higher) meaning the main heat resistance in that zone is the gas side. The wall temperature is, in that regard, very close from the boiling temperature. Moreover, the continuity at the transition liquid/two-phase and two-phase/vapor is shown in Figure 4.1. This continuity is due to the form of equation (4.12) where $\alpha_{f_{2\phi}}(q=0) = \alpha_{f_{liq}}$ and $\alpha_{f_{2\phi}}(q=1) = \alpha_{f_{vap}}$.



(a) (b)

Figure 4.1 – Heat transfer coefficient profiles EGR (a) and exhaust (b) boilers

4.1.3 Working fluid properties

Usually, working fluids' properties are computed based on a thermodynamic database such as in Eric. W. Lemmon (2013), regrouping fluid information and thermodynamic and transport property models. The link between the database and the simulation model is generally done via the use of external subroutines or look up tables, which increases the computational complexity of the model (Bell et al. (2015)). Here, in order to avoid this, the working fluid properties are approximated using a mathematical model under the form of nonlinear functions of pressure and enthalpy only. This approximation also creates continuity in derivative terms during the single / two phase transition.

- Temperature model:

$$T_f = \begin{cases} a_{T_{liq}} h_f^2 + b_{T_{liq}} h_f + c_{T_{liq}} & \text{if } h_f \leq h_{sat_{liq}} \\ T_{sat_{liq}} + q\left(T_{sat_{vap}} - T_{sat_{liq}}\right) & \text{if } h_{sat_{liq}} \geq h_f \leq h_{sat_{vap}} \\ a_{T_{vap}} h_f^2 + b_{T_{vap}} h_f + c_{T_{vap}} & \text{if } h_f \geq h_{sat_{vap}}, \end{cases} \tag{4.14}$$

  where $a_.$, $b_.$ and $c_.$ are first-order polynomial expressions function of pressure and q is computed with equation (4.13). The saturation temperature (T_{sat}) is approximated with the Wagner equation with adapted coefficient for liquid and vapor saturation Kleiber et al. (2010) and allows to make a smooth transition between each phase.

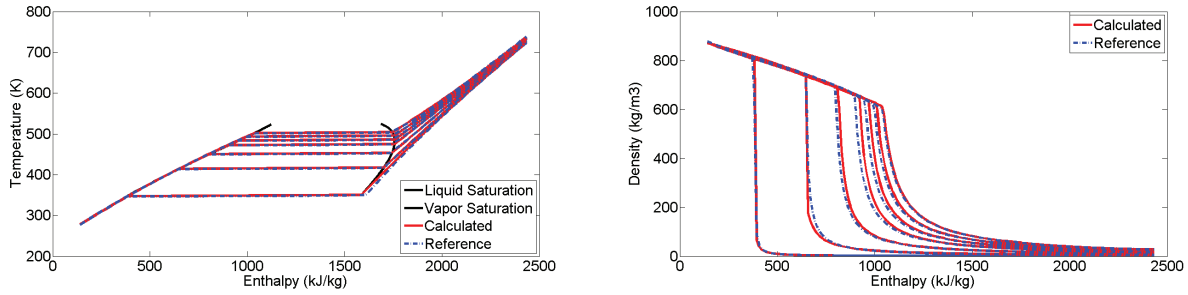
- Density model:

$$\rho_f = \begin{cases} a_{\rho_{liq}} h_f^2 + b_{\rho_{liq}} h_f + c_{\rho_{liq}} & \text{if } h_f \leq h_{sat_{liq}} \\ \dfrac{1}{a_{\rho_{2\phi}} h_f + b_{\rho_{2\phi}}} & \text{if } h_{sat_{liq}} \geq h_f \leq h_{sat_{vap}} \\ a_{\rho_{vap}} h_f^2 + b_{\rho_{vap}} h_f + c_{\rho_{vap}} & \text{if } h_f \geq h_{sat_{vap}}. \end{cases} \tag{4.15}$$

  In single-phase transfers (liq and vap), the coefficient $a_.$, $b_.$ and $c_.$ are evaluated based on third order polynomial function of the working fluid pressure. In the two-phase region the following expressions are used:

$$\begin{aligned} a_{\rho_{2\phi}} &= \frac{1}{a_{\rho_{2\phi_1}} P_f + a_{\rho_{2\phi_0}}} \\ b_{\rho_{2\phi}} &= \frac{1}{b_{\rho_{2\phi_1}} P_f + b_{\rho_{2\phi_0}}}. \end{aligned} \tag{4.16}$$

  All coefficients mentioned before are evaluated by means of fitting routines written in Matlab. Figure 4.2 demonstrates a comparison between calculated temperature and density using equations (4.14) and (4.15) and properties coming from Eric. W. Lemmon (2013) for pressure ranging from 1 to 80 bar for a mixture composed of 20% of water and 80% of ethanol by volume.



(a) (b)

Figure 4.2 – Temperature (a) and density (b) model validation

4.1.4 Spatial discretization

To be implemented in the simulation environment, the continuous model mentioned by equations (4.1), (4.3), (4.4), (4.5) is discretized with respect to space based on finite differences method. The heat exchanger is divided into n longitudinal cells where a backward Euler scheme [1] is applied for the space derivative terms. The dynamic response of the i^{th} cell can be described by the following nonlinear dynamic system:

$$\dot{x}_i \quad = \quad f_i\left(x_i, u\right), \tag{4.17}$$

where

$$x_i{}^T = \begin{bmatrix} h_{f_i} & T_{w_{int_i}} & T_{g_i} & T_{w_{ext_i}} \end{bmatrix}$$
$$u^T = \begin{bmatrix} \dot{m}_{f_0} & P_{f_0} & h_{f_0} & \dot{m}_{g_L} & T_{g_L} \end{bmatrix}$$

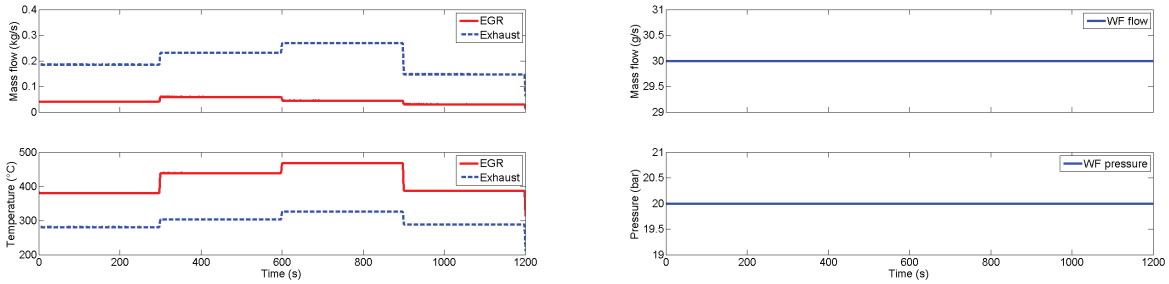
$$f_i(x,u) = \begin{bmatrix} \dfrac{\left(\dot{m}_{f_{i-1}} h_{f_{i-1}} - \dot{m}_{f_i} h_{f_i}\right) - \alpha_{f_i} A_{exch_{int_f}} \left(T_{f_i} - T_{w_{int_i}}\right)}{\rho_{f_i} V_f} \\ \dfrac{\alpha_{f_i} A_{exch_{int_f}} \left(T_{f_i} - T_{w_{int_i}}\right) + \alpha_g A_{exch_{int_g}} \left(T_{g_i} - T_{w_{int_i}}\right)}{\rho_{w_{int}} V_{w_{int}}} \\ \dfrac{\dot{m}_g c_{p_g}(T_{g_i})\left(T_{g_{i-1}} - T_{g_i}\right) - \alpha_g \left[A_{exch_{int_g}} \left(T^*_{g_i} - T_{w_{int_i}}\right) - A_{exch_{ext_g}} \left(T_{g_i} - T_{w_{ext_i}}\right)\right]}{\rho_{g_i} V_g c_{p_g}\left(T_{g_i}\right)} \\ \dfrac{\alpha_{amb} A_{exch_{ext_{amb}}} \left(T_{amb} - T_{w_{ext_i}}\right) + \alpha_g A_{exch_{ext_g}} \left(T_{g_i} - T_{w_{ext_i}}\right)}{\rho_{w_{ext}} V_{w_{ext}}} \end{bmatrix}. \tag{4.18}$$

Note that the ambient temperature T_{amb} is assumed constant around the entire HEX.

4.1.5 Simulation results

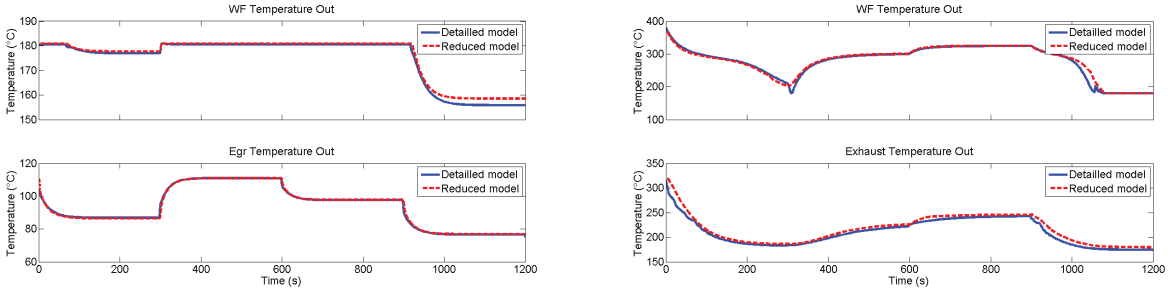
A first step in the validation procedure of the reduced model is to use as process simulator the detailed model presented in 2.2.5. The disturbance inputs are changed to assess different regions of the evaporators and check if appearance and disappearance of the different phases are well handled by the model. The EGR and exhaust flow rates and temperatures vary over time whereas the working fluid mass flow rate and pressure are kept constant for the simulation. Figure 4.3 shows the inputs used to compare the detailed and reduced model. The model outputs are shown in Figure 4.4. The latter ones are very well predicted by the reduced model with regard to both the steady state and the dynamic behaviors seeing as the reduced model fits well with the detailed evaporator model for every fluid state; liquid, two-phase and superheated can be observed. The maximum error that can be observed is 3K for the EGR evaporator and 7K for the tailpipe boiler. Once

[1] constraint of the implementation platform



(a) (b)

Figure 4.3 – Detailed-reduced model comparison: gas (a) and fluid (b) model inputs



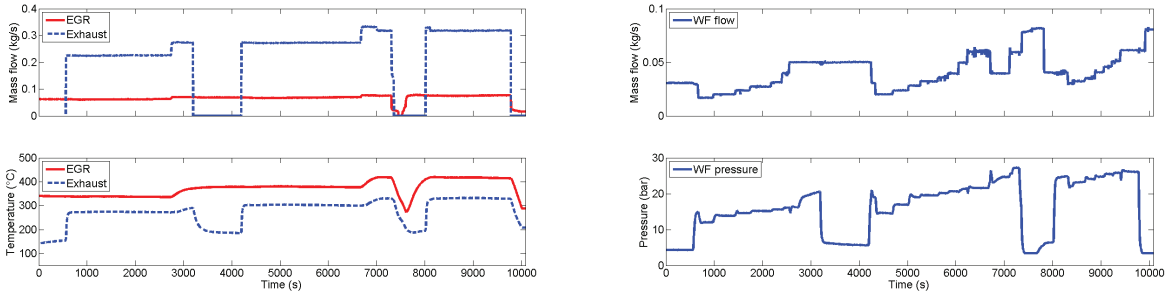
(a) (b)

Figure 4.4 – Detailed-reduced model comparison: EGR (a) and exhaust (b) model outputs

implemented under Simulink and with a sampling time of about 20ms, the model runs 100 times faster than real time (Dell Precision laptop with Intel Core i7 and 8 Gb RAM). The model is then suitable for many purposes but it seems difficult to use it in an advanced controller and especially in an iterative framework such as the model predictive controller where an optimization problem is solved under a finite time horizon.

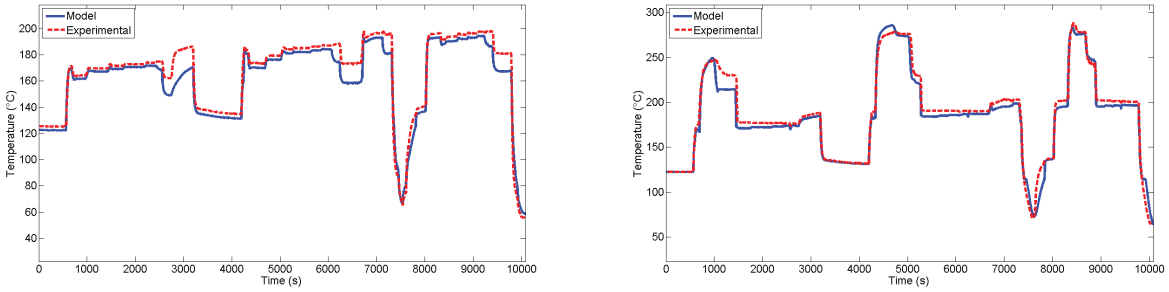
4.1.6 Experimental results

The second step in the reduced model validation procedure is carried out by using experimental data. The reduced model is then fed with experimental inputs (shown in Figure 4.5) and the outputs are compared to the real measurements. Figure 4.6 shows the working fluid temperature after each boiler. This quantity is well fitted since the maximum difference that can be observed is around 20K. A difference can be observed in the real and calculated saturation temperature. This can come from a difference in mixture composition during the evaporation process or from the database (Eric. W. Lemmon (2013)) used to create this quantity. The gas temperatures after the recovery processes show small errors in the range of 15K, especially as the EGR temperatures exiting the boiler do fit with a maximum absolute error of 6K. Main discrepancies come from the assumption that gas composition is the same regardless of the engine operating point. The air fuel ratio could change a lot during engine operation and impacts the gas specific heat. Other effects, such as temperature distribution or non-homogeneous fluid flow are possible sources of error. However, the objective has been to create a model faster than real time and implementable into an automotive electronic control unit. Those two goals are achieved, since the model reflects working fluid and gas temperatures with a relative error of less than 5% in real time in an ECU.



(a) (b)

Figure 4.5 – Experimental validation: gas (a) and fluid (b) model inputs



(a) (b)

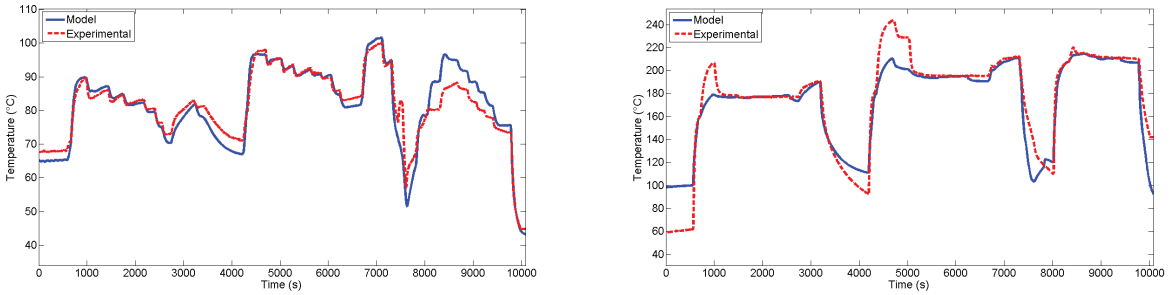
Figure 4.6 – Working fluid temperature experimental validation: EGR (a) and exhaust (b) boiler outlet

4.1.7 Analysis

The reduced model is experimentally validated but a discussion about its performance needs to be conducted. The calibration effort of such a model is huge and needs to be balanced with the model performance. Indeed, in the automotive industry the cost and development constraints are more and more important and standardized procedures for control software calibration are of primary importance. This is antagonistic with the use of such models where non-measurable parameters estimation, such as $\alpha_{f_{liq_{ref}}}$ in equation (4.11), is needed. In addition to this, the reduced model presented here, with a sampling time of 20ms, is 100 times faster than real time. This is an asset for simulation but when it comes to a advanced control system development it could be hard to use it as it is. The integration of such nonlinear model in a model predictive controller framework, where an optimization problem over a prediction horizon is solved at each sampling time, as the implementation constraints relative to the automotive industry is almost impossible. Simple mathematics can help to understand this, since the sampling time has to be 20ms and with a model 100 times faster than real time it gives maximum prediction horizon of 100 (20 seconds) without taking into account the optimization problem solving. This enlightens the needs for simpler model when, it comes to advanced controller development.

4.2 Multi linear model

For sake of simplicity and computational time reduction, a new approach should be considered. A good alternative is the use of a multi-linear model approach where each linear model represents the



(a) (b)

Figure 4.7 – Gases temperature experimental validation: EGR (a) and exhaust (b) boiler outlet

plant on one of the multiple considered operating points. Then, by tracking the transitions from one regime to another, a global model can be estimated. Banerjee et al. (1997) have shown that a combination of linear models can be used to approximate the true behavior of one nonlinear process. Each local model should greatly describe the plant in one operating region but when the plant moves from this region the same model may gives poor performance. First applications of multiple models are reported in the aerospace industry. Aircraft are known to behave nonlinearly and a multiple model adaptive controller perfectly suits for this application (Athans et al. (1977)). A more recent overview of multiple linear model approaches can be found in Murray-Smith and Johansen (1997), when general design method for this kind of problems can be found in Li et al. (2005). In general, the bank of local models is designed a priori where all the operating conditions are screened. In some processes, this step is not possible but the approach is still applicable (He et al. (1986)). Other usage of multi models are reported, such as fault detection (Rodrigues et al. (2008)) where models are representing faulty and normal operation. During engine development, the operating conditions are screened and the multiple models approach takes sense.

4.2.1 Model structure selection and validation

First, a linear model has to be developed. This linear model can be either identified directly from the experiments (i.e. without existing model requirement) or derived by linearization of an existing validated detailed first principle nonlinear model. Here, modeling and identification are obtained from the validated model presented in chapter 2. By considering the previous model to be a single input single output (SISO) plant of the form:

$$\dot{x} = f(x,u), \tag{4.19}$$
$$y = g(x,u), \tag{4.20}$$

where u is the WF mass flow entering into the boiler and y is the WF temperature exiting the boiler. This input/output pair is chosen accordingly to the final control objective, which is to reduce the deviation of the working fluid temperature around a set point by acting on the working fluid mass flow rate. In the present case, the dynamic relation between the variation of u and y (also called manipulated variable (MV) and controlled variable (CV)) around an operating point can be described by a first-order plus time delay (FOPTD) transfer function:

$$\frac{\Delta T_{f,out}(s)}{\Delta \dot{m}_{f,in}(s)} = \frac{G}{1+\tau s} e^{-Ls}, \tag{4.21}$$

which is a commonly adopted linear model in the industry, especially for further simple model based control development. The main issue with that approximation is the introduction of dead time or a

time delay which in the continuous domain has an infinite dimension (Normey-Rico (2007)). This can be better understood by considering the Taylor expansion of the time delay of (4.21):

$$e^{-Ls} = \frac{1}{1 + \sum_{i=1}^{\infty} \frac{(sL)^i}{i!}}. \tag{4.22}$$

The denominator of equation (4.22) is of infinite degree and the corresponding state space representation has an infinite dimension. Therefore, mathematical study of such a system is strongly complex, which is in itself a large area of research study (Richard (2003); Lu et al. (2014)). To overcome this problem, we consider a finite approximation of the delay. The implementation in the controller then relies on a discrete representation of the model or on a truncation of the infinite series. Although, approximating the process by a first-order plus time delay does not capture all the behavior of high order processes, Cohen and Coon (1953) shows that it gives a reasonable description of the plant gain, overall time constant and dead time. This model structure is validated here by comparing outputs around two extreme operating points of the validated detailed model and the identified ones. As it can be seen in Figure 4.8 the agreement between both approaches the 98%.

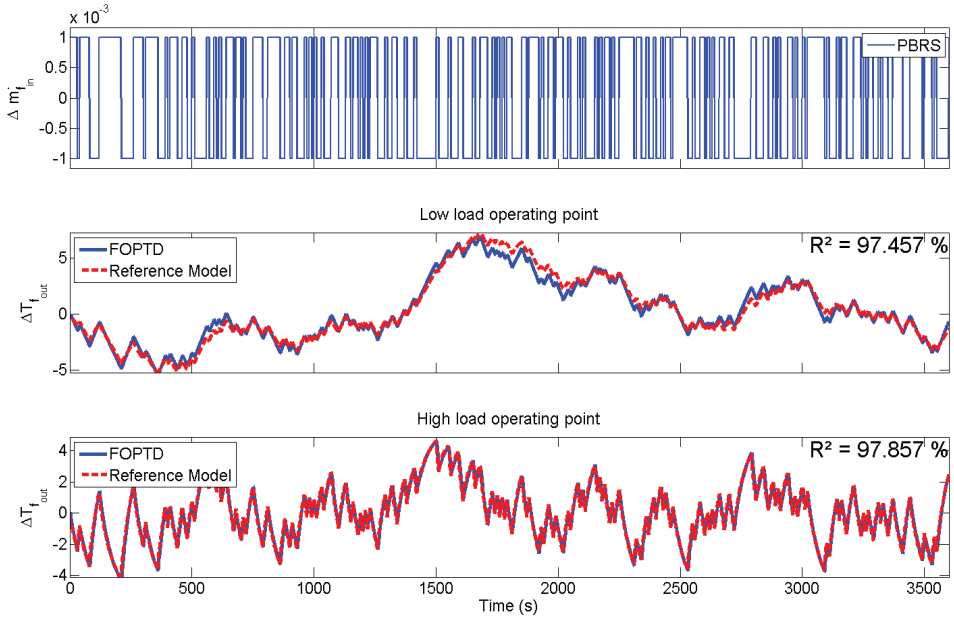


Figure 4.8 – FOPTD model validation based on the reference model

4.2.2 The piecewise linear approach

The nonlinear behavior of the system can be split into several local operating regimes and for each one a linear model can be built (Murray-Smith and Johansen (1997)) . By plant experiments or simulation by means of the detailed nonlinear model (presented in chapter 2), the relationship between the MV and the CV defined in the nonlinear SISO system (4.19) can be identified by a series of FOPTD models (each with a subscript $i \in [1, N]$), where the model parameters are the static gain G_i, the time constant τ_i and the delay L_i:

$$F_i(p) = \frac{y_i}{u} = \frac{G_i}{1 + \tau_i p} e^{-L_i p}. \tag{4.23}$$

In the sequel, the scalar MV is u and the scalar CV is y_i. These N local models have to be combined in order to obtain a global model.

In Banerjee et al. (1997) two different approaches are reported.

1. One is based on the construction of a global model by interpolating between the N models thanks to time-varying weights identified online in order for the output of the global model to match the output of the process.

2. The second estimates the probability of one or several models among N to be valid. By means of a comparison of the plant measurements to each local model output, the most valid models are used to compute the global model output. The model validity is based on the plant-model mismatch represented by the i^{th} model error (ϵ_i) at the current time t_k between the real measurement $y_{p,k}$ and the i^{th} model output $y_{i,k}$.

$$\epsilon_{i,k} = y_{p,k} - y_{i,k}. \tag{4.24}$$

   The weighting scheme then attributes a weight $w_{i,k}$ to each linear model depending on the value of $\epsilon_{i,k}$ (usually the lower $\epsilon_{i,k}$ the higher $w_{i,k}$).

Following on from this, first a state of the art weighting scheme relying on a recursive probability estimation of one model among the bank to be valid has been implemented. Then, in the aim to reduce the calibration effort (and so the number of tuning parameters) a new scheme has been developed.

4.2.2.1 Bayesian estimator

Most of the studies on multiple linear models found in the literature use the Bayesian estimator as adaptive estimation technique to select the best model at each time step (Rao et al. (1999); Aufderheide and Bequette (2003); Nandola and Bhartiya (2008)). It is based on model probabilities calculation $P(i)$, representing the probability of the i^{th} model to be valid. This weighting scheme assigns a value between 0 and 1 to each model outputs where the weights sum is equal to 1 to ensure that the global model is always bounded by the extreme values of the N models in the bank. It also allows an exact, if it appears, model to be the only prediction model. The recursive Bayesian weighting scheme is a conditional probability of the i^{th} model present in the N model bank to be true given the model population in the bank and its past history of probabilities. It is written as follows:

$$p_{i,k} = \frac{\exp(-\frac{1}{2}\epsilon_{i,k}K_i\epsilon_{i,k}p_{i,k-1})}{\sum_{m=1}^{N}(\exp(-\frac{1}{2}\epsilon_{m,k}K_m\epsilon_{m,k}p_{m,k-1})}. \tag{4.25}$$

$$w_{i,k} = \begin{cases} \frac{p_{i,k}}{\sum_{m=1}^{N} p_{m,k}} & \text{for } p_{i,k} > \delta_{cut\ off} \\ 0 & \text{for } p_{i,k} < \delta_{cut\ off}. \end{cases} \tag{4.26}$$

In the probability calculation of equations (4.25)-(4.26), a vector K containing convergence factor K_i ($i \in [1\ N]$) is used to improve the convergence to a single model. If more combination of the different models contained in the bank is desired, this factor should be detuned and set at a low value. To keep each model of the bank alive, an artificial probability is introduced such that all $p_{i,k}$ never go below this artificial lower limit $\delta_{cut\ off}$ (which is a tuning parameter). This one is called in the following cut-off probability and is set to improve the estimator performances. However, each

model having this lower saturation value as probability are excluded from the weight computation as it is shown in equation (4.26). The model output is then defined at the current time t_k by:

$$y_k = \sum_{i=1}^{N} w_{i,k}\ y_{i,k}. \tag{4.27}$$

The number of tuning parameters with the Bayesian recursive scheme is $N+2$ (K, N and $\delta_{cut\ off}$). The calibration effort is then dependent on the number of models composing the bank. Indeed, when it comes to the selection of N it is obvious that the higher the better but it increases the complexity for an optimal setting of the N elements composing the vector K. In practice, all the elements constituting the vector K are set to the same value in order to reduce the calibration time to the detriment of the estimation.

4.2.2.2 New developed estimator

To simplify the weighting scheme and reduce the number of setting parameters, a new scheme has been developed. All values denoted by a superscript, $\tilde{}$, refer to normalized values. First, the normalized i^{th} model error $\tilde{\epsilon}_i$ is computed at the current time t_k and is bounded between 0 and 1:

$$\tilde{\epsilon}_{i,k} = \frac{\epsilon_{i,k}^2}{\sum_{m=1}^{N} \epsilon_{m,k}^2}. \tag{4.28}$$

The lower $\tilde{\epsilon}_{i,k}$ the more valid the i$^{\text{th}}$ model. Then, the raw absolute weight ($c_{i,k}$) of the i^{th} linear model composing the bank is calculated according to:

$$c_{i,k} = (1 - \tilde{\epsilon}_{i,k}) \prod_{j \neq i, j=1}^{j=N} \tilde{\epsilon}_{j,k}, \tag{4.29}$$

which is also normalized to be bounded between 0 and 1:

$$\tilde{c}_{i,k} = \frac{c_{i,k}}{\sum_{m=1}^{N} c_{m,k}}. \tag{4.30}$$

The normalization of $\tilde{c_{i,k}}$ allows the global output to be bounded between the extreme values of the model composing the bank. By analyzing, $\tilde{c}_{i,k}$, it is obvious that the lower $\tilde{\epsilon}_{i,k}$ the closer from 1 $\tilde{c}_{i,k}$. If one model represents exactly the process at the current time (meaning $\tilde{\epsilon}_{i,k} = 0$), the corresponding normalized raw weight $\tilde{c}_{i,k}$ is exactly the unity and the scheme converges to only one model.
The value $\tilde{c_{i,k}}$ computed based on equation (4.30) is then filtered through a first-order transfer function with unit static gain to remain bounded. A tuning parameter, τ_{filt}, is here introduced permitting to, when this latter is set at a low value, increase the convergence to the most accurate models. Increasing the value of τ_{filt} creates more mixing between the models of the bank and then, more continuity in the global model parameters. In a certain manner, τ_{filt} is a scalar playing a similar role than the convergence matrix K used in Bayesian approach (4.25).

$$w_i(s) = \frac{1}{1 + \tau_{filt} s} \tilde{c}_i(s), \tag{4.31}$$

Here also the global model output is calculated at each time step using the equation (4.27).
The number of tuning parameters is then decreased to only two parameters (N and τ_{filt}) instead of $N+2$ (K, N and $\delta_{cut\ off}$) in the Bayesian recursive scheme. The tuning is therefore simplified to the selection of those two scalars and that independently of the size of the model's bank.

4.2.3 Simulation results

In a first step, the multiple models approach is compared to the detailed first principle nonlinear model. Both weighting schemes are used in order to compare their estimation performance in open loop. An unknown operating point is applied to the system and the outputs of the detailed and the global identified model (calculated according to equation (4.27)) are compared to each other. The different tuning parameters, namely K, $\delta_{cut\ off}$ and τ_{filt}, are optimally set to obtain the best performance. Figure 4.9 shows the simulated case for the two weighting schemes and three scenarios concerning the number of models in the bank. It can be remarked that with the developed weighting scheme the number of models in the bank does not really matter (in this example a minimum number of 3 models is needed to represent the process) whereas with the Bayesian scheme there is an increase in the R^2 when N is increased. This phenomenon is due to the quick convergence of the recursive Bayesian scheme to the most valid model no matter of the global model output. The developed weighting scheme could use only one model only if that one is perfectly representing the process behavior at the current time t_k. By using more blending between the models composing the bank, the plant output (y) is better approximated when the size of the databank is limited.
However, the agreements are very good for both methods and do not allow to draw any conclusions on the scheme to scheme comparison. It should be noted that with both schemes the same models constitute the bank.

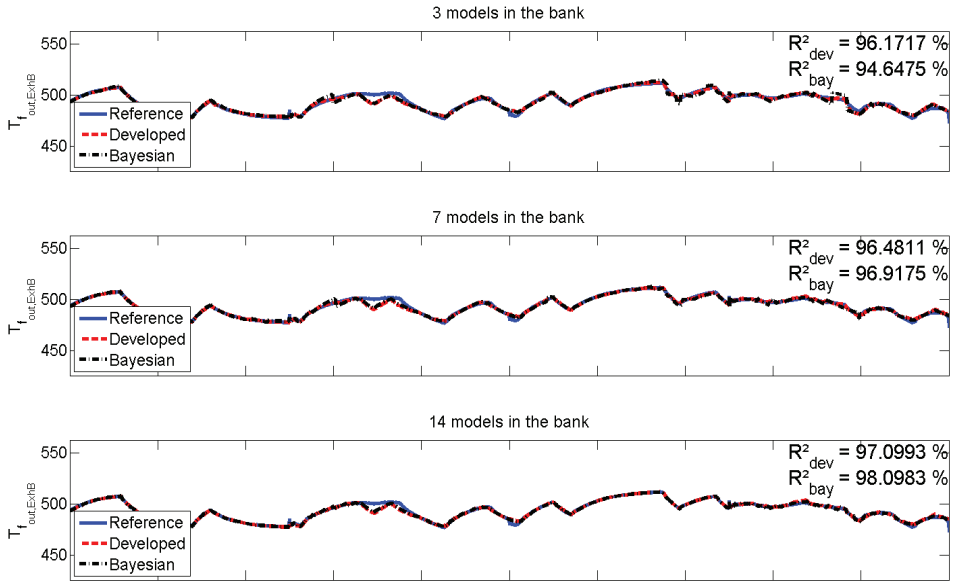
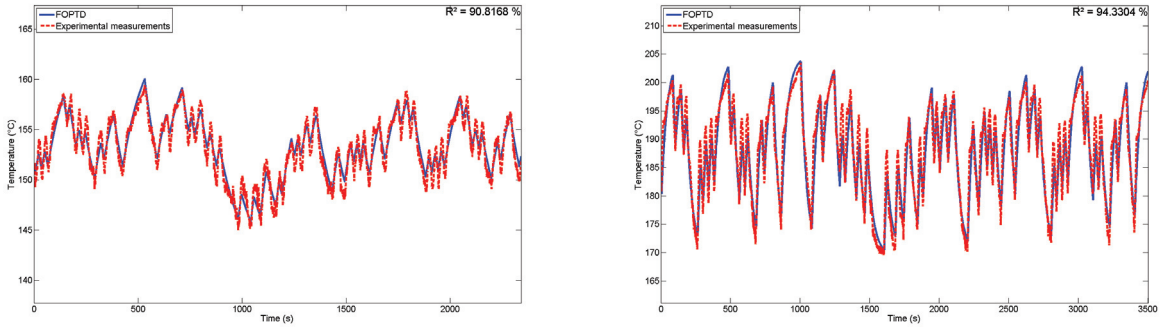


Figure 4.9 – Open loop comparison of multi-model approach

4.2.4 Experimental results

As shown previously, first-order plus time delay models are identified around several operating points. This model structure has been selected and validated on the detailed model developed in chapter 2. It needs to be validated on the experimental setup presented in appendix A. Figure 4.10 shows the identified first-order plus time delay model responses on a low (4.10a) and highly loaded (4.10a) engine operating point. The coefficient of determination is still good (larger than 90%) and the dynamic behavior of the working fluid temperature is correctly represented.



(a) Operating conditions 1 (b) Operating conditions 2

Figure 4.10 – FOPTD model experimental validation in open loop

Then an open loop validation of the multiple models approach is performed on the experimental set up. Due to time constraints in the experimental setup, the set of linear models composing the model bank has been reduced to 12 elements. To fairly evaluate the two implemented weighting schemes, tuning parameters are set to obtained the best estimation. In addition to that, the number of models is reduced to $N = 8$ and $N = 4$. Indeed, to lower the development and calibration time, good performance should be obtained with a limited number of models in the bank since the identification procedure for each linear model is generally long and can take several hours. This is particularly good in an industrial perspective where the objective to reduce development cost is more and more present. The performance of both weighting schemes are then evaluated on the experimental setup. A pseudo-random binary sequence (PRBS) is carried out around an operating point and measurements are compared to the Bayesian and developed scheme. This operating point is chosen such that, one linear model composing the bank could not perfectly represent the process around it bounded by the extreme models composing the bank. Figures 4.11, 4.12, 4.13 show the model validation with a varying number of models in the data bank (respectively 4, 8 and 12 models), when the tuning parameters τ_{filt}, K and $\delta_{cut\ off}$ are shown in Table 5.2. Note that, in the same way than in simulation, the bank is constituted of the same linear models for each weighting scheme. The developed weighting scheme clearly outperforms the Bayesian one especially when the number of models that contain the data bank is reduced. This is due to the method itself. While the Bayesian scheme searches for one model to be valid among N at the time step t_k, the developed approach uses the most valid models of the bank to create the global output. In addition to estimate in a better way the output quantity, it shows a better continuity in the estimation. Indeed, the Baysesian scheme creates a chattering effect when switching from one model to another, that could lead to some unstable behavior when using this approach in a closed loop framework. However, this could be avoided by derating the values in the convergence matrix K which creates more blending in the global output estimation but with a clear effect on the estimator performance.

Tuning parameters	τ_{filt}	K	$\delta_{cut\ off}$
Developed weighting scheme	0.2	N/A	N/A
Bayesian weighting scheme	N/A	11	0.008

Table 4.1 – Weighting schemes tuning parameters values

Conclusion. *In this chapter two control-oriented models are presented. One is based on a reduction of the detailed validated model presented in chapter 2 by means of fastest dynamics cancellation and*

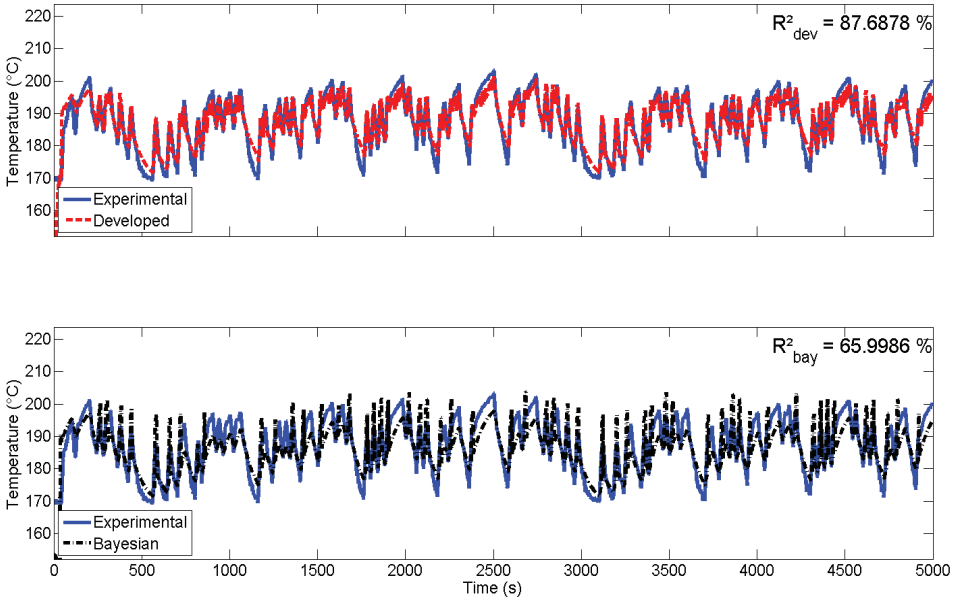


Figure 4.11 – Multi model approach experimental validation with $N = 4$

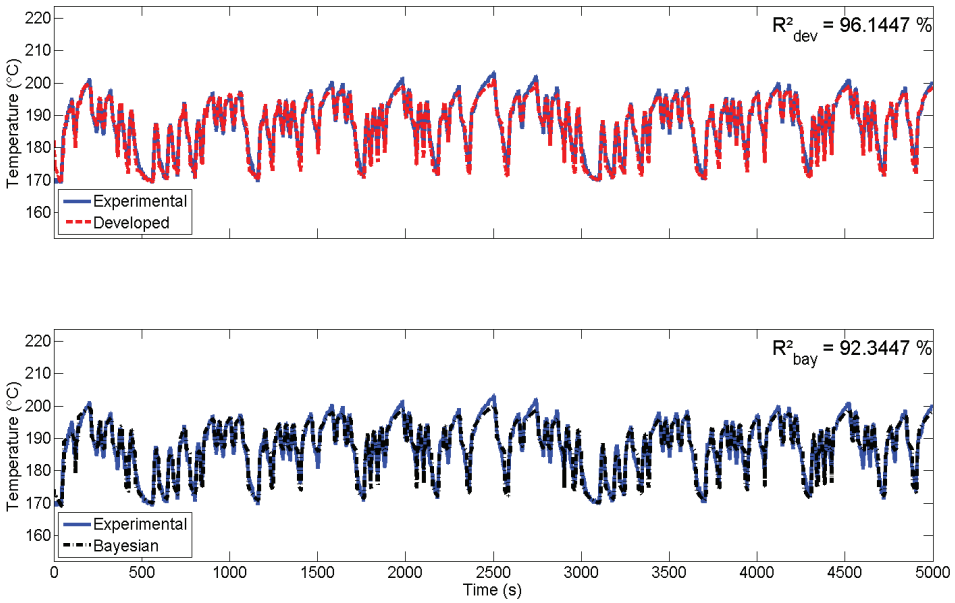


Figure 4.12 – Multi model approach experimental validation with $N = 8$

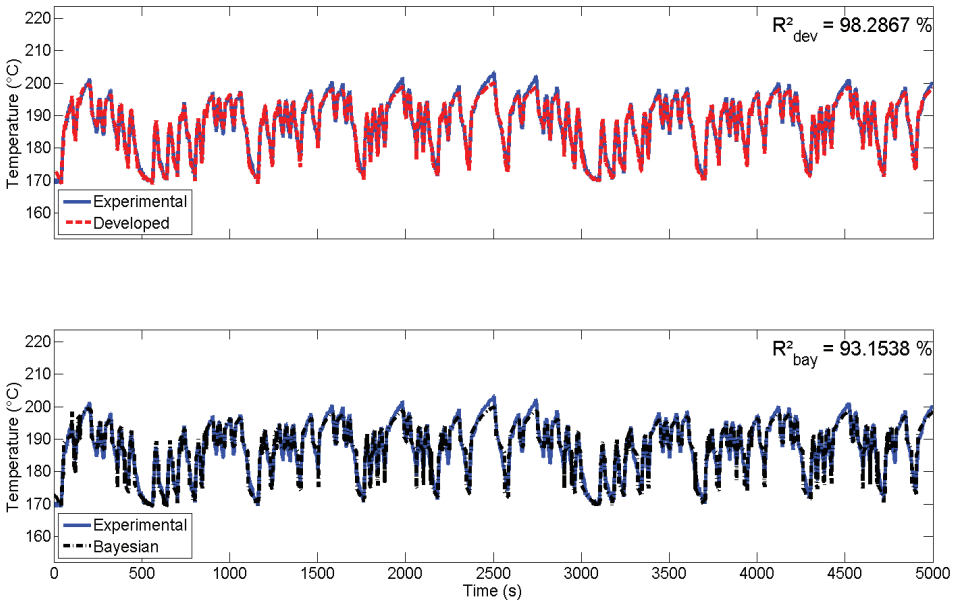


Figure 4.13 – Multi model approach experimental validation with $N = 12$

internal simplification. The second model is based on a piecewise linear approach where two different weighting scheme have been implemented. One is a classical scheme used for multi-model whereas the second has been especially developed for this application. It shows better performance concerning the output estimation and behaves more smoothly.
The next chapter will target closed loop strategies for Rankine cycle based heat recovery system applied to heavy-duty trucks where the main objective is to improve the superheat level control. Both simulation and experimental results will be presented and a discussion about the development effort will be performed.

Chapter 5

Rankine system control strategies

Abstract. *The development of control oriented models in chapter 4 is the basis for closed loop strategy implementation. The constraints inherent to the automotive industry in terms of advanced control algorithms are explained and used in this chapter to link the methodologies used. Four different controllers are developed in this section ranging from linear time invariant such as PID to model predictive controller. Each one is assessed in the detailed validated model. Unfortunately due to cost constraints and the limited availability of the experimental set-up only some have been validated experimentally.*

5.1 Rankine control system: challenges and opportunities

In most stationary applications of Rankine cycle that produce electricity, the control objective is to adapt the power production to the needs of the electrical grid (Mier et al. (2015)). This has to be done by ensuring safe operation and optimal cycle efficiency. While the regulation of the heat flow rate of the heat source makes it possible to respond to the first objective by managing the heat entering into the system, the second objective is achieved by managing the working fluid mass flow and the expansion machine speed. The working media flow rate ensures the necessary superheat when adjusting the expansion machine speed allows it to run at its best efficiency point (Kusters (2003)). Due to the coupled process, the control problem is generally complex although facilitated by the slow nature of the input disturbances and the predictable operation (Zhang et al. (2013)).
For mobile applications, the objectives are the same but the highly transient nature of the heat sources makes the problem even more complex. The driver answers its own control problem, which is generally to keep the vehicle speed constant regardless of the road conditions and the engine operation changes constantly in order to meet this objective (Guzzella and Onder (2004)). This results in very fast and frequent transient behavior of the heat sources which now act as input disturbances. In addition, the WHRS operation is limited by numerous parameters such as the cooling capacity and the power request of the engine or vehicle. Last but not least, the industrial context should not be forgotten. On a vehicle, both the computational capacity and the possible measurements are limited, which constrains strategy development and implementation. Previous work reports the use of model based controllers (Ammann et al. (2003)) or model predictive controllers (Del Re et al. (2010)) but there is still a long way to go before such strategies are implementated in mass production (Pretschner et al. (2007)). Indeed, automotive ECU are really cheap compared to laptops and their low performance constraints software implementation. Sampling time is fixed and equal at 20

ms, classical matrix operations are not possible and most of the problems have to be rescaled to avoid involving too many floating number operations, which consume a lot of memory. This makes it difficult to implement advanced control strategies.
This chapter focuses on the management of the working fluid superheat at the expansion machine inlet. Indeed, this objective is the most important for Rankine cycle based recovery system for vehicle application since it ensures the safe operation of the components and maximizes the fuel saving induced by the WHRS. By keeping the superheat constant and low during the system operation, the expansion machine can be fed during the whole vehicle mission and the system can generate substantial gains in terms of fuel consumption (Horst et al. (2013)). This is achieved by adjusting the working medium mass flow rate through the evaporator by means of a pump speed variation if this is coupled to an electric motor or by throttling the working fluid via a proportional valve if the pump speed is not controllable. Another proportional valve is present to bypass the exhaust gases entering the system. That latter is usually used for safety purposes regarding the overheating of the working fluid, overly limited cooling capacity, excessive fan engagement or diesel particulate filter regeneration.

5.2 State of the art automotive controller

Despite the increase in complexity of modern vehicles, the control strategies used in this sector have not changed to a very great extent. Indeed, due to cost and complexity constraints most of the controllers are open loop and map based (Kiencke and Nielsen (2000)). Those maps result from experimental tests carried out during the engine development which reduces the use of advanced control strategies.
The usual closed loop control strategies used in the automotive industry are based on the proportional integral derivative (PID) controller. It is well known, easy to implement and with low computational complexity. In its simplest form, this controller has only three tuning parameters but these are often poorly tuned. The first robust tuning method was introduced by Ziegler and Nichols (1942) and since, the number of systematic parameters tuning procedures has been increasing. Some classical methods can be cited such as the IMC-PID tuning proposed by Rivera et al. (1986) or the direct synthesis methods proposed in Smith and Corripio (1985). The Ziegler-Nichols method are known to give good disturbance responses but have aggressive settings. Conversely, the IMC settings give good responses for set point changes and are generally robust but give very poor disturbance responses. A general tuning method has been proposed by Skogestad (2003) for both set points and load disturbances, and also works for integration as pure time delay processes. It is a two-step procedure:

- 1. Obtain a first or second order plus time delay model. For higher order systems, a model reduction technique is presented.
- 2. Derive model based PID controller settings. Note that for a first order system the author proposes to use a PI but for a second order a PID.

The work done in Madhuranthakam et al. (2008) presents generalized correlations for the optimal tuning of PID controllers for different processes: first order plus time delay (FOPTD), second order plus time delay (SOPTD) and second order plus time delay with lead (SOPTDLD) systems. The settings are derived to achieve a minimization of the integrated absolute error either on a load or a set point change.
As the Rankine system is strongly nonlinear, a linear type invariant (LTI) controller is not suited to managing the superheat during dynamic driving cycles. The first idea is to schedule the controller parameters and adapt them to the operating conditions in order to take into account those strong

nonlinearities. Alleyne and Rasmussen (2007) and Tona et al. (2012) propose scheduling the PID parameters to obtain better results in transient operation. The gain scheduling approach takes into account the strong nonlinearities of a system by adapting the controller parameters to the operating conditions. It consists of building a nonlinear command by interpolating several linear commands which are performant locally. As it is can be implemented simply and has a low computational complexity is is widely used in industry. However, it requires a certain number of variables representative of the operating points which catch the nonlinearities of the system to control. In Rasmussen (2006), the author proposes approaching the nonlinearities of a refrigeration system via the evaporating pressure.
A second idea is to switch to an adaptive structure. Adaptive means the controller parameters and/or its structure are modified on line when the operating conditions change (Åström (1991)). One classical adaptive technique referred to as multi-model based control, is well known and reported (Narendra and Balakrishnan (1997); Murray-Smith and Johansen (1997)). It consists of using a linear model bank to represent the nonlinear system over its entire operating region and to synthesize a controller online at each sampling. A linear time variant controller is then created by mixing different linear time invariant controllers. It makes it possible to adapt either the controller structure or its parameters to the system's operation in real time. Advanced control strategies are a field that is poorly addressed when it comes to Rankine cycle based heat recovery systems. In Peralez et al. (2014), a state feedback controller using an observer is designed to control the pressure inside the system by acting on the exhaust flap. In Luong and Tsao (2014a), a linear quadratic integral controller is used to track the superheat on a system recovering heat from EGR and exhaust in parallel. The strategy outperforms a classical PI structure but needs to be coupled with an additional actuator. In Peralez (2015), an inverted moving boundary heat exchanger model is used as dynamic feedforward on different Rankine systems with success. The model then calculates the manipulated variable corresponding to the desired output set point at each sampling time and a conservative feedback controller adjusts the working fluid mass flow rate to track the superheat set point. This strategy gives tremendous results but its implementation is not addressed by the author.
The model predictive controller is currently the most advanced controller structure used for industrial applications. This controller structure is very popular and particularly in petrochemical process control, due to its ability to handle dead time, multivariable and constrained problems. This is also the only controller that systematically integrate constraints (Darby and Nikolaou (2012)). In many processes, MPC shows improved performance over traditional controllers (Muske and Rawlings (1993)) since it integrates the process model and considers plant dynamic behavior in the future. The basic framework of the model predictive controller can be summarized in four basic steps:

1. Predict deviation from a set point from the current time to the prediction horizon by means of a model of the process.
2. Minimize a cost function by adjusting the manipulated variable moves over a control horizon.
3. Control the MV with the first control action calculated at the previous step and measure the plant answer.
4. Update the model by means of the new measurement and go back to the first step.

The associated diagram is shown in Figure 5.1 (Dai et al. (2 05)).
With highly nonlinear processes where distinct input-output behavior depending on the operating region can be observed, the use of a nonlinear model can lead to complex optimization problems where the convergence to a global optimum is not certainly guaranteed (Aufderheide and Bequette (2003)). The optimization problem solving can take a significant fraction of the sampling time which is not acceptable here. MPC use for Rankine systems has been poorly addressed (Luong and Tsao (2014b); Feru et al. (2014)) and implementation and experimental validation of those strategies

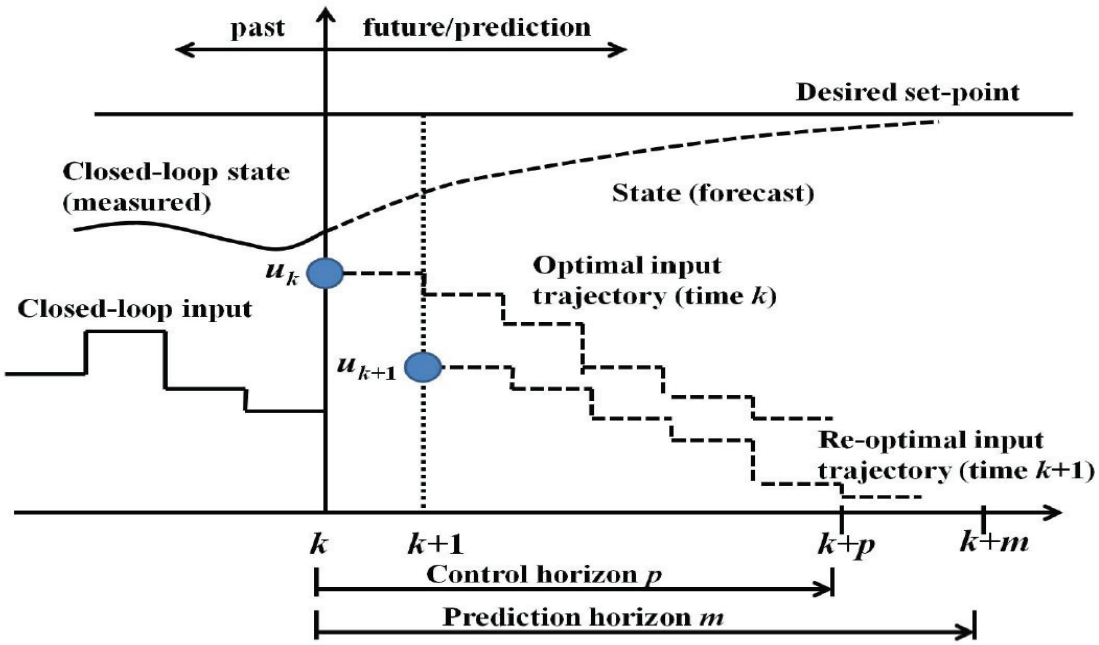


Figure 5.1 – Model predictive controller diagram

have never been carried out. In Mier et al. (2015), a linear MPC is designed based on a state space representation of the Rankine process. The use of only one linear model to represent the steam cycle gives satisfactory results on stationary applications due to the slow or even non-existent transient behavior of the heat sources. With mobile applications, those transients occur during normal operation. To overcome this problem , many studies report the use of multi-model predictive controllers (MMPC) where the process model is approximated by a bank of linear models (Rao et al. (1999); Aufderheide and Bequette (2003); Nandola and Bhartiya (2008)). In Guolian et al. (2010) this control structure has been used in a stationary power plant and the author shows better performance, robustness and disturbance rejection compared to classical PID.

5.3 Gain scheduled PID

Firstly, and as a basis for all future developments, a classical PID structure has been implemented. Note that, in the following the parallel form of the PID controller (also called non-interacting) is used:

$$c(s) = K_p \left(1 + \frac{1}{T_i\ s} + T_d\ s\right). \tag{5.1}$$

The main issue with LTI structure is the high parameter variation between two operating points. One set of parameters determined at one operating point can be totally different from another. This can be illustrated by looking at different operating points encountered during engine utilization. Let us define 14 operating points over the engine map each representing an area of 10 kW of the heat wasted by the engine. A partial experimental map representing the engine normal operation is shown in Figure 5.2. Those operating points differ in terms of engine speed and torque, which results in a variation in the working fluid pressure, EGR mass flow rate, temperature and exhaust mass flow rate. The other system input disturbance, namely, inlet working fluid temperature is kept constant. Indeed, the temperature variations in the fluid reservoir are very slow due to its thermal inertia (there is a large amount of fluid in the tank compared to the fluid mass flow).

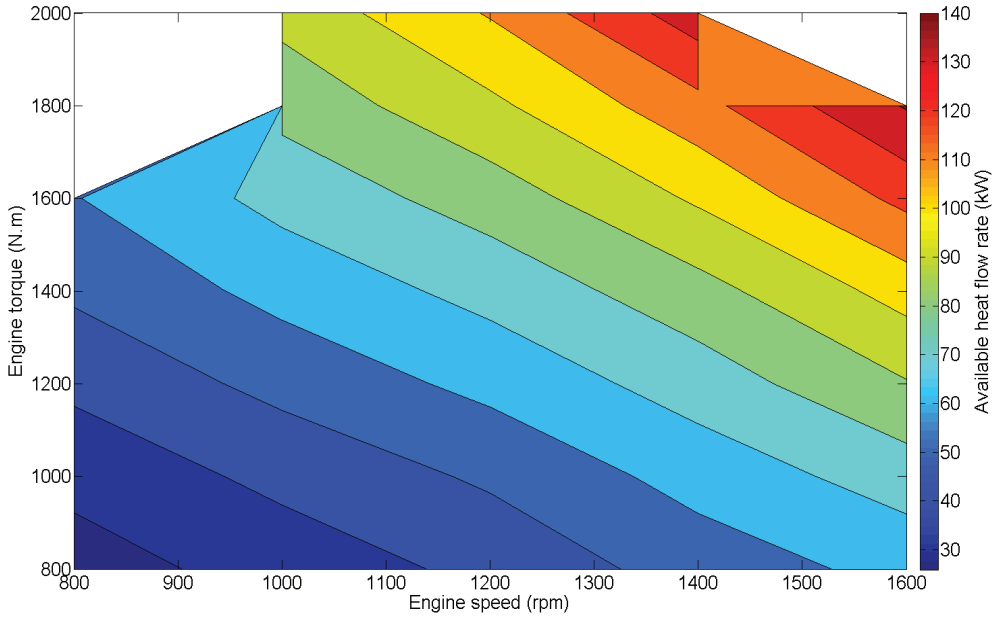


Figure 5.2 – Engine wasted heat map

Based on the step responses at each operating point, a FOPTD model structure is chosen, where the parameters are identified using a minimization output error algorithm. The identified model parameter variation according to the input signal is shown in Figure 5.3. A simple scheduling

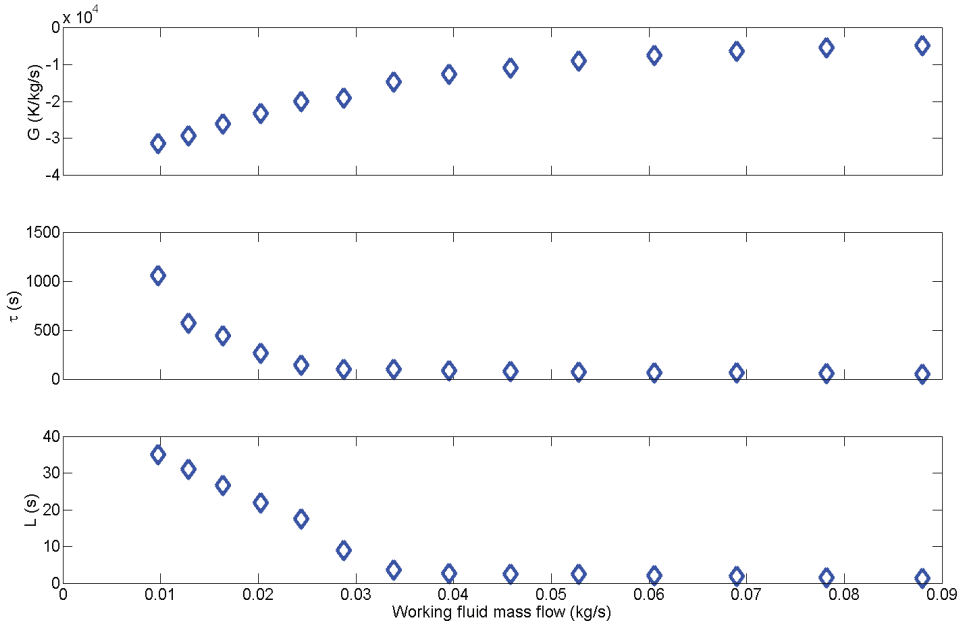


Figure 5.3 – FOPTD model parameters

approach would be to interpolate the controller parameters according to the heat flow rate entering the system $\dot{Q}_{heat,in}$ calculated as follows:

$$\dot{Q}_{heat,in} = c_p(T^*)\left[\dot{m}_{egr}\left(T_{egr,in} - T_{f,in}\right) + \dot{m}_{exh}\left(T_{exh,in} - T_{f,sat}\right)\right], \tag{5.2}$$

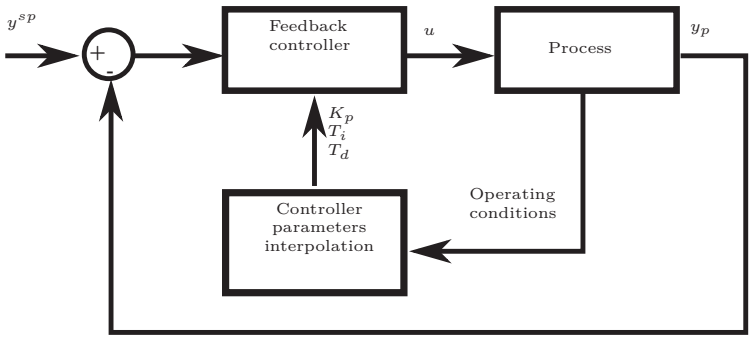


Figure 5.4 – Gain scheduled PID block diagram

where $T^* = \frac{T_{egr,in}+T_{exh,in}}{2}$ and $T_{f,sat}$ is only a function of the working fluid pressure. It includes the four main input disturbances and is easy to obtain since measurements of those values are available for the engine. However, another approach is proposed herein, which is based on the interpolation of the controller parameters by means of the working fluid mass flow rate which is the manipulated variable. Although no theoretical proof of the stability of such a method is shown here, the simulation results show a better performance from the controller when this approach is used (in comparison to scheduling the controller parameters by means of input disturbances). The associated block diagram to the gain scheduled feedback controller is shown in Figure 5.4.

5.3.1 PID settings comparison

Firstly, in order to select the correct PID setting method, a comparison has been made between the different controller parameter tuning methods cited previously. They are compared in terms of performance as well as in terms of control effort on a step load change. The performance index use is the integrated absolute error (IAE) while the control effort is represented by the total variation (TV):

$$IAE = \int_0^\infty |CV(t) - SP(t)|dt, \tag{5.3}$$

$$TV = \int_0^\infty \overbrace{\dot{MV}}(t)dt. \tag{5.4}$$

where $CV(t)$ is the controlled output signal, $SP(t)$ is the setpoint signal and $\overbrace{\dot{MV}}(t)$ is the time derivative of the manipulated variable. Table 5.1 summarizes the two performance indexes used to compare the tuning methods. The optimal tuning for load change proposed by (Madhuranthakam et al. (2008)) gives the best tracking performance but is very aggressive which can cause some robustness issues. Therefore, the SIMC method proposed by Skogestad (2003) is selected as the best tuning method. It also has the advantage of having a setting parameter to make it faster if this is desired.

Tuning method	*IAE*	*TV*
Ziegler-Nichols in closed loop Ziegler and Nichols (1942)	84.6325	0.0065
IMC Smith and Corripio (1985)	940.3763	0.0064
SIMC Skogestad (2003)	208.5099	0.0047
Optimal load change Madhuranthakam et al. (2008)	48.6754	0.0204

Table 5.1 – PID tuning method comparison

5.3.2 Duty cycle and simulation model environment

To correctly assess all the control strategies developed in this thesis , real driving conditions are used as input disturbances. These represent the normal operation of a long haul truck. Figure 5.5 shows these input disturbances used in the simulation. As the primary focus of the developed control is

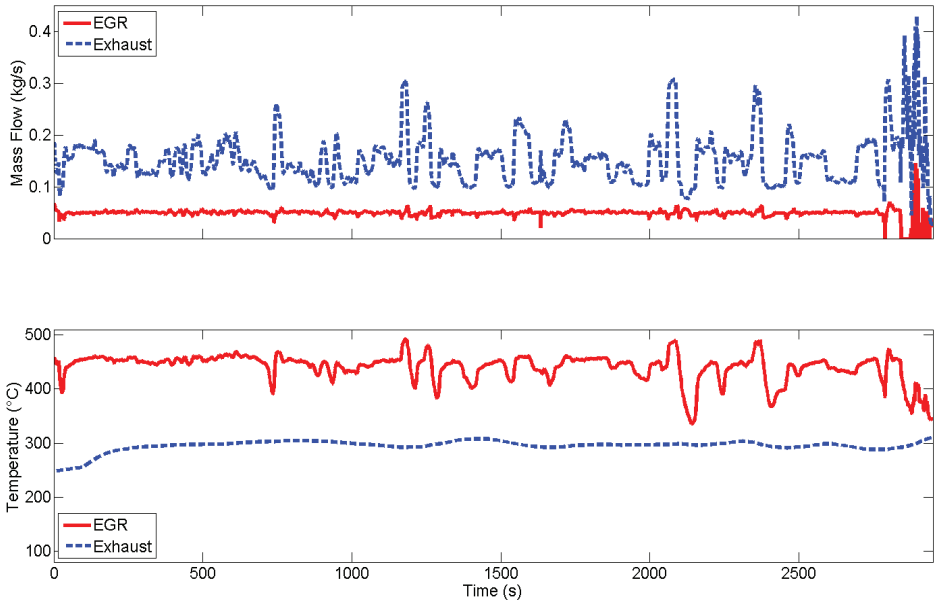


Figure 5.5 – Experimental input disturbances for all controller evaluation

to reduce the standard variation of the superheat at the set point, the high and low pressure parts of the circuit are decoupled. The simulated process is then composed of detailed validated models:

- Working fluid pump linked to an infinite sink at constant temperature and pressure.
- EGR and an exhaust evaporator linked to the corresponding heat sources.
- Kinetic turbine expander rotating at 100 times the engine speed.

The model development and validation of all those components are detailed in chapter 2.

5.3.3 Simulation results

By simulation, the control strategy performance can be assessed over the driving cycle shown in Figure 5.5. The set point is changed at t = 1500s to check whether the control system is also reacting well to variation in this variable. Those first results are promising since they show continuous superheated vapor production on this dynamic driving cycle. This means the expansion machine can continuously be fed with superheated working fluid and generate power. This results in better power production and indeed greater cycle efficiency since the expansion machine can operate at higher isentropic efficiency zones. Figure 5.6 shows the tracking error and the manipulated variable over the driving cycle. The superheat remains in a +/-5K window and reacts well to the set point change since that latter is taken into account by the controller very quickly (less than 30s) and accurately (stable behavior). Figure 5.7 shows the interpolated PID controller parameters K_p, T_i

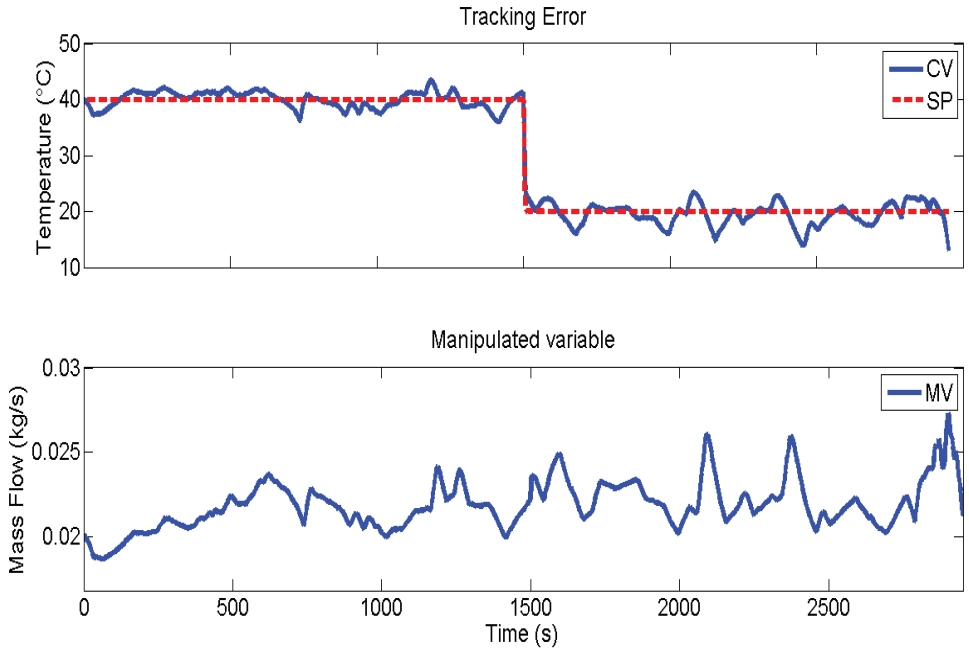


Figure 5.6 – Gain scheduled PID: tracking error and manipulated variable

and T_d (note that with the tuning methodology proposed by Skogestad (2003), only PI rather than PID controllers are used for FOPTD). It is seen that during the first 500 seconds of the simulation the controller parameters do not vary to any great extent. Then the K_p variation is of magnitude 2 (minimum -8.10^4, maximum -4.10^4) when the variation of T_i is of magnitude 3 (minimum 40, maximum 120).

In terms of experimental validation, unfortunately, due to the time development constraints and the limited availability of the experimental set-up, this control strategy was not implemented on a real set-up and experimental results cannot therefore be discussed. Indeed, the time spent in the test cell with the experimental set-up was relatively short and the focus was done on the other control strategies developed later in this thesis. Anyway this type of command does not appear to offer a sufficiently high level of performance in the case of highly transient heat source conditions which can appear during truck usage (Horne (2013); Neveu (2014)). In order to improve performance, an adaptive strategy where the controller parameters are computed on line (and not off line and then tabulated) is developed in the next section.

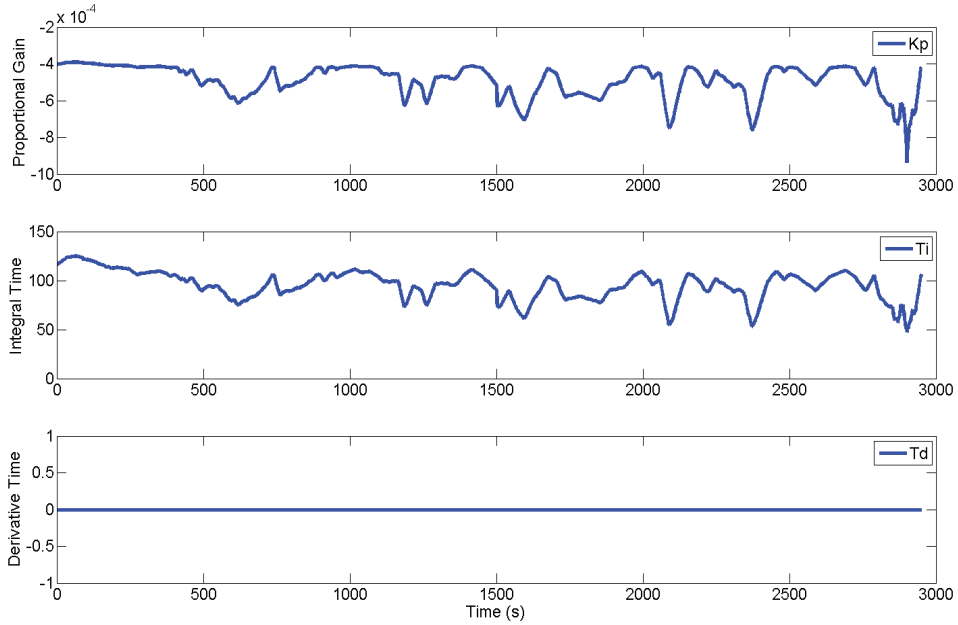


Figure 5.7 – Gain scheduled PID controller parameters versus time

5.4 Multi-model based PID strategy

Adaptive strategy, based on a multi-model approach, finds its motivation in the complex behavior of many systems that can be, at least, locally approximated by a set of simple models. Two key design issues can be then stated. The first one is on the selection of the good model among the number of models composing the data bank and has been addressed in chapter 4. The second one is on the online calculation of the controller parameters.

5.4.1 Online PID controller parameters calculation

The PID controller parameters can be computed from the global model estimation obtained using one of the two explicit weighting schemes in the previous section. The PID controller is the same as in the gain scheduling structure and is denoted by equation (5.1). Using the FOPTD global model and the PID tuning procedure from (Skogestad (2003)) (the PID tuning selected in the previous simulation results), the controller settings can be calculated on line at each current time t_k from the N models and the on-line adapted weights

$$\begin{aligned} K_p &= \sum_{i=1}^{N} \frac{1}{w_{i,k}G_i} \frac{w_{i,k}\tau_i}{\theta_c + w_{i,k}L_i} \\ T_i &= \min\left\{ \sum_{i=1}^{N} w_{i,k}\tau_i, 4\left(\theta_c + \sum_{i=1}^{N} w_{i,k}L_i\right)\right\} \\ T_d &= 0, \end{aligned} \tag{5.5}$$

where G_i, τ_i and L_i are the parameters of the identified FOPTD presented in (4.23), $w_{i,k}$ is the weight of each model composing the bank (denoted by equation (4.26) for the Bayesian weighting scheme and (4.31) for the developed one) and θ_c is a tuning parameter set to obtain a trade-off between:

- Fast speed and good disturbance rejection (corresponding to a small value of θ_c).

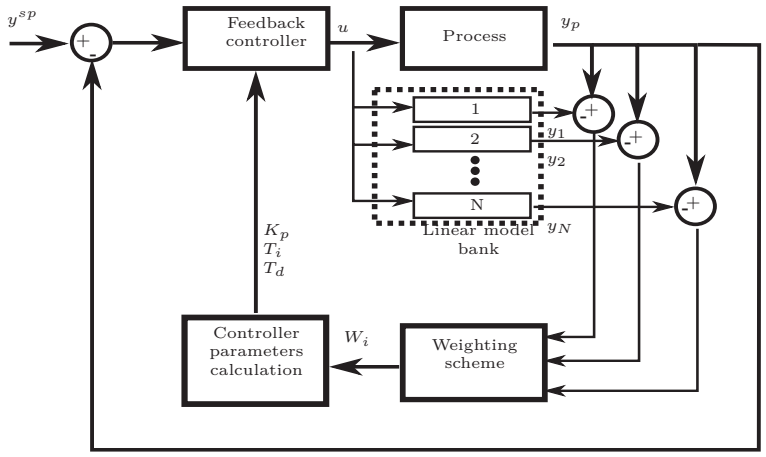


Figure 5.8 – MPID block diagram

- Good stability and small input variation (obtained with large value of θ_c).

As a design rule, θ_c is calculated as a fraction of the identified global delay:

$$\theta_c = a_c \sum_{i=1}^{N} w_{i,k} \; L_i, \tag{5.6}$$

where $a_c \in \mathbb{R}^+$. The resulting block diagram of this multi-model based PID (MPID) strategy is shown in Figure 5.8.

5.4.2 Simulation results

The controller shown in Figure 5.8 is used in the simulation environment depicted in 5.3.2. Both weighting schemes ((4.26) for the Bayesian weighting scheme and (4.31) for the developed one) are compared on their ability to allow the controlled output to follow a set point under highly transient input conditions. As open loop tests gave better results with an increase in the number of models in the bank, N has been set to 14 and tuning parameters, namely K, $\delta_{cut\ off}$, τ_{filt} and θ_C, are optimally set to obtain the best performance on the set point tracking. Figure 5.9 shows the simulation results using the multi-model based PID strategy. It can be noticed that both weighting schemes (denoted by equation (4.26) and (4.31)) give good results and only a performance index, such as the IAE, allows to conclude on scheme to scheme performance. This one is lower with the developed weighting scheme but the gap is not that huge, which explains the very similar command signal. The biggest difference that can be observed is in the controller parameters (shown in Figure 5.10). Indeed, for the Bayesian weighting scheme the best performance is achieved by setting the convergence vector to a high value, which increases the convergence to a single model but produces very fast change in controller parameters. On the other hand, the tuning parameter of the developed weighting scheme, τ_{filt}, is set to an intermediate value which increases the blending between the models of the bank and gives a smoother behavior in the controller parameters. Table 5.2 shows the different tuning parameters values set in the simulated case. Note that in practice all values of the convergence vector K are set to the same values.

Tuning parameters	τ_{filt}	K	$\delta_{cut\ off}$	a_c
Developed weighting scheme	5.33	N/A	N/A	0.78
Bayesian weighting scheme	N/A	11	0.08	1.23

Table 5.2 – MPID: tuning parameters values

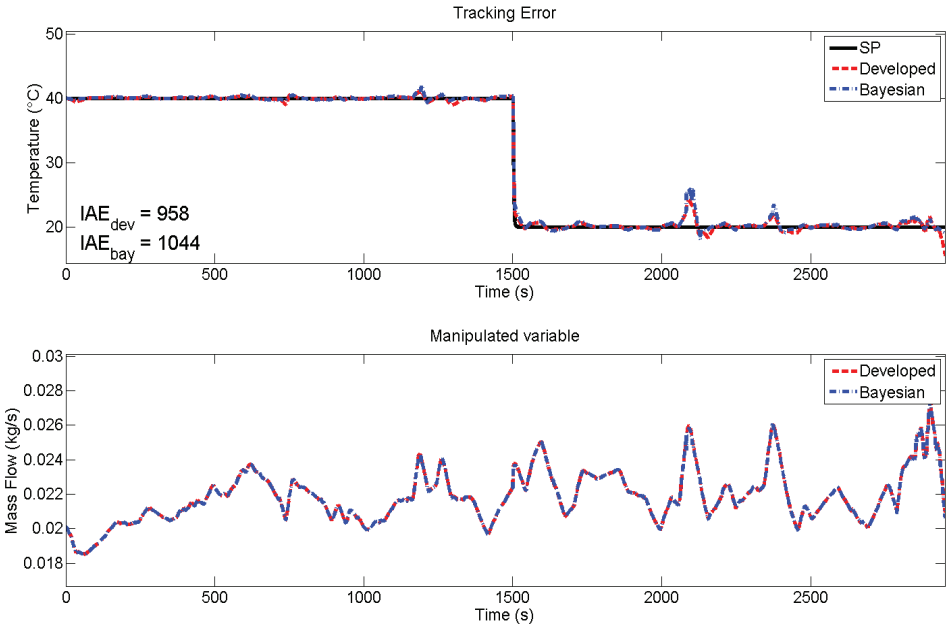


Figure 5.9 – MPID: tracking error and manipulated variable

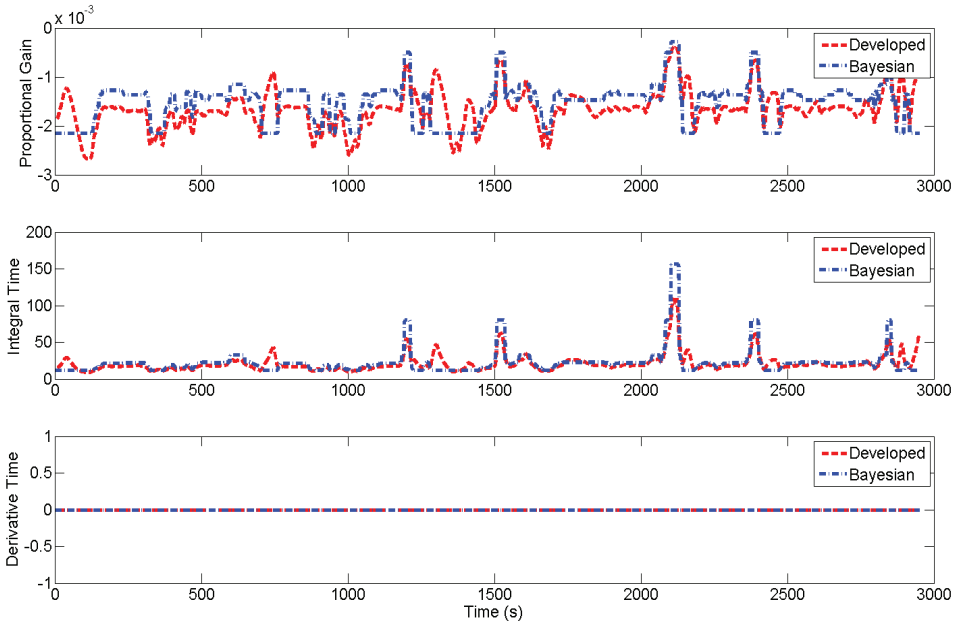


Figure 5.10 – MPID controller parameters

5.4.3 Experimental results

The strategy is then tested on the experimental setup (see appendix A) first on the steady state operating point (see appendix B) and then on a dynamic profile. In this experimental setup, since the pump has been oversized, its speed is kept constant and a fluid distributor valve is used to control the working fluid mass flow. That valve, being a fast actuator, is therefore considered as a static negative gain. In the following experimental results, neither the time constant and time delay are impacted by this actuator change but the FOPTD model gain changes in sign as well as in magnitude. The FOPTD model bank has been identified as a result. A driving cycle representative of a long haul truck usage is carried out where the engine speed and torque vary over time. The engine speed and torque over this dynamic driving cycle (called Boras Landvetter Boras or BLB) is depicted in Figure 5.11. As shown, a fairly long period is associated to a zero torque demand (between 700 and 1000s) and corresponds to a downhill on the route. The linked available heat flow rate entering into the Rankine system is shown in Figure 5.12. It can be observed that two times over the driving cycle, the available waste heat is very low (between 700 and 1000s and between 1700 and 1950s) and maintaining the vapor production during those phases can be difficult or even impossible. If the superheat is not high enough during those periods the expander by pass opens and no power is produced.

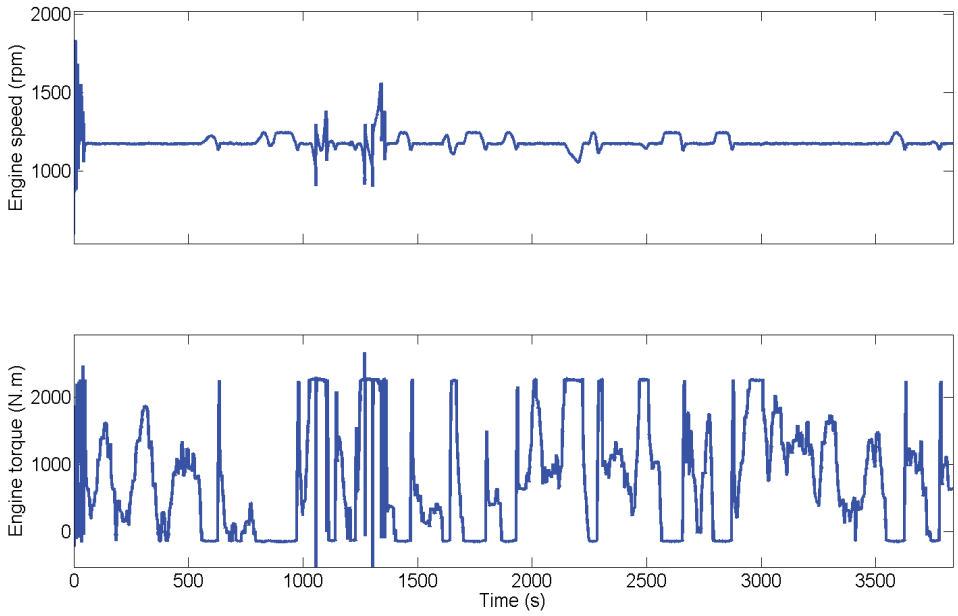


Figure 5.11 – Engine speed and torque over Boras Landvetter Boras cycle

The superheat for the two different implemented weighting schemes (namely the Baysesian and the developed one and presented in chapter 4) can be examined in Figure 5.13. As illustrated by the wasted heat, the vapor production cannot be held during any engine torque phases and the expansion machine should be bypassed, no matter of the weighting scheme used. On this figure, it can be observed that, during the vapor production phases, the developed weighting scheme reduces the deviation from the set point to maximum 4K instead of 9K with the Bayesian approach. The manipulated variable (namely the working fluid mass flow rate) for each weighting scheme is shown in Figure 5.14. The fact that the superheat is not maintained is also explained by the saturation of the working fluid mass flow rate at its minimum level. Indeed, it has been decided to limit the minimum mass flow rate to 4 g/s in order to avoid a complete dry-out of the evaporator which could

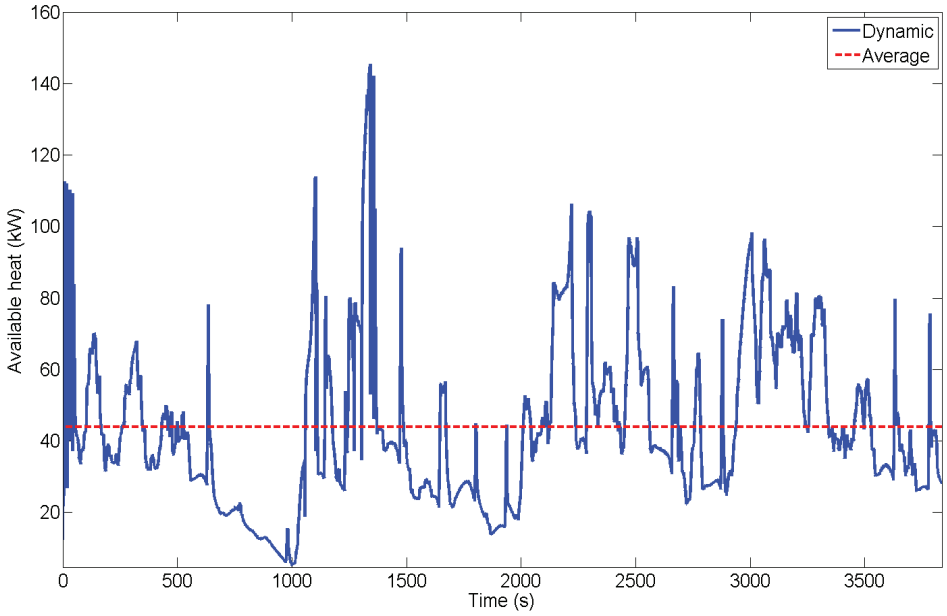


Figure 5.12 – Engine wasted heat over Boras Landvetter Boras cycle

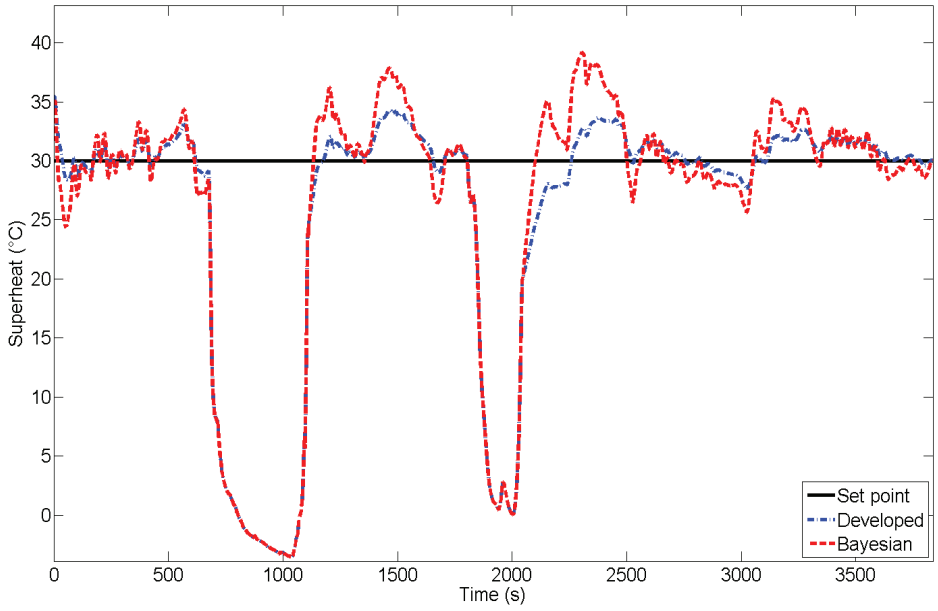


Figure 5.13 – MPID over BLB driving cycle using Bayesian and developed weighting scheme: experimental tracking error

result in localized overheat of the metal composing the latter, which increases the thermal stress and in some cases leads to cracking of the component.

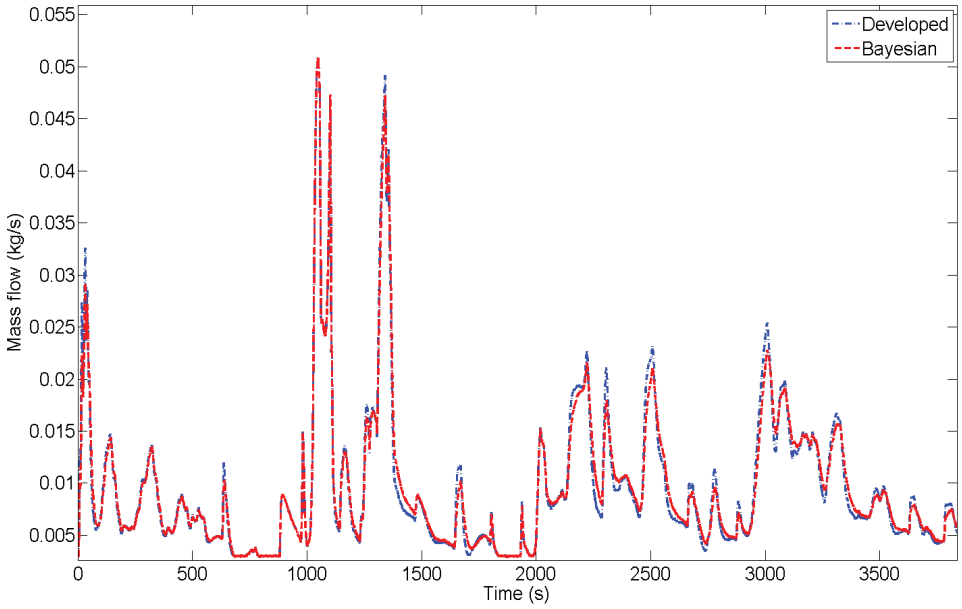


Figure 5.14 – MPID over BLB driving cycle using Bayesian and developed weighting scheme: experimental manipulated variable

5.5 Nonlinear controller

Literature survey reports the use of inverted nonlinear moving boundary model as dynamic feedforward (Peralez et al. (2013, 2014)). As a moving boundary model does not respect the implementation constraints inherent to the automotive ECU (especially due to the integration method), the finite volume reduced model presented in chapter 4 is used as feedforward after being inverted.

5.5.1 Controller structure

The main idea is to remove the fastest dynamics in order to obtain an explicit expression of the desired MV u, in this case the WF mass flow ($\dot{m}_{f_0}$), function of the slowest states which are, here, the internal and external wall temperatures. The model (4.17) owns four states and even if the number of finite volumes has been reduced to a minimum number (i.e. $i = 6$) allowing good convergence, this model is still too complex to be used as it is. In Munch Jensen and Tummescheit (2002), a physical analysis of a moving boundary model eigenvalues is proposed, and slow and fast dynamics for usual evaporators can be identified. The slowest corresponding states, though depending on the component and working fluid considered, are the wall temperatures. In Peralez et al. (2013), the same analysis is done and fastest states, such as zone lengths or fluid enthalpy, are approximated by quasi static variables. In the model (4.17), the dynamics of the fastest states, i.e. h_{f_i} and T_{g_i}, are neglected and only the time derivative of the internal and external walls is conserved. Using

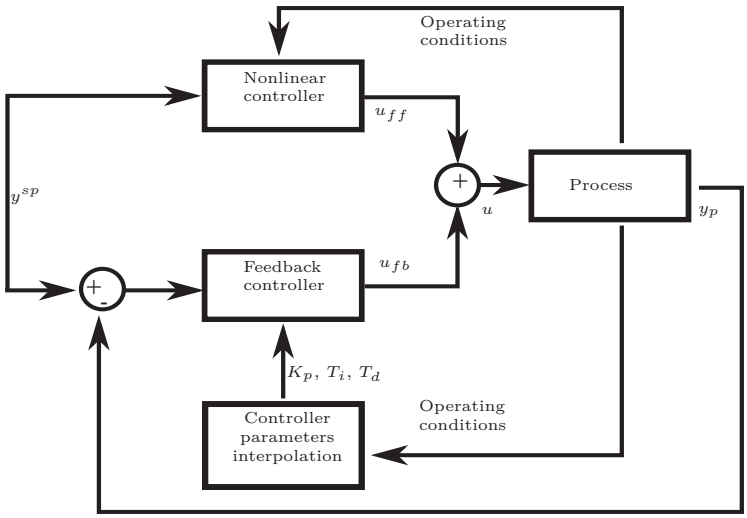


Figure 5.15 – Nonlinear controller block diagram

the update of the input disturbances measure (P_{f_0}, h_{f_0}, $\dot{m}_{g_L}$, T_{g_L}), the system of equations defining the response of the i^{th} cell of the reduced model is then:

$$\begin{cases} 0 &= \dot{m}_f \left(h_{f_{i-1}} - h_{f_i}\right) + \dot{Q}_{f_{int_i}} \\ \frac{dT_{w_{int_i}}}{dt} &= \frac{1}{\rho_{w_{int}} V_{w_{int_i}} c_{w_{int}}} \left(\dot{Q}_{f_{int_i}} + \dot{Q}_{g_{int_i}}\right) \\ 0 &= \dot{m}_g c_{p_g} \left(T_{g_{i-1}} - T_{g_i}\right) + \dot{Q}_{g_{int_i}} + \dot{Q}_{g_{ext_i}} \\ \frac{dT_{w_{ext_i}}}{dt} &= \frac{1}{\rho_{w_{ext}} V_{w_{ext_i}} c_{w_{ext}}} \left(\dot{Q}_{g_{ext_i}} + \dot{Q}_{amb_{ext_i}}\right). \end{cases} \tag{5.7}$$

The expression of the feedforward term MV $\dot{m}_f$ is then straightforward and equals to:

$$\dot{m}_f = \frac{\sum_{i=1}^{N} \dot{Q}_{f_{int_i}}}{h_{f_0} - h_{f_L}}. \tag{5.8}$$

Figure 5.15 shows the block diagram of the nonlinear controller. The feedforward part is composed of the nonlinear evaporator inverted model whereas the feedback part is made of the gain scheduled controller presented in section 5.3.

5.5.2 Simulation results

The performance of this controller structure is first tested on the same simulation environment with the same duty cycle (shown in Figure 5.5) than for the other strategies. Figure 5.16 shows the tracking error and the manipulated variable over the entire driving cycle. The superheat remains in a very narrow window of 1K around the set point and the controller reacts almost immediately to the set point change. In order to assess the performance of such a strategy, model uncertainties have been introduced in the heat transfer coefficient on each side (α_g and α_f) and on the boiler's geometries ($A_{exch_{int_g}}$,$A_{exch_{int_f}}$ and $A_{exch_{ext_g}}$). Each case has been simulated separately in order to check the sensitivity on those parameters. Discrepancies from -50 to +50 % have been introduced on those parameters (the three areas are considered as only one case study and regrouped under the label Geom). Figure 5.17 shows the IAE (5.3) for the different parameters uncertainties on simulation environment presented in section 5.3.2. The geometry has the biggest influence on the controller performance since the inertia is contained in those parameters and the model inversion

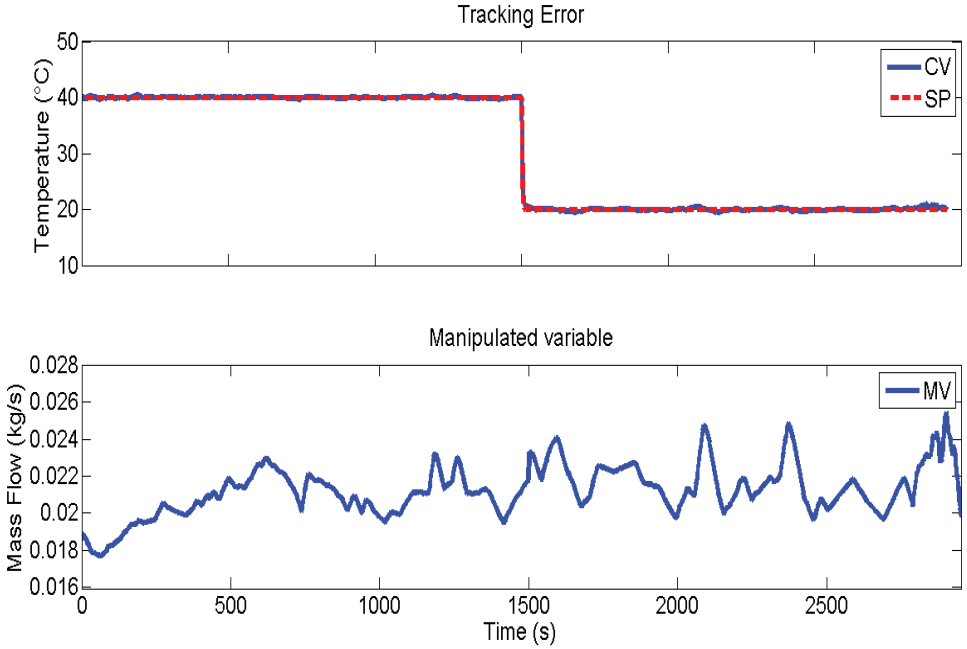


Figure 5.16 – Nonlinear controller: tracking error and manipulated variable

keep the slowest dynamics which are the wall states. An uncertainty between +/- 20% on any parameters gives an IAE below 1000 which was the performance obtained with the multi-model based PID controller presented in section 5.4. This is important when considering, the deviation that could exist between the different heat exchangers of a same model.

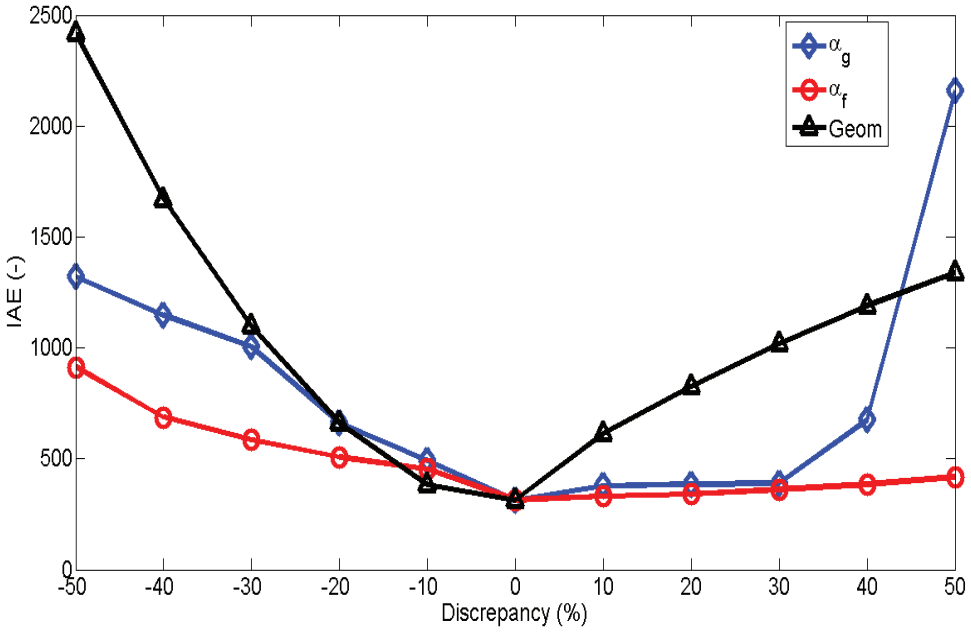


Figure 5.17 – Nonlinear controller: IAE with model uncertainties

5.6 Multi-model predictive controller

Even if the previous strategy gives good results, development of a good nonlinear first principle model is a severe effort (many parameters are usually hard to get from experimental results) and may be implemented with difficulty into an online model based control strategy (due to the online model resolution task). Therefore, current integration constraints lead to the development of a simple and fast controller. In section 5.4, it has been shown that the multiple linear approach could lead to good results with a simple PID controller. The model denoted by equation (4.21) and (4.27) is now used in a MMPC framework to ensure tracking of the process output to the set-point, accounting for the control move effort Δu.

5.6.1 Controller structure

Since the technical integration is a major issue, it is important to decrease the computational load, first by decreasing the number of optimization arguments: the control horizon is first set to its minimum: 1 ($u(t) = u(t_k) = u_k$ over the control horizon t_p). Therefore, the MMPC algorithm aims to find, at each current time t_k, the optimal step input u_k^* that minimizes the cost function J:

$$\left\{\begin{array}{rcl} \min J(u_k) & = & \int\limits_{t_k}^{t_k+t_p} (y_p(t) - y^{sp}(t))^2 + w_u \Delta u_k^2 \; dt \\ \text{where: } \Delta u_k & = & u_k - u_{k-1} \\ \text{where: } u_{inf} & \leq & u_k \leq u_{sup}. \end{array}\right. \tag{5.9}$$

where w_u is a scaling factor and a penalty weight for the control move. In this quadratic form, the ideal optimal solution leads to $J(u_k^\star) = 0$, i.e.: the tracking is perfect ($y_p(t) = y^{sp}\ \forall t$) and the control is at a steady state ($\Delta u_k = 0\ \forall t$).
In the internal model control structure, the control u is both applied to the process and to the model(s) (in a multi-model control approach). Hence, it allows to compute the modeling error e_k at each k:

$$e_k = y_{p,k} - y_k, \tag{5.10}$$

which is assumed constant into the future and used to get the output prediction $y_p(t)$ in (5.9) with the model:

$$y_p(t) = y(t) + e_k. \tag{5.11}$$

In the same way, the set point y^{sp} is taken constant on the prediction horizon and updated each time k. The question is now how to write the model response $y(t)$ according to u_k (and also the constant values and the parameters updated at each k). Let us start from the definition of the output response $y_i(t)$ of one linear FOPTD model i with any input profile $u(t)$ from any current time t_k, and starting from the current process output $y_{p,k}$:

$$y_i(t) = y_{p,k} e^{\frac{-(t-t_k)}{\tau_i}} + \int_{t_k}^{t} (e^{\frac{-(t-s)}{\tau_i}} \frac{G_i}{\tau_i} u(s - L_i)) ds \tag{5.12}$$

(5.12) can be developed as:

$$y_i(t) = y_{p,k} e^{\frac{-(t-t_k)}{\tau_i}} + \frac{G_i}{\tau_i} e^{\frac{-t}{\tau_i}} \int_{t_k}^{t} (e^{\frac{s}{\tau_i}} u(s - L_i)) ds. \tag{5.13}$$

To proceed, we need to define, based on the time delay L_i:

$$\left\{\begin{array}{rcl} \lambda_i & = & max(a_i \in \mathbb{N} | a_i \leq \frac{L_i}{T_s}) \\ \Delta L_i & = & L_i - \lambda_i T_s, \in \mathbb{R}^+, \end{array}\right. \tag{5.14}$$

which allows to define $u(.)$ used in the integration interval of (5.13), based on past known input values and the future input value of u. Then, the integration in (5.13) is done by parts, where the $\lambda_i + 2$ time intervals are given in Table 5.3:

s	$s - L_i$	$u(s - L_i)$
$t_k \to t_k + \Delta L_i$	$t_k - L_i \to t_{k-\lambda_i}$	$u(t_{k-\lambda_i-1})$
$t_k + \Delta L_i \to t_k + \Delta L_i + T_s$	$t_{k-\lambda_i} \to t_{k-\lambda_i+1}$	$u(t_{k-\lambda_i})$
$\dots$	$\dots$	$\dots$
$t_k + \Delta L_i + (\lambda_i - j)T_s \to t_k + \Delta L_i + (\lambda_i - j + 1)T_s$	$t_{k-j} \to t_{k-j+1}$	$u(t_{k-j})$
$\dots$	$\dots$	$\dots$
$t_k + \Delta L_i + (\lambda_i - 1)T_s \to t_k + L_i$	$t_{k-1} \to t_k$	$u(t_{k-1})$
$t_k + L_i \to t$	$t_k \to t - L_i$	$u(t_k) = u_k$

Table 5.3 – MMPC: input sequence definition.

$$\begin{aligned} y_i(t) &= y_{p,k} e^{\frac{-(t-t_k)}{\tau_i}} \\ &+ \frac{G_i}{\tau_i} e^{\frac{-t}{\tau_i}} u(t_{k-\lambda_i-1}) \int_{t_k}^{t_k+\Delta L_i} e^{\frac{s}{\tau_i}} ds \\ &+ \frac{G_i}{\tau_i} e^{\frac{-t}{\tau_i}} \left(\sum_{j=1}^{j=\lambda_i} u(t_{k-j}) \int_{t_k+\Delta L_i+(\lambda_i-j+1)T_s}^{t_k+\Delta L_i+(\lambda_i-j)T_s} e^{\frac{s}{\tau_i}} ds \right) \\ &+ \frac{G_i}{\tau_i} e^{\frac{-t}{\tau_i}} u(t_k) \int_{t_k+L_i}^{t} e^{\frac{s}{\tau_i}} ds \end{aligned} \tag{5.15}$$

(5.15) can be summarized as a linear expression in the optimization argument u_k:

$$\begin{aligned} &y_i(t) = y_{p,k} f_{1i}(\tau_i, t_k, t) + f_{2i}(T_s, G_i, \tau_i, \Delta L_i, \lambda_i, t_k, t, u(past)) \\ &+ u_k f_{3i}(G_i, \tau_i, L_i, t_k, t), \end{aligned} \tag{5.16}$$

where the f_i may be explicitly defined offline and numerically updated online at each time t_k. $u(past)$ contains the past applied input.
Therefore, replacing first (5.16) in the computation of the global model output from the considered model outputs (4.27), assuming that the weights $w_{i,k}$ are constant over the prediction horizon, then combining this result with (5.10) and (5.11) in (5.9), the cost function to minimize can be written as:

$$J(u_k) = \int_{t_k}^{t_k+t_p} \left(\left(\sum_{i=1}^{N} (w_{i,k} y_i(t)) + e_k - y^{sp}(t) \right)^2 + w_u \Delta u_k^2 \right) dt, \tag{5.17}$$

where $t_p = max(t_{pi})\ \forall i$ is each prediction horizon t_{pi} has to be tuned according:

$$\begin{cases} t_{pi} = \gamma_p * \tau_i + L_i;\ \gamma_p \in \mathbb{R}^+, \\ \text{e.g.: } \gamma_p = 1 \text{ (63\% of the dynamics is predicted)} \\ \text{or } \gamma_p = 3 \text{ (95\% of the dynamics is predicted).} \end{cases} \tag{5.18}$$

Based on the step response series (5.15) of the N linear FOPTD models, the expression (5.17) is a quadratic one in u_k:

$$\begin{aligned} &J(u_k) = \beta_{2,k}(N, G_i, \tau_i, L_i, t_p, w_u, w_{i,k}) u_k^2 \\ &+ \beta_{1,k}(N, T_s, G_i, \tau_i, L_i, t_p, \Delta L_i, \lambda_i, w_u, y_{p,k}, y_k^{sp}, e_k, u(past), w_{i,k}) u_k \\ &+ \beta_{0,k}(N, T_s, G_i, \tau_i, L_i, t_p, \Delta L_i, \lambda_i, w_u, y_{p,k}, y_k^{sp}, e_k, u(past), w_{i,k}). \end{aligned} \tag{5.19}$$

The $\beta_{i,k}(.)$ can be explicitly defined offline (expressions are in the appendix C) and updated each time t_k. Since J is convex in u_k (due to the fact that $\beta_{2,k} > 0$, by definition), let us then define

$$u_k^{min}(N, T_s, G_i, \tau_i, L_i, t_p, \Delta L_i, \lambda_i, w_u, y_{p,k}, y_k^{sp}, e_k, u(past), w_{i,k}) \tag{5.20}$$

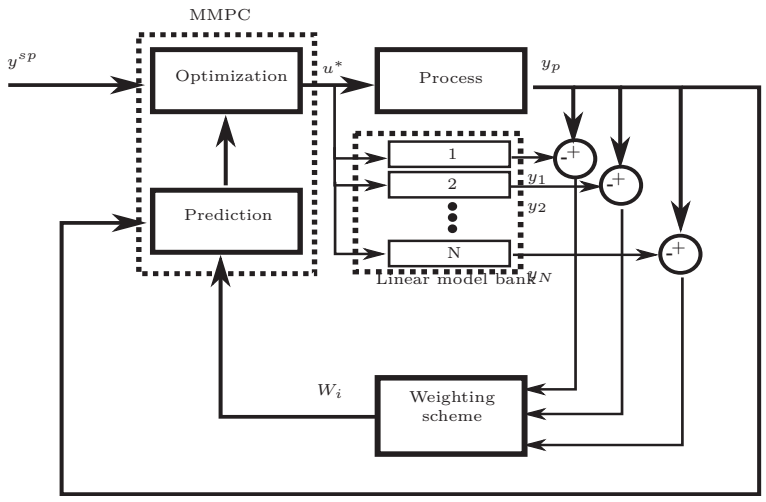


Figure 5.18 – MMPC block diagram

the solution of the minimization of (5.19) obtained with the first order optimality at each t_k:

$$\frac{\partial J}{\partial u_k} = 0 \text{ at } u_k = u_k^{min}. \tag{5.21}$$

The calculation of u_k^{min} is then straightforward:

$$u_k^{min} = \frac{-\beta_{1,k}}{2\beta_{2,k}}, \tag{5.22}$$

which leads to the explicit formulation of the solution $u_k^\star$ of the constrained optimization problem 5.9:

$$\begin{cases} \text{if:} & u_{inf} \leq u_k^{min} \leq u_{sup} : \ u_k^\star = u_k^{min} \\ \text{if:} & u_k^{min} \leq u_{inf} : \ u_k^\star = u_{inf} \\ \text{if:} & u_{sup} \leq u_k^{min} : \ u_k^\star = u_{sup}, \end{cases} \tag{5.23}$$

which is, as required by our integration constraints, very fast to compute (no online optimization task, no online dynamic model resolution). The two tuning parameters of the MMPC framework, namely the prediction horizon γ_p and the control move penalty $w_u >$, are strictly positive real numbers.
The diagram of this multi-model predictive controller is shown in Figure 5.18.

5.6.2 Simulation results

The explicit MMPC formulation being a generic method that could be applied on any kind of systems, it has been first validated on a simple benchmark process found in the literature. It is then used as controller in the detailed simulation environment presented in section 5.3.2.

5.6.2.1 Benchmark process

First the controller is tested and validated on a benchmark process. This one is taken from Dougherty and Cooper (2003). The process is simulated by three different transfer functions combined to represent a nonlinear plant. Each transfer function has the following form:

$$T_p(s) = \frac{G_p \left(\tau_L s + 1\right) e^{-L_p s}}{\left(\tau_{p,1} s + 1\right)\left(\tau_{p,2} s + 1\right)}. \tag{5.24}$$

These three set of parameters represent, each, the process behavior at a specific value of the measured process variable. These transfer functions, denoted by equation (5.24), are then summed using linear weighting function. Each transfer functions is approximated here by a simpler FOPTD model used in the MMPC framework developed in the previous section 5.6. All parameters used in the case study are listed in Table 5.4.

	Lower level	Intermediate level	Upper level
Process variable value (%)	20	50	80
SOPTD with lead time model parameters			
G_p	1	3	6
τ_L	-15	-10	-5
$\tau_{p,1}$	10	20	30
$\tau_{p,2}$	5	10	15
L_p	3	6	9
FOPTD model parameters			
G'_p	1.20	3.13	6.12
τ'_p	15.3	25.3	37.7
L'_p	15.9	21.2	23.7

Table 5.4 – Case study parameters (Dougherty and Cooper (2003))

This first simulations, in addition to validate the methodology developed in section 5.6, lead to a better understanding of the tuning parameters, i.e. γ_p and w_u actions on the MMPC strategy. Figure 5.19 and 5.20 show respectively the controlled and manipulated variable for this case study. The w_u influence can be noticed: increasing the move penalty factor influence as well the rapidity of the controller as its stability since undershoot disappears.

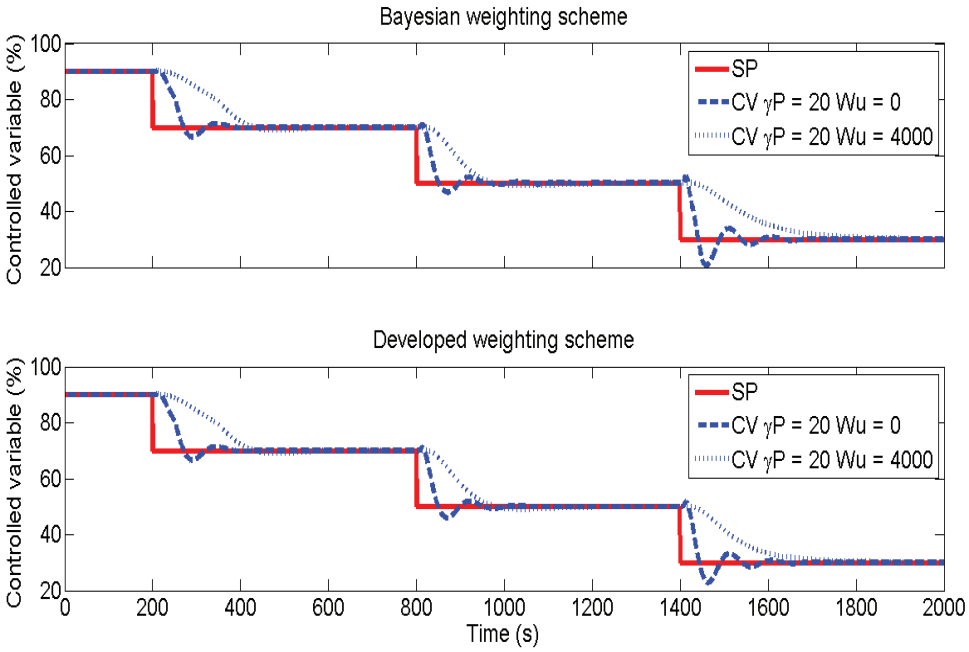


Figure 5.19 – MMPC simulation results on benchmark process: controlled variable

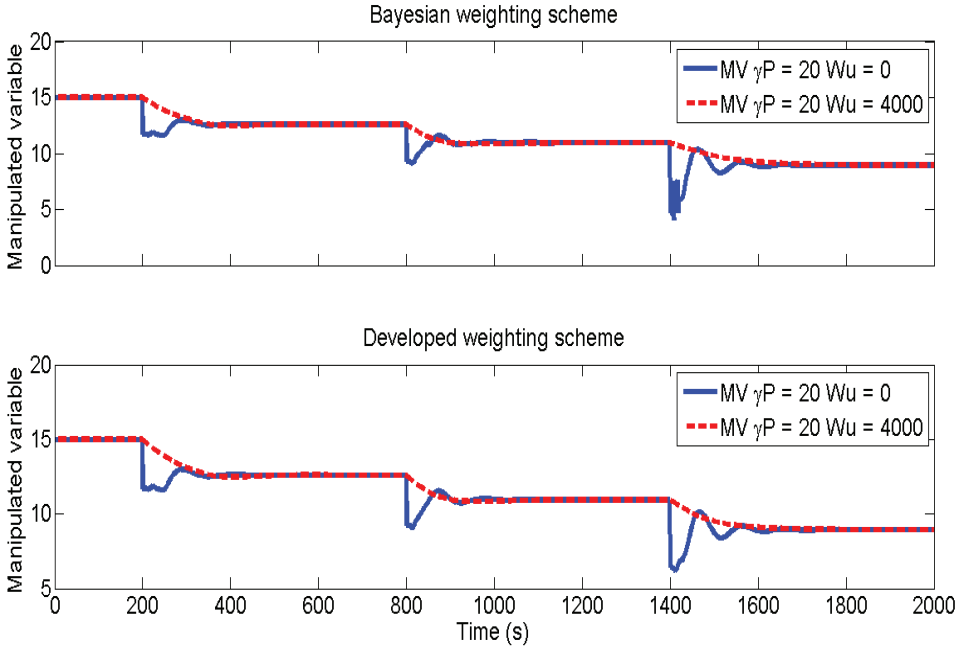


Figure 5.20 – MMPC simulation results on benchmark process: manipulated variable

5.6.2.2 Detailed Rankine process model

As for the other control strategies, the MMPC performance is evaluated on the reference detailed simulation environment presented in 5.3.2 using the same dynamic inputs than for the other strategies. Figure 5.21 shows the simulation results for the controlled and manipulated variables using both weighting schemes. It can be noted that for both implemented schemes, the controlled variable does not deviate from the set point more than 1°C, except when the set point is changed at time $t = 1500s$. When moving the superheat set point from 40°C to 20°C the multi-model predictive controller could be considered slow compared to the previously implemented controller. In practice this slow behavior is due to the non-prediction of future set points which is considered impossible to predict. Here again the set point was changed only to assess controllers' performance under disturbance and set point changes. On a real setup the superheat set point is constant over the entire operation of the system.
Concerning the scheme to scheme comparison the Bayesian weighting scheme reacts faster to the set point change since it converges more quickly to a model with a smaller time constant. The developed weighting scheme uses more blending by construction and is generally slower to answer to fast operating region changes.
The manipulated variables, as in the MPID case presented in section 5.4, are similar but slightly different which is beneficial since it means no additional effort for the actuator.

5.6.3 Experimental results

The controller is then implemented and tested on the experimental setup. The relatively low time spent in the test cell explains why only the developed weighting scheme was tested, rather than the Bayesian one. In addition to that, during the tests, a drift in the actuator appeared and discredited the different linear models while not enough time was left to re-identify the different models. The results presented here were obtained before the actuator drifting on simple engine torque variation (presented in Figure 5.22). Figure 5.23 shows the superheat tracking and the working fluid mass

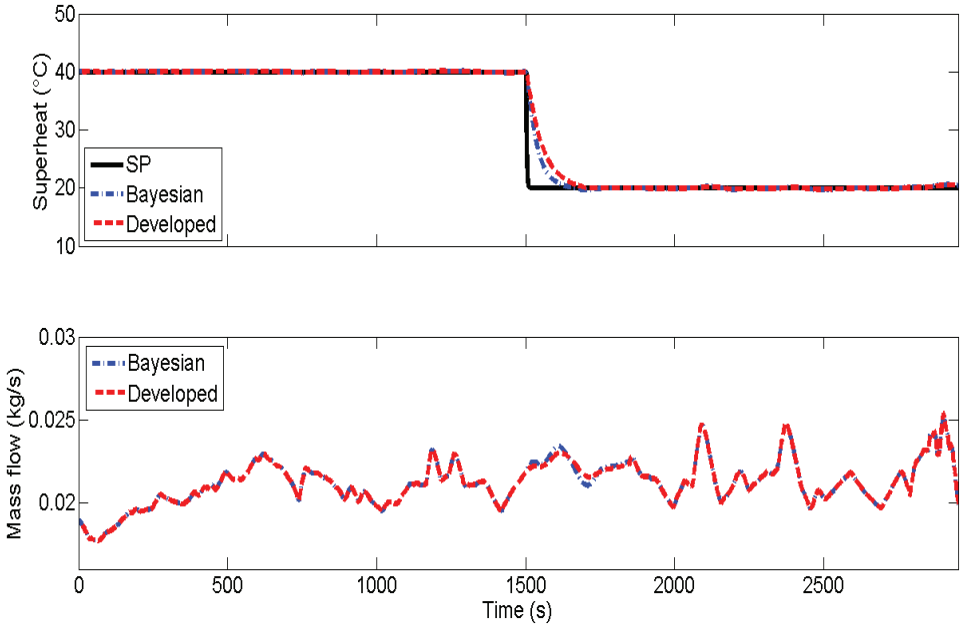


Figure 5.21 – MMPC simulation results on Rankine process: tracking error and manipulated variable

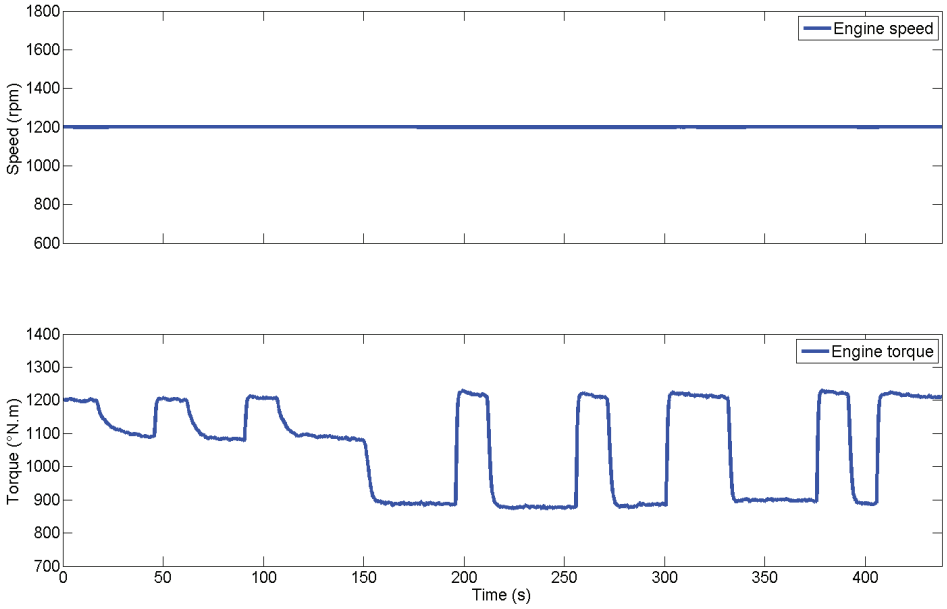


Figure 5.22 – Engine speed and torque variation

flow obtained with the multi-model predictive controller. Obviously the changes in operating conditions were less important than in a driving cycle but it gives first impression about the MMPC performance. The superheat tracking error is shown by Figure 5.23. It can be seen that the deviation to the set point is less than 1K for the biggest torque steps (corresponding to 300 N.m). Figure 5.24 shows the estimation of the working fluid temperature at the expansion machine inlet by means of the developed weighting scheme during this experiment. It can be noted that the multi-model control approach gave satisfactory results once implemented in the controller since the maximum deviation is 2.5K and the temperature dynamic behavior is well calculated.
This model-based control strategy demonstrates very good performance with only 4 tuning parameters (namely N, τ_{filt}, γ_p and w_u), which is perfectly in line with the industrial needs and standardized procedure.

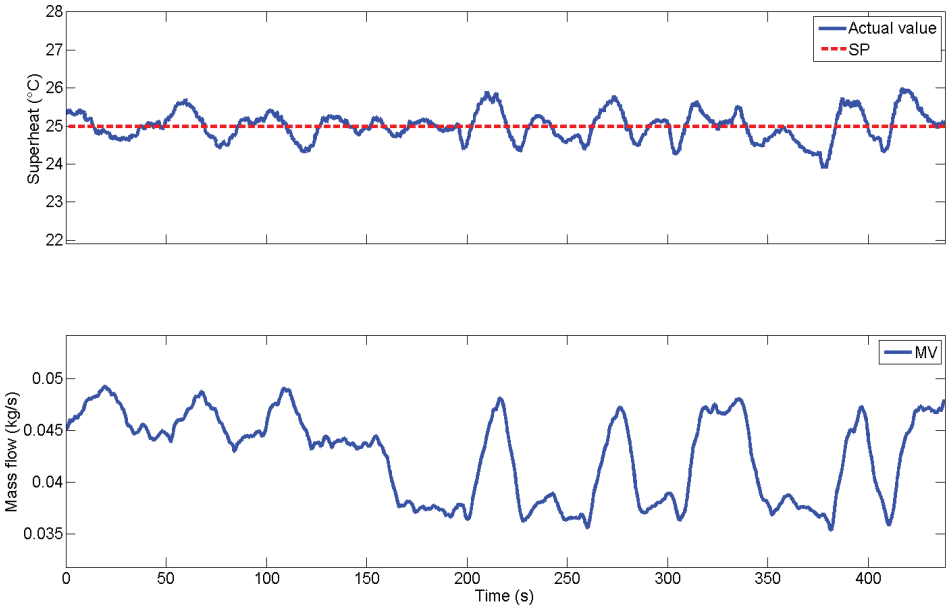


Figure 5.23 – MMPC: experimental tracking error and manipulated variable

5.7 Controller comparison

As exactly the same environment has been used to assess the different controller performance via simulation they can be compared on the basis of the integrated absolute error (denoted by equation (5.3)). Figure 5.25 shows the IAE for the 6 implemented controllers. It can be seen that the poorest performance is given by the gain scheduled PID whereas the nonlinear inverted model presented in section 5.5 gives the best results. For the controller based on the multi-model approach, namely the MPID and the MMPC, the performance is more or less the same with an IAE around 1000. The multi-model predictive controller despite the weighting scheme had a very high IAE due to the low dynamic response when it has to deal with a set point change. This behavior obviously increases the performance indicator but that latter remains anyway low. When it comes to the scheme to scheme comparison for the controller using the multi-model approach, it is hard to give an answer for which one is the best. For the multi-model based PID strategy the developed weighting scheme gives slightly higher performance whereas for the MMPC it is the other way around. In any case, a trade-off between performance and tuning effort should be taken into account for a fair comparison.

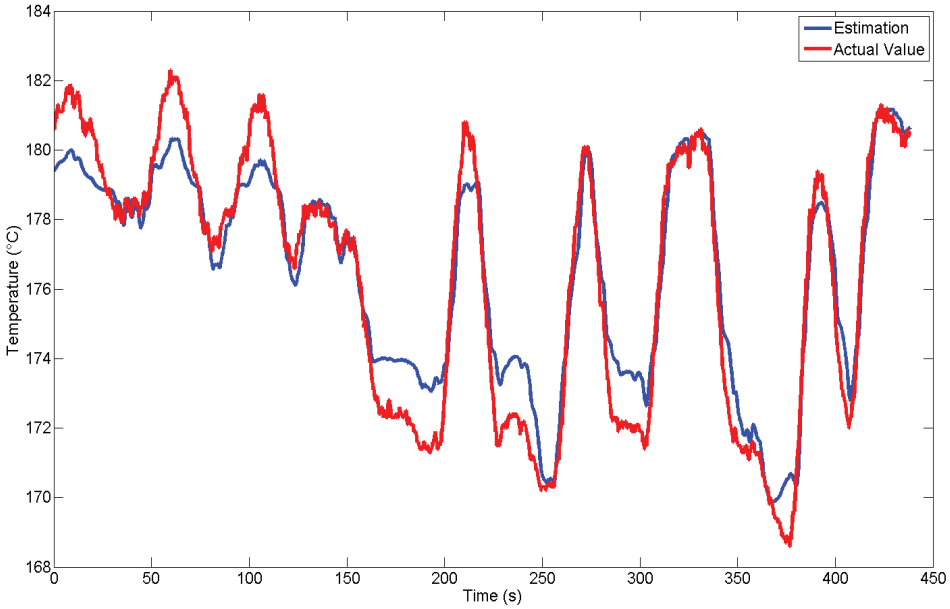


Figure 5.24 – MMPC: experimental validation of the working fluid temperature estimation at the expansion machine inlet

Last but not least, it can be noted that this comparison is based on a detailed validated simulation model where the bank of linear models has been built with perfection. When considering the physical setup it has been shown that the developed weighting scheme shows better performance than the Bayesian since it uses more blending between the model. This results into lower IAE for the developed scheme than the Bayesian one and should also be true for the MMPC framework.

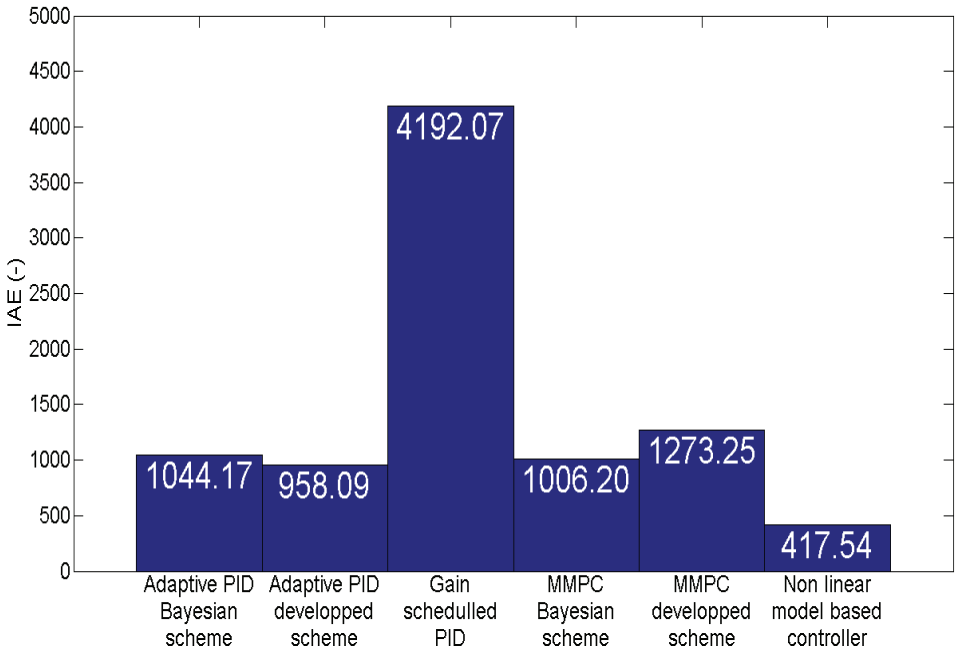


Figure 5.25 – Different implemented controller comparison: IAE

Conclusion. *In this chapter, different control strategies adapted to Rankine cycle heat recovery system for heavy-duty truck application are presented and compared. The need for high performance controller at low calibration effort is clear in the industry and the work presented here fits with this idea. Apart from the nonlinear controller which requires identifying non-measurable parameters that could demand a huge effort, the other strategies developed in this part contains a maximum of 4 tuning parameters When considering the developed weighting scheme (this is not true for the Bayesian scheme where the number of tuning parameters depends on the number of models in the bank). The multi-model approach developed in chapter 4 has been used to create two new strategies. One is based on a PID controller where its parameters are adapted online to improve the performance. The other is based on a MMPC framework where the process behavior is predicted by means of an explicit formulation of the FOPTD's response over a prediction horizon. Some strategies are experimentally validated which proves the viability of such controllers.*
The next chapter will focus on the real-time estimation of a global adaptive FOPTD in order to remove the offline identification part and creates even more efficient strategies.

Chapter 6

Observer based control strategy

Abstract. *In this chapter an observer is built to replace the offline linear model identification phase used in the multi-model approach. This may help to drastically reduce the development time required for the MPID and the MMPC strategies developed in chapter 5 and increase the model robustness. However, since it does not respect the implementation constraints the observer is only validated offline using experimental data.*

6.1 Model design

The multi-linear model approach presented in chapter 4 and then used as a basis for the feedback controllers developed in sections 5.4 and 5.6 of the previous chapter is based on an offline identification of first-order plus time delay model bank. Multiple models can be identified and combined via a weighting scheme but the controller calibration goes through an open loop phase where dynamic relation between an input and an output is established. This phase is usually costly in terms of time especially for the studied systems which have a long response time. Moreover, important controlled outputs are in open loop during this identification task, which is an undesired uncontrolled behavior. To avoid this and save development time, online identification algorithms could be used Landau and Zito (2006). Another benefit of the online identification is the robustness of the controller since the model identified online takes care of the possible current drifts of the system. For further control designs, the idea is here to get an online adapted FOPTD SISO model, with the online observation of its gain, time constant and lag.

6.1.1 Linear model approximation with the half rule method

Due to the infinite dimension of the time delay, as underlined in section 4.2.1, we need to approximate it in finite dimension. In Skogestad (2003), the author shows an approximation method for high order linear SISO model that contains multiple time constants. By considering a model of the form

$$\frac{\prod_j \left(-T_{j0}^{inv} s + 1\right)}{\prod_i \tau_{i0} s + 1} e^{-L_0 s} \tag{6.1}$$

where the time constants τ_{i0} are ranked according to their magnitude (i.e. $\tau_{10} \geq \tau_{20} \geq \ldots \geq \tau_{i0}$), T_{j0}^{inv} represents the inverse response time constant and L_0 is the original delay. Note that in equation

(6.1), $T_{j0}^{inv} \geq 0$ and $L_0 \geq 0$ (i.e, there might be no initial delay). Based on the half rule applied on the initial full order model (6.1), one understands the lower order FOPTD model of the form:

$$F(p) = \frac{e^{-Ls}}{1+\tau s}. \tag{6.2}$$

where:

$$\begin{aligned} \tau &= \tau_{10} + \frac{\tau_{20}}{2}, \\ L &= L_0 + \frac{\tau_{20}}{2} + \sum_{i\geq 3} \tau_{i0} + \sum_j T_{j0}^{inv}. \end{aligned} \tag{6.3}$$

Based on this method used in the other way around, a finite approximation of the lag is possible: starting from the FOPTD model (6.2) where lag is present, the initial lagged model can be approximated by a non lagged model (6.1) where $L_0 = 0$. That one presents a lower order than the initial model (due to the infinite dimension of the lag (Normey-Rico (2007))) and is used in the following part.

6.1.2 Considered model structure

In section 4.2.1, it has been shown that evaporators used in Rankine cycle based heat recovery system could be modeled by a bank of FOPTD models. The idea is here to replace this bank of FOPTD models identified offline by a single FOPTD model with parameters estimated online. By using the half rule of Skogestad (2003) explained in section 6.1.1, the identified FOPTD around an operating point can be approximated in finite dimension by a second order (SO) model.

$$\frac{y}{u}(s) = \frac{G}{\tau s+1} e^{-Ls} \approx \frac{G}{(\tau_1 s+1)(\tau_2 s+1)}. \tag{6.4}$$

Indeed this approximation method is validated here since for all FOPTD models previously found $\tau >> L$ (see Figure 5.3). Therefore, based on the half-rule, we are able to define the relations between the FOPTD model parameters and the SO model parameters:

$$L = \frac{\tau_2}{2},\ \tau = \tau_1 + \frac{\tau_2}{2},\ (\text{hence, } \tau_1 > \tau_2), \tag{6.5}$$

which leads to:

$$\tau_1 = \tau - L, \tau_2 = 2L. \tag{6.6}$$

This model is formulated in state-space form as following :

$$\tau_1\tau_2 \ddot{y}(t) + (\tau_1+\tau_2)\,\dot{y}(t) + y(t) = Gu(t). \tag{6.7}$$

Furthermore, considering the following notations :

$$\begin{cases} x_1(t) &= y(t) \\ x_2(t) &= \dot{y}(t), \end{cases} \tag{6.8}$$

we obtain the following state representation:

$$\begin{cases} \dot{x_1}(t) &= x_2(t) \\ \dot{x_2}(t) &= \dfrac{-x_1(t) - (\tau_1+\tau_2)\,x_2(t) + Gu(t)}{\tau_1\tau_2}. \end{cases} \tag{6.9}$$

In the following section, the FOPTD model parameter vector $[\tau\ G\ L]'$ is considered to be unknown and varying slowly when compared to the other relevant dynamics of the system. They will be

identified online using a nonlinear observer. Hence, by making the following change of coordinates, $x_3(t) = \frac{1}{\tau_1\tau_2}$, $x_4(t) = \frac{\tau_1+\tau_2}{\tau_1\tau_2}$ and $x_5(t) = \frac{G}{\tau_1\tau_2}$, the following augmented state space is obtained:

$$\begin{cases} \dot{x_1}(t) &= x_2 \\ \dot{x_2}(t) &= -x_1(t)x_3(t) - x_2(t)x_4(t) + x_5(t)u \\ \dot{x_3}(t) &= 0 \\ \dot{x_4}(t) &= 0 \\ \dot{x_5}(t) &= 0. \end{cases} \tag{6.10}$$

In the following section using x_1 measurement, the augmented state vector is estimated using a nonlinear observer.

6.2 Observer design

Observers aim to provide an estimate of the internal states of a given system. They are used more and more to gain access to states or/and parameters of a process, which are non-physically measurable or to replace sensors that are too costly. Also called software sensors, they are at each sampling k giving an online estimation of internal states based on a process model and using both inputs and outputs of the process plant (as seen in Figure 6.1).
Observers have been first introduced by Kalman and Bucy (Kalman and Bucy (1961)) for linear systems in a stochastic environment. Luenberger (Luenberger (1964)) developed a general formulation for linear systems introducing concept for reduced observer. Since then, observer theory is an area of research in automatic control (Gauthier and Kupka (2001); Besançon (2007)) where both linear and nonlinear systems are studied.

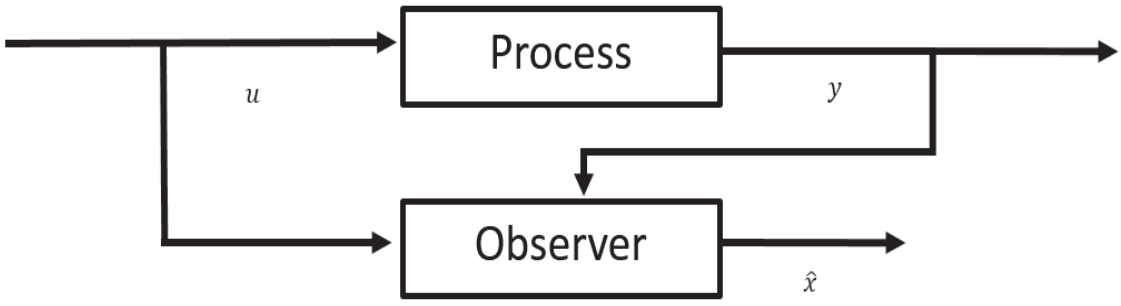


Figure 6.1 – Observer block diagram

Considering the general form of a nonlinear system:

$$\begin{cases} \dot{x} &= f(x,u) \\ y &= h(x), \end{cases} \tag{6.11}$$

where x denotes the state vector taking values in a subset X of $\mathbb{R}^n$, u is the vector of known external inputs taking values in U of R^m and y denotes the vector of measured outputs taking values in a subset Y of $\mathbb{R}^p$. f and h are nonlinear functions of suitable dimensions.
An observer for system (6.11) can be described in a general form as follows:

$$\begin{cases} \dot{\hat{x}} = f(\hat{x},u) + \zeta(t, h(\hat{x}) - y) \\ \text{with} \quad \zeta(t,0) = 0, \end{cases} \tag{6.12}$$

where $\hat{x}$ is the estimated state vector and ζ is a function of estimation error to be designed depending on the model structure.

6.2.1 Observability

A system is said to be uniformly observable, if for any possible choice of input vectors, the current state can be determined only using the outputs of the system. In other words, it means that the system behavior can be determined from its outputs.
The pair (f, h) can being said to be observable in the rank sense if the differential of h with the differential of the successive Lie derivatives of f until the order $n-1$ (n being the order of f) are independent. i.e. :

$$Rank\left\{dh, dL_f h, \ldots, dL_f^{n-1}h\right\} = n, \tag{6.13}$$

where

$$dL_f^k h = \left(\frac{\partial L_f^k h}{\partial x_1}, \frac{\partial L_f^k h}{\partial x_2}, \ldots \frac{\partial L_f^k h}{\partial x_n}\right). \tag{6.14}$$

As the observability depends on the inputs, some values could be found of those where observability vanishes. We must therefore examine the inputs.
The model (6.10) can now be written in the form (6.11) where:

$$f(x,u) = \begin{bmatrix} x_2 \\ -x_1x_3 - x_2x_4 + x_5u \\ 0 \\ 0 \\ 0 \end{bmatrix}, \tag{6.15}$$

and

$$h(x) = x_1. \tag{6.16}$$

Knowing the physical operating region of the studied Rankine cycle based heat recovery device, it can easily be demonstrated that the rank condition (6.13) holds for system (6.10) in the physical domain.

6.2.2 Observer structure

An extended Kalman observer for system (6.11) is given by (for more details, see for instance (Besançon (2007))):

$$\begin{cases} \dot{\hat{x}} = f(\hat{x}, u) - \kappa S C^T (C\hat{x} - y) \\ \dot{S} = AS + SA^T - SC^T\kappa^{-1}C^TS + Q \\ S(0) = S(0)^T > 0, \end{cases} \tag{6.17}$$

where Q is a constant symmetric positive definite (SPD) matrix, κ is a real positive constant and $A = \frac{\partial f}{\partial x}|_{(\hat{x},u)}$, $C = \frac{\partial h}{\partial x}|_{(\hat{x},u)}$.
The observer (6.17) is then validated using experimental data.

6.3 Experimental validation

The experimental input and output of the Rankine system with the MMPC controller presented in section 5.6 are fed into the observer.
Experimental comparison of the working fluid temperature at the expansion machine inlet measured, predicted by the multi-model approach presented in section 4.2 and predicted by the observer (6.17) is shown in Figure 6.2. The associated R^2 of the estimated variables are respectively 97.7% for the observer approach and 92.3% for the multi-model approach. This highlights the visual impression

that the observer predicts in a better way the working fluid temperature at the expansion machine inlet. Another benefit compared to the multi-model approach is that the observer looks less affected by the presence of noise. In the multi-model approach, this could force the weighting to move from one model to another and creates some chattering effect.
Figure 6.3 shows the FOPTD model parameter predicted by the observer and the multi-model

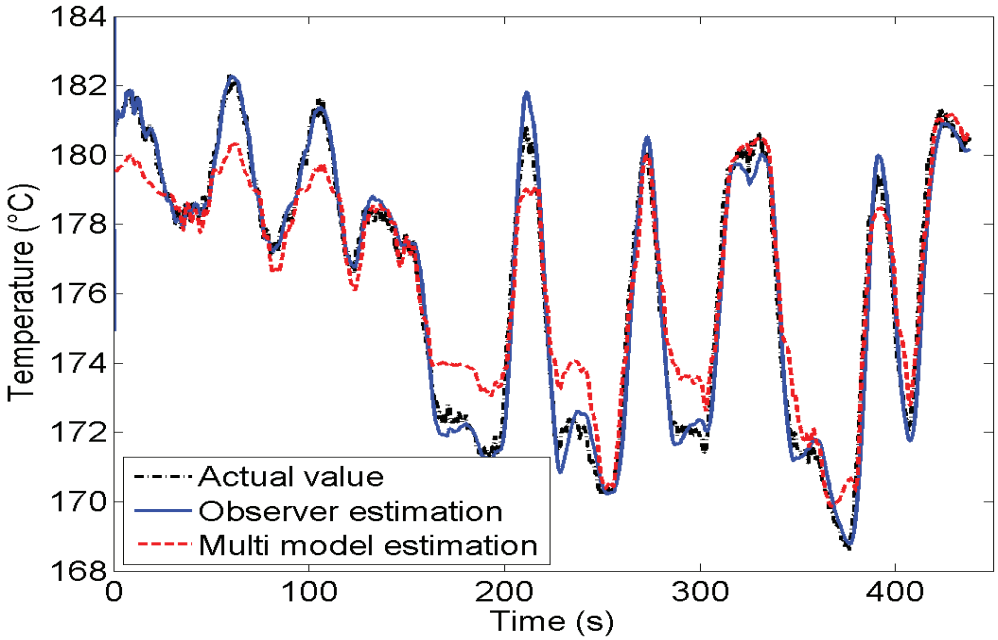


Figure 6.2 – Observer validation: comparison between temperature measured, observed and estimated by means of the multi-model approach

approach. It can be seen that the model parameters, namely $\hat{G}$, $\hat{\tau}$ and $\hat{L}$ (called G_{obs}, τ_{obs} and L_{obs} on Figure 6.3) and G_{mm}, τ_{mm} and L_{mm}, do not change much during the first 200s. This is mainly because the working fluid temperature variations are not as large during that phase. When a bigger variation from the heat source is observed (corresponding to bigger variation in the engine torque) the FOPTD model parameters estimated by both the observer and the multi-model approach vary in a more important way and seem to follow the same trends. It should be noted that unlike Figure 5.3 the static gains G_{mm} and $\hat{G}$ predicted by the two methods are not negative due to the implemented valve to act on the working fluid mass flow. The static gain $\hat{G}$ varies in a proportion of magnitude 3 whereas $\hat{\tau}$ and $\hat{L}$ vary in a more considerable way (ratio of 10 for the time constant and 25 for the lag). The biggest difference that can be observed between the two methods relies in the estimation of that latter which seems better predicted by the observer since the output estimation is also better.
Anyway, the model parameters of the single FOPTD considered now appear to be well predicted and could be used in a closed loop framework in order to replace the FOPDT model bank.

6.4 Observer based PID

The methodology in section 5.4.1 is used in combination with the observer (6.17) to create an observer based PID (OPID). The controller parameters are updated online based on the model

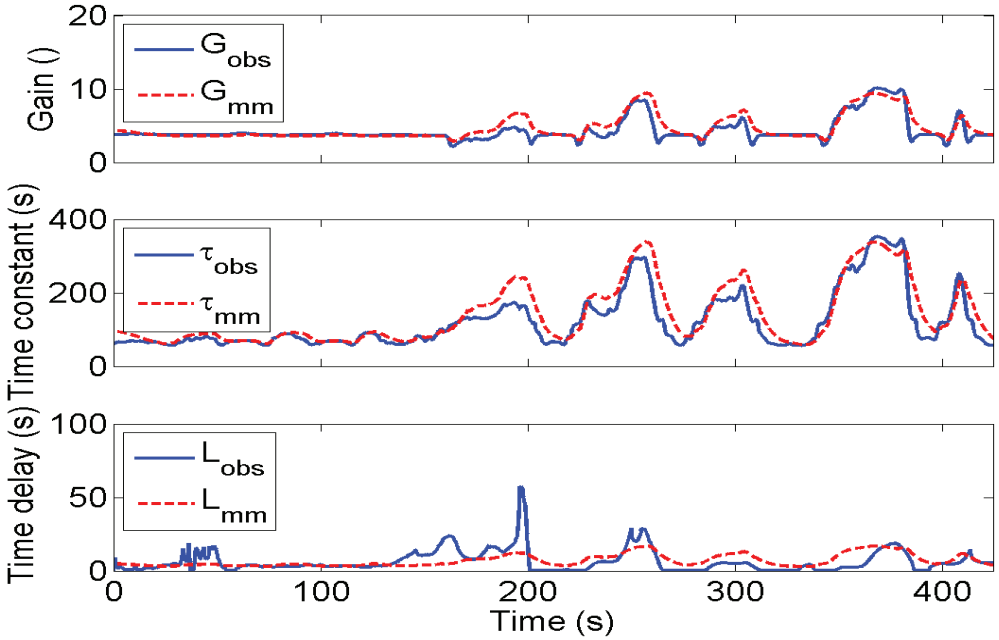


Figure 6.3 – Observer validation: comparison between FOPTD model parameters estimated via the observer (G_{obs},τ_{obs},L_{obs}) and the multi-model approach (G_{mm},τ_{mm},L_{mm})

parameter estimation according to:

$$\begin{aligned} K_p &= \frac{1}{\hat{G}}\frac{\hat{\tau}}{\theta_c+\hat{L}} \\ T_i &= \min\left\{\hat{\tau}, 4\left(\theta_c+\hat{L}\right)\right\} \\ T_d &= 0, \end{aligned} \tag{6.18}$$

where $\hat{G}$, $\hat{\tau}$ and $\hat{L}$ are the parameters of the single identified FOPTD and θ_c is a tuning parameter set to obtain a trade-off between good disturbance rejection (low value of θ_c) and stability (high value of θ_c). As a design rule, θ_c is calculated as a fraction of the estimated delay:

$$\theta_c = a_c\hat{L}, \tag{6.19}$$

where, like in equation (5.6), $a_c \in \mathbb{R}^+$ (typically $a_c \in [0.5\ 1.5]$). The resulting block diagram of this observer based PID strategy is shown in Figure 6.4.

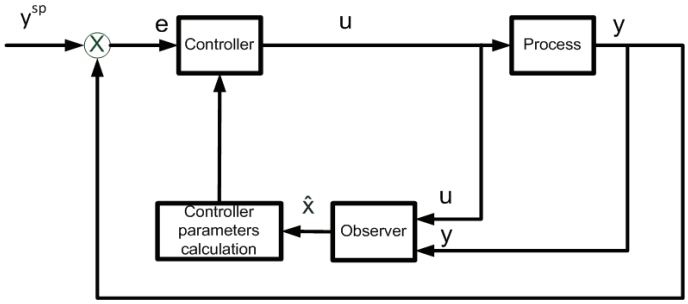


Figure 6.4 – OPID block diagram

Unfortunately, due to the lack of availability of both the detailed simulation model and the experimental setup at the time of this method development, this controller framework has not been evaluated.

6.5 Observer based model predictive controller

The multi-model predictive controller developed in section 5.6 is then adapted to be coupled with the observer. The MMPC framework is then reduced to a new observer based model predictive controller (OMPC). It is based on a single FOPTD model with parameters adapted online by the observer, and is solution of the following optimization problem:

$$\begin{cases} \min\ J(u_k) &= \int_{t_k}^{t_k+t_p} (y_p(t) - y^{sp}(t))^2 + w_u \Delta u_k^2\ dt \\ \text{where: } \Delta u_k &= u_k - u_{k-1} \\ \text{where: } u_{inf} &\leq u_k \leq u_{sup}. \end{cases} \tag{6.20}$$

The expression of y_p can now be formulated based on the observed FOPTD model parameter $\hat{G}$, $\hat{\tau}$ and $\hat{L}$.
First, the modeling error is defined such as the difference between the process and the observed variable:

$$e_k = y_{p,k} - \hat{y}_k, \tag{6.21}$$

where $\hat{y}_k$ is the estimated output given by the observer (6.17) at t_k. Again both modeling error e_k and the process variable set point (y_k^{sp}) are assumed constant over the prediction horizon. Based on equation (5.13) the following expression can be derived:

$$y(t) = y_{p,k} e^{\frac{-(t-t_k)}{\hat{\tau}}} + \frac{\hat{G}}{\hat{\tau}} e^{\frac{-t}{\hat{\tau}}} \int_{t_k}^{t} (e^{\frac{s}{\hat{\tau}}} u(s - \hat{L}))ds. \tag{6.22}$$

Based on the observed time delay $\hat{L}$, one can defined:

$$\begin{cases} \lambda &= max\left(a \in \mathbb{N} | a \leq \frac{\hat{L}}{T_s}\right) \\ \Delta L &= \hat{L} - \lambda T_s, \end{cases} \tag{6.23}$$

which helps to define the different integration intervals needed in (6.22). Those $\lambda + 2$ intervals are given in Table 6.1: Using this input sequence definition the equation (6.22) becomes:

s	$s - \hat{L}$	$u(s - \hat{L})$
$t_k \to t_k + \Delta L$	$t_k - \hat{L} \to t_{k-\lambda}$	$u(t_{k-\lambda-1})$
$t_k + \Delta L \to t_k + \Delta L + T_s$	$t_{k-\lambda} \to t_{k-\lambda+1}$	$u(t_{k-\lambda})$
$\dots$	$\dots$	$\dots$
$t_k + \Delta L + (\lambda - j)T_s \to t_k + \Delta L + (\lambda - j + 1)T_s$	$t_{k-j} \to t_{k-j+1}$	$u(t_{k-j})$
$\dots$	$\dots$	$\dots$
$t_k + \Delta L + (\lambda - j + 1)T_s \to t_k + \hat{L}$	$t_{k-1} \to t_k$	$u(t_{k-1})$
$t_k + \hat{L} \to t$	$t_k \to t - \hat{L}$	$u(t_k) = u_k$.

Table 6.1 – OMPC: input sequence definition.

$$\begin{aligned} y(t) &= y_{p,k} e^{\frac{-(t-t_k)}{\hat{\tau}}} \\ &+ \frac{\hat{G}}{\hat{\tau}} e^{\frac{-t}{\hat{\tau}}} u(t_{k-\lambda-1}) \int_{t_k}^{t_k+\Delta L} e^{\frac{s}{\hat{\tau}}} ds \\ &+ \frac{\hat{G}}{\hat{\tau}} e^{\frac{-t}{\hat{\tau}}} \left(\sum_{j=1}^{j=\lambda} u(t_{k-j}) \int_{t_k+\Delta L+(\lambda-j)T_s}^{t_k+\Delta L+(\lambda-j+1)T_s} e^{\frac{s}{\hat{\tau}}} ds \right) \\ &+ \frac{\hat{G}}{\hat{\tau}} e^{\frac{-t}{\hat{\tau}}} u(t_k) \int_{t_k+\hat{L}}^{t} e^{\frac{s}{\hat{\tau}}} ds. \end{aligned} \tag{6.24}$$

Based on the prediction of the process output (6.21) (based on the model prediction, the output estimation and the measured output), the cost function (6.20) can now be formulated as:

$$J(u_k) = \int_{t_k}^{t_k+t_p} \left((y(t) + e_k - y^{sp}(t))^2 + w_u \Delta u_k^2 \right) dt, \tag{6.25}$$

where the prediction horizon t_p is adapted online:

$$\begin{array}{rcl} t_p & = & \gamma_p \, \hat{\tau} + \hat{L}; \; \gamma_p \in \mathbb{R}^+, \\ \text{e.g.: } \gamma_p & = & 1 \text{ (63\% of the dynamics is predicted)} \\ \text{or } \gamma_p & = & 3 \text{ (95\% of the dynamics is predicted).} \end{array} \tag{6.26}$$

The expression (6.25) can now be summarized as a quadratic function of u_k:

$$\begin{array}{l} J(u_k) = \hat{\beta}_{2,k} \left(\hat{G}, \hat{\tau}, \hat{L}, t_p, w_u \right) u_k^2 \\ + \hat{\beta}_{1,k} \left(T_s, \hat{G}, \hat{\tau}, \hat{L}, \Delta L, \lambda, w_u, y_{p,k}, y_k^{sp}, e_k, u(past) \right) u_k \\ + \hat{\beta}_{0,k} \left(T_s, \hat{G}, \hat{\tau}, \hat{L}, \Delta L, \lambda, w_u, y_{p,k}, y_k^{sp}, e_k, u(past) \right), \end{array} \tag{6.27}$$

where the $\hat{\beta}_{i,k}; i = 0, 1, 2$ can be defined offline (see appendix D) and updated at each sampling time k. As the expression of J given by (6.27) is convex in u_k (since $\hat{\beta}_{2,k} > 0$ by definition) and using the first order optimality equality (5.21), the solution for the unconstrained minimization of (6.27) is:

$$u_k^{min} = \frac{-\hat{\beta}_{1,k}}{2 \; \hat{\beta}_{2,k}}. \tag{6.28}$$

The solution $u_k^\star$ of the constrained optimization problem (6.20) is given by:

$$\left\{ \begin{array}{lll} \text{if:} & u_{inf} & \leq u_k^{min} \leq u_{sup} : \; u_k^\star = u_k^{min} \\ \text{if:} & u_k^{min} & \leq u_{inf} : \; u_k^\star = u_{inf} \\ \text{if:} & u_{sup} & \leq u_k^{min} : \; u_k^\star = u_{sup} \end{array} \right. \tag{6.29}$$

The observer based MPC controller block diagram is shown in Figure 6.5. Unfortunately, due to

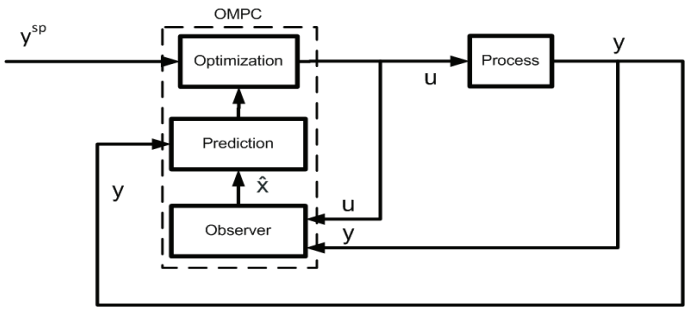


Figure 6.5 – OMPC block diagram

the lack of availability of both the detailed simulation model and the experimental setup at the time of this method development, this controller framework has not been evaluated and implemented. It still has to be validated on a reference process but could be used on numerous problem since it relies on a method validated by simulation on different processes (see section 5.6.2) and on a Rankine experimental setup (see section 5.6.3).

Conclusion. *In this chapter, an observer has been developed for the online prediction of the single FOPTD model parameters used as a basis for closed loop control strategies developed in chapter 5. The extended Kalman observer is based on a model order reduction and is experimentally validated offline. First results show better prediction than the multi-linear model approach used in the previous chapters. Based on this observer, an adaptation of the PID and MPC seen in the previous chapter has been shown.*
This generic method can be adapted to numerous control problems where the plant dynamic behavior can be locally reduced to a first-order plus time delay model. The validation of both OPID and OMPC strategies still have to be done both by simulations and experimental tests.

Global conclusion

The future commercialization of a Rankine cycle based heat recovery system in long haul heavy-duty trucks requires an optimization of both the architecture and control system.
The WHRS architecture and its performance are strongly linked to vehicle implementation and the reference mission. A complete vehicle simulation platform has been used to assess and optimize the system. The modeling and simulation phase is an important step in the development cycle of a product.
Different levels of modeling have been developed here for different purposes. Starting from system evaluation and thermodynamic optimization on the design point to fuel economy assessment models from 0D to dynamic 1D are necessary. Those models have been successfully integrated into a model-based conception methodology starting from scratch, where integration constraints were taken into account. Numerous limitations inherent to the automotive application going from environmental to purely technical have been explained in this manuscript. It is demonstrated that reaching the 5% fuel economy which is targeted by many OEM's is challenging with current components. An optimization of the system integration into the cooling package is also proposed which results into an increase in performance around 11%.
The successful system integration also goes hand in hand with good performance over large and frequent transient that can appear on a driving cycle. The system performance should be maintained over a large range of operating conditions with simple and fast control strategies compliant with automotive electronic control unit.
The work presented in this thesis contributes to this where different controller frameworks have been compared on a detailed simulation model. Each strategy has been implemented on the targeted ECU but only some have been experimentally validated. The primary focus was to reduce the calibration effort and has been addressed through the use of a multi-linear model approach with which a simple and efficient weighting scheme has been developed. Advanced controller development has been examined via the creation of an explicit multi-model predictive controller which has been validated on the experimental setup and which shows good tracking behavior. Experimental validation of both adaptive PID and MMPC controllers shows good performance with regards to disturbance rejection and set point tracking. The control strategy coupling a feedback controller and a dynamic feedforward based on an inverted heat exchanger model, even if it shows tremendous results in simulation, seems too complicated to be calibrated and to be used on a mass produced system.
Beyond the pure scientific work proposed here, the industrial context should be taken into account. The development of such a technology is a major challenge for a heavy-duty truck manufacturer and special attention is paid by the industrial to the cost and development time. The time devoted to research topics is usually little and the work is usually constrained by the implementation. Some of those latter are explained in this manuscript such as the development guidelines for control strategies but when it comes to the integration of a Rankine cycle based heat recovery system into a vehicle the constrains could be even stronger. Evaluation of such a technology should pay attention not only to the pure performance but also to the additional weight, volume and cost. New performance indicators taking care of that should be then introduced to understand the real potential of the system once implemented on a vehicle.

Concerning the system itself, there is little remaining development and the major actors should now focus on the control strategies. In the next coming years, computational capacity of ECU will increase for sure and will open doors for advanced controller development.
The integration method, limited here by the ECU platform to a simple Euler scheme, should be also addressed. By substituting this for a more advanced scheme with a variable time step, the development will be facilitated and new methods can be implemented.
Another stream of development can be the use of field programmable gate array (FPGA). As a reconfigurable hardware, FPGA is gaining popularity and have been applied in applications ranging from signal processing, aerospace, to robotics. It allows parallelization of computation using the advantages of the chip resources and to structure the FPGA in order to fit a control algorithms and not the other way around.
New observer structure for time delayed system could be introduced avoiding the finite approximation of the delay. The observer based controller presented in chapter 6 could become implementable and will help to save time and make the control strategy more robust.
In this manuscript only the constant superheat set point is used and implemented. Meanwhile it has been shown that online adaptation of the superheat increase the system performance. Therefore evaluation of such an optimal online time varying set point design could be valuable.

Bibliography

Aghaali, H. and Ångström, H.-E. (2015). A review of turbocompounding as a waste heat recovery system for internal combustion engines. *Renewable and Sustainable Energy Reviews*, 49:813 – 824.

Alleyne, A. and Rasmussen, B. (2007). Advances in energy systems modeling and control. In *American Control Conference, 2007. ACC '07*, pages 4363–4373.

Ammann, M., Fekete, N. P., Guzzella, L., and Glattfelder, A. (2003). Model-based control of the vgt and egr in a turbocharged common-rail diesel engine: theory and passenger car implementation. Technical report, SAE Technical Paper.

Armstead, J. R. and Miers, S. A. (2014). Review of waste heat recovery mechanisms for internal combustion engines. *Journal of Thermal Science and Engineering Applications*, 6(1):014001.

Åström, K. (1991). Adaptive control. In Antoulas, A., editor, *Mathematical System Theory*, pages 437–450. Springer Berlin Heidelberg.

Athans, M., Castanon, D., Dunn, K. P., Greene, C. S., Lee, W. H., Sandell, N. R., and Willsky, A. S. (1977). The stochastic control of the f-8c aircraft using a multiple model adaptive control (mmac) method–part i: Equilibrium flight. *Automatic Control, IEEE Transactions on*, 22(5):768–780.

Aufderheide, B. and Bequette, B. (2003). Extension of dynamic matrix control to multiple models. *Computers and Chemical Engineering*, 27(8–9):1079 – 1096.

Bachman, L. J., Erb, A., and Sellers, J. (2014). Quantitative estimate of the relation between rolling resistance on fuel consumption of class 8 tractor trailers using both new and retreaded tires. In *SAE Technical Paper*. SAE International.

Banerjee, A., Arkun, Y., Ogunnaike, B., and Pearson, R. (1997). Estimation of nonlinear systems using linear multiple models. *AIChE Journal*, 43(5):1204–1226.

Bell, I. H., Quoilin, S., Georges, E., Braun, J. E., Groll, E. A., Horton, W. T., and Lemort, V. (2015). A generalized moving-boundary algorithm to predict the heat transfer rate of counterflow heat exchangers for any phase configuration. *Applied Thermal Engineering*, 79:192 – 201.

Bergman, T. L., Incropera, F. P., and Lavine, A. S. (2011). *Fundamentals of heat and mass transfer*. John Wiley & Sons.

Besançon, G. (2007). *Nonlinear observers and applications*, volume 363. Springer.

Bredel, E., Nickl, J., and Bartosch, S. (2011). Waste heat recovery in drive systems of today and tomorrow. *MTZ worldwide eMagazine*, 72(4):52–56.

Cayer, E., Galanis, N., and Nesreddine, H. (2010). Parametric study and optimization of a transcritical power cycle using a low temperature source. *Applied Energy*, 87(4):1349 – 1357.

Cohen, G. and Coon, G. (1953). Theoretical consideration of retarded control. *Trans. Asme*, 75(1):827–834.

Dai, L., Xia, Y., Fu, M., and Mahmoud, M. S. (2012-12-05). Advances in discrete time systems.

Daimler Trucks North America, . (2015). Freightliner supertruck presentation.

Darby, M. L. and Nikolaou, M. (2012). MPC: Current practice and challenges. *Control Engineering Practice*, 20(4):328 – 342. Special Section: IFAC Symposium on Advanced Control of Chemical Processes - ADCHEM 2009.

Del Re, L., Allgöwer, F., Glielmo, L., Guardiola, C., and Kolmanovsky, I. (2010). *Automotive model predictive control: models, methods and applications*, volume 402. Springer.

Dickson, J., Ellis, M., Rousseau, T., and Smith, J. (2014). Validation and design of heavy vehicle cooling system with waste heat recovery condenser. *SAE International Journal of Commercial Vehicles*, 7:458–467.

Dougherty, D. and Cooper, D. (2003). A practical multiple model adaptive strategy for single-loop MPC. *Control Engineering Practice*, 11(2):141 – 159. Automotive Systems.

Doyle, E. DiNanno, L. and Kramer, S. (1979). Installation of a diesel-organic rankine compound engine in a class 8 truck for a single-vehicle test. In *SAE Technical Paper*, number 790646. SAE International.

Dávila, A. and Nombela, M. (2011). Sartre - safe road trains for the environment reducing fuel consumption through lower aerodynamic drag coefficient. In *SAE Technical Paper*. SAE International.

Edwards, S., Eitel, J., Pantow, E., Geskes, P., Lutz, R., and Tepas, J. (2012). Waste heat recovery: The next challenge for commercial vehicle thermomanagement. *SAE International Journal of Commercial Vehicles*, 5:395–406.

Elliott, M. and Rasmussen, B. (2008). Model-based predictive control of a multi-evaporator vapor compression cooling cycle. In *American Control Conference, 2008. ACC '08*, pages 1463–1468.

Eric. W. Lemmon, M. L. H. (2013). Refprop nist standard reference database 23 (version 9.0)), thermophysical properties division, national institute of standards and technology, boulder, co.

Espinosa, N. (2011). *Contribution to the Study of Waste Heat Recovery Systems on Commercial Truck Diesel Engines*. PhD thesis, University of Liege, National Polytechnic Institute of Lorraine.

Feru, E., Kupper, F., Rojer, C., Seykens, X., Scappin, F., Willems, F., Smits, J., Jager, B. D., and Steinbuch, M. (2013). Experimental validation of a dynamic waste heat recovery system model for control purposes. In *SAE Technical Paper*. SAE International.

Feru, E., Willems, F., de Jager, B., and Steinbuch, M. (2014). Modeling and control of a parallel waste heat recovery system for euro-vi heavy-duty diesel engines. *Energies*, 7(10):6571.

Fischer, J. (2011). Comparison of trilateral cycles and organic rankine cycles. *Energy*, 36(10):6208 – 6219.

Flik, M. Edwards, S. and Pantow, E. (2009). Emissions reduction in commercial vehicles via thermomanagement. In *Proceedings of the 30th wiener motorensymposium*. Vienna, Austria.

Franke, M., Bhide, S., Liang, J., Neitz, M., and Hamm, T. (2014). Development trends for commercial and industrial engines. *SAE Int. J. Engines*, 7:1629–1636.

Freymann, R., Strobl, W., and Obieglo, A. (2008). The turbosteamer: A system introducing the principle of cogeneration in automotive applications. *MTZ worldwide*, 69(5):20–27.

Gauthier, J.-P. and Kupka, I. (2001). *Deterministic observation theory and applications*. Cambridge university press.

Grelet, V., Reiche, T., Guillaume, L., and Lemort, V. (2014). Optimal waste heat recovery rankine based for heavy duty applications. In *35th FISITA world automotive congress*.

Guolian, H., Jinfang, Z., Junjun, L., and Jianhua, Z. (2010). Multiple-model predictive control based on fuzzy adaptive weights and its application to main-steam temperature in power plant. In *5th IEEE Conference on Industrial Electronics and Applications (ICIEA), 2010*, pages 668–673.

Guzzella, L. and Onder, C. (2004). *Introduction to Modeling and Control of Internal Combustion Engine Systems*. Springer.

He, W., Kaufman, H., and Roy, R. (1986). Multiple model adaptive control procedure for blood pressure control. *Biomedical Engineering, IEEE Transactions on*, BME-33(1):10–19.

He, W., Zhang, G., Zhang, X., Ji, J., Li, G., and Zhao, X. (2015). Recent development and application of thermoelectric generator and cooler. *Applied Energy*, 143:1 – 25.

Hiereth, H., Drexl, K., and Prenninger, P. (2007). *Charging the internal combustion engine*. Springer Science & Business Media.

Holmqvist, T. (2006). Air flow measurements in vfl performed in the ae project chgt5: Alternative placement of heat exchangers. Technical report.

Horne, T. (2013). Construction and test of a rankine waste heat recovery (whr) system on a volvo 13 liter euro vi (euro 6) engine, including controls configuration. Confidential, Volvo Trucks.

Horst, T. A., Rottengruber, H.-S., Seifert, M., and Ringler, J. (2013). Dynamic heat exchanger model for performance prediction and control system design of automotive waste heat recovery systems. *Applied Energy*, 105(0):293 – 303.

Horst, T. A., Tegethoff, W., Eilts, P., and Koehler, J. (2014). Prediction of dynamic rankine cycle waste heat recovery performance and fuel saving potential in passenger car applications considering interactions with vehicles' energy management. *Energy Conversion and Management*, 78(0):438 – 451.

Hou, G., Sun, R., Hu, G., and Zhang, J. (2011). Supervisory predictive control of evaporator in organic rankine cycle (orc) system for waste heat recovery. In *Advanced Mechatronic Systems (ICAMechS), 2011 International Conference on*, pages 306–311.

Ibaraki, S., Endo, T., Kojima, Y., Takahashi, K., Baba, T., and Kawajiri, S. (2007). Study of efficient on-board waste heat recovery system using rankine cycle. *Review of automotive engineering*, 28(3):307–313.

(IRU), I. R. T. U. (2014). Economic and competiveness gains from the adoption of best practices in intermodal maritime and road transport in the americas.

Johnson, K. G., Mollenhauer, K., and Tschöke, H. (2010). *Handbook of diesel engines*. Springer Science & Business Media.

Kalman, R. E. and Bucy, R. S. (1961). New results in linear filtering and prediction theory. *Journal of Fluids Engineering*, 83(1):95–108.

Kardos, Z. and Klingberg, K. (2013). Cooler arrangement for a vehicle powered by a supercharged combustion engine.

Karellas, S., Schuster, A., and Leontaritis, A.-D. (2012). Influence of supercritical ORC parameters on plate heat exchanger design. *Applied Thermal Engineering*, 33–34(0):70 – 76.

Katrašnik, T. (2007). Hybridization of powertrain and downsizing of IC engine – a way to reduce fuel consumption and pollutant emissions – part 1. *Energy Conversion and Management*, 48(5):1411 – 1423.

Kiencke, U. and Nielsen, L. (2000). Automotive control systems: for engine, driveline, and vehicle. *Measurement Science and Technology*, 11(12):1828.

Kleiber, M., Joh, R., and Span, R. (2010). *Properties of Pure Fluid Substances*. VDI Buch. Springer.

Kunte, H. and Seume, J. (2013). Partial admission impulse turbine for automotive orc application. In *SAE Technical Paper*. SAE International.

Kusters, K. (2003). Control strategy for rankine cycle of rankine compression gas turbine. Technical report.

Landau, I. and Zito, G. (2006). *Digital Control Systems: Design, Identification and Implementation*. Communications and Control Engineering. Springer-Verlag London.

Larnaud, A. (2010). Study and selection of the working fluid for waste heat recovery rankine cycle system. Confidential, Volvo Trucks.

Latz, G., Andersson, S., and Munch, K. (2013). Selecting an expansion machine for vehicle waste-heat recovery systems based on the rankine cycle. In *SAE Technical Paper*. SAE International.

Latz, G., Erlandsson, O., Skare, T., Contet, A., Andersson, S., and Munch, K. (2015). Water-based rankine cycle waste heat recovery systems for engines: chalenges and opportunities. In *3rd International Seminar on ORC Power Systems (ORC15), 2015*.

LeBlanc, S. (2014). Thermoelectric generators: Linking material properties and systems engineering for waste heat recovery applications. *Sustainable Materials and Technologies*, 1–2:26 – 35.

Lecompte, S., Huisseune, H., van den Broek, M., Schampheleire, S. D., and Paepe, M. D. (2013). Part load based thermo-economic optimization of the organic rankine cycle (ORC) applied to a combined heat and power (CHP) system. *Applied Energy*, 111:871 – 881.

Lecompte, S., Van den Broek, M., and De Paepe, M. (2014). Optimal sizing of heat exchangers for organic rankine cycles (ORC) based on thermo-economics. *Proceedings of 15th international heat transfer conference. Kyoto, Japan*, page 14.

Li, X., Zhao, Z., and Li, X.-B. (2005). General model-set design methods for multiple-model approach. *Automatic Control, IEEE Transactions on*, 50(9):1260–1276.

Lu, H., Di Loreto, M., Eberard, D., and Simon, J.-P. (2014). Approximation of distributed delays. *Systems and Control Letters*, 66:16–21.

Luenberger, D. G. (1964). Observing the state of a linear system. *IEEE Transactions on Military Electronics*, 8(2):74–80.

Luong, D. and Tsao, T.-C. (2014a). Linear quadratic integral control of an organic rankine cycle for waste heat recovery in heavy-duty diesel powertrain. In *American Control Conference (ACC), 2014*, pages 3147–3152.

Luong, D. and Tsao, T.-C. (2014b). Model predictive control of organic rankine cycle for waste heat recovery in heavy-duty diesel powertrain. In *ASME 2014 Dynamic Systems and Control Conference*, pages V002T21A001–V002T21A001. American Society of Mechanical Engineers.

Madhuranthakam, C., Elkamel, A., and Budman, H. (2008). Optimal tuning of PID controllers for FOPTD, SOPTD and SOPTD with lead processes. *Chemical Engineering and Processing: Process Intensification*, 47(2):251 – 264.

Mago, P. J., Chamra, L. M., and Somayaji, C. (2007). Performance analysis of different working fluids for use in organic rankine cycles. *Proceedings of the Institution of Mechanical Engineers, Part A: Journal of Power and Energy*, 221(3):255–263.

Mammetti, M., Gallegos, D., Freixas, A., and Muñoz, J. (2013). The influence of rolling resistance on fuel consumption in heavy-duty vehicles. In *SAE Technical Paper*. SAE International.

Manente, V., Zander, C.-G., Johansson, B., Tunestal, P., and Cannella, W. (2010). An advanced internal combustion engine concept for low emissions and high efficiency from idle to max load using gasoline partially premixed combustion. In *SAE Technical Paper*. SAE International.

Mier, D., Mollenbruck, F., Jost, M., Grote, W., and Monnigmann, M. (2015). Model predictive control of the steam cycle in a solar power plant. In *IFAC International Symposium on Advanced Control of Chemical Processes (ADCHEM)*, pages 711–716.

Munch Jensen, J. and Tummescheit, H. (2002). Moving boundary models for dynamic simulations of two-phase flows. *Modelica'2002 Proceedings*, pages 235–244.

Murray-Smith, R. and Johansen, T., editors (1997). *Multiple Model Approaches to Modelling and Control*. Taylor and Francis systems and control book series. Taylor and Francis, London, UK.

Muske, K. R. and Rawlings, J. B. (1993). Model predictive control with linear models. *AIChE Journal*, 39(2):262–287.

Nandola, N. N. and Bhartiya, S. (2008). A multiple model approach for predictive control of nonlinear hybrid systems. *Journal of Process Control*, 18(2):131 – 148.

Narendra, K. and Balakrishnan, J. (1997). Adaptive control using multiple models. *Automatic Control, IEEE Transactions on*, 42(2):171–187.

Neveu, J.-M. (2014). Refrigerant rankine system: system verification and application on tigre vehicle. Confidential, Volvo Trucks.

Normey-Rico, J. E. (2007). *Control of dead-time processes*. Springer Science & Business Media.

Oomori, H. Ogino, S. (1993). Waste heat recovery of passenger car using a combination of rankine bottoming cycle and evaporative cooling system. In *SAE Technical Paper*, number 930880. SAE International.

Papadopoulos, A. I., Stijepovic, M., and Linke, P. (2010). On the systematic design and selection of optimal working fluids for organic rankine cycles. *Applied Thermal Engineering*, 30(6–7):760 – 769.

Park, T., Teng, H., Hunter, G. L., van der Velde, B., and Klaver, J. (2011). A rankine cycle system for recovering waste heat from hd diesel engines - experimental results. In *SAE Technical Paper*. SAE International.

Patel, P. and Doyle, E. (1976). Compounding the truck diesel engine with an organic rankine-cycle system. In *SAE Technical Paper*, number 760343. SAE International.

Peralez, J. (2015). *Rankine cycle for waste heat recovery on board vehicles: control and energy management.* PhD thesis, Université Claude Bernard Lyon 1.

Peralez, J., Nadri, M., Dufour, P., Tona, P., and Sciarretta, A. (2014). Control design for an automotive turbine rankine cycle system based on nonlinear state estimation. In *Decision and Control (CDC), 2014 IEEE 53rd Annual Conference on*, pages 3316–3321.

Peralez, J., Tona, P., Lepreux, O., Sciarretta, A., Voise, L., Dufour, P., and Nadri, M. (2013). Improving the control performance of an organic rankine cycle system for waste heat recovery from a heavy-duty diesel engine using a model-based approach. In *52nd Annual IEEE Conference on Decision and Control (CDC)*, pages 6830–6836.

Pretschner, A., Broy, M., Kruger, I. H., and Stauner, T. (2007). Software engineering for automotive systems: A roadmap. In *2007 Future of Software Engineering*, FOSE '07, pages 55–71, Washington, DC, USA. IEEE Computer Society.

Quoilin, S., Aumann, R., Grill, A., Schuster, A., Lemort, V., and Spliethoff, H. (2011). Dynamic modeling and optimal control strategy of waste heat recovery organic rankine cycles. *Applied Energy*, 88(6):2183 – 2190.

Rao, R., Aufderheide, B., and Bequette, B. (1999). Multiple model predictive control of hemodynamic variables: an experimental study. In *Proceedings of the 1999 American Control Conference (ACC), 1999.*, volume 2, pages 1253–1257 vol.2.

Rasmussen, Bryan P.; Alleyne, A. G. (2006). Dynamic modeling and advanced control of air conditioning and refrigeration systems. Technical report.

Rasmussen, B. and Alleyne, A. (2010). Gain scheduled control of an air conditioning system using the youla parameterization. *IEEE Transactions on Control Systems Technology*, 18(5):1216–1225.

Rasmussen, B., Alleyne, A., Bullard, C., Hmjak, P., and Miller, N. (2002). Control-oriented modeling and analysis of automotive transcritical ac system dynamics. In *American Control Conference, 2002. Proceedings of the 2002*, volume 4, pages 3111–3116 vol.4.

Redon, F., Kalebjian, C., Kessler, J., Rakovec, N., Headley, J., Regner, G., and Koszewnik, J. (2014). Meeting stringent 2025 emissions and fuel efficiency regulations with an opposed-piston, light-duty diesel engine. In *SAE Technical Paper*. SAE International.

Regner, G., Johnson, D., Koszewnik, J., Dion, E., Redon, F., and Fromm, L. (2013). Modernizing the opposed piston, two stroke engine for clean, efficient transportation. In *SAE Technical Paper*. The Automotive Research Association of India.

Reiche, T. (2010). The waste heat recovery potential of different secondary thermodynamic cycle mode. Confidential, Volvo Trucks.

Richard, J.-P. (2003). Time-delay systems: an overview of some recent advances and open problems. *Automatica*, 39(10):1667 – 1694.

Rivera, D. E., Morari, M., and Skogestad, S. (1986). Internal model control: PID controller design. *Industrial & engineering chemistry process design and development*, 25(1):252–265.

Rodrigues, M., Theilliol, D., Adam-Medina, M., and Sauter, D. (2008). A fault detection and isolation scheme for industrial systems based on multiple operating models. *Control Engineering Practice*, 16(2):225 – 239. Special Issue on Advanced Control Methodologies for Mining, Mineral and Metal (MMM) Processing IndustriesThe 11th Mining, Mineral and Metal (MMM) Symposium.

Ronan, L. and Abernathy, W. (1979). The development and introduction of the automotive turbocharger: A case of innovation in response to fuel economy regulation. Technical report.

Saidur, R., Rezaei, M., Muzammil, W., Hassan, M., Paria, S., and Hasanuzzaman, M. (2012). Technologies to recover exhaust heat from internal combustion engines. *Renewable and Sustainable Energy Reviews*, 16(8):5649 – 5659.

Schuster, A., Karellas, S., and Aumann, R. (2010). Efficiency optimization potential in supercritical organic rankine cycles. *Energy*, 35(2):1033 – 1039. {ECOS} 200821st International Conference, on Efficiency, Cost, Optimization, Simulation and Environmental Impact of Energy Systems.

Sermeno, S., Bideaux, E., Morgan, T., and Nguyen, D. (2014). Heavy duty vehicle cooling system auxiliary load management control: Evaluating the maximum gain of implementing an advanced control strategy. In *SAE Technical Paper*. SAE International.

Sims, R., Schaeffer, R., Creutzig, F., Cruz-Núñez, X. D'Agosto, M., Dimitriu, D., Figueroa Meza, M., Fulton, L., Kobayashi, S., Lah, O., McKinnon, A., Newman, P., Ouyang, M., Schauer, J., Sperling, D., and G., T. (2014). Mitigation of climate change. contribution of working group iii to the fifth assessment report of the intergovernmental panel on climate change. *Cambridge, United Kingdom and New York, USA*.

Skogestad, S. (2003). Simple analytic rules for model reduction and PID controller tuning. *Journal of Process Control*, 13(4):291 – 309.

Smith, C. A. and Corripio, A. B. (1985). *Principles and practice of automatic process control*, volume 2. Wiley New York.

Stanton, D. W. (2013). Systematic development of highly efficient and clean engines to meet future commercial vehicle greenhouse gas regulations. *SAE Int. J. Engines*, 6:1395–1480.

Stijepovic, M. Z., Linke, P., Papadopoulos, A. I., and Grujic, A. S. (2012). On the role of working fluid properties in organic rankine cycle performance. *Applied Thermal Engineering*, 36(0):406 – 413.

Stobart, R., Hounsham, S., and Weerasinghe, R. (2007). The controllability of vapour based thermal recovery systems in vehicles. In *SAE Technical Paper*. SAE International.

Stobart, R. and Weerasinghe, R. (2006). Heat recovery and bottoming cycles for si and ci engines - a perspective. In *SAE Technical Paper*. SAE International.

Sun, J. and Li, W. (2011). Operation optimization of an organic rankine cycle (ORC) heat recovery power plant. *Applied Thermal Engineering*, 31(11–12):2032 – 2041.

Suresh, A., Langenderfer, D., Arnett, C., and Ruth, M. (2013). Thermodynamic systems for tier 2 bin 2 diesel engines. *SAE Int. J. Engines*, 6:167–183.

TA Engineering INC. (2012). DOE supertruck program benefits analysis.

Teng, H., Regner, G., and Cowland, C. (2007a). Waste heat recovery of heavy-duty diesel engines by organic rankine cycle part i: Hybrid energy system of diesel and rankine engines. In *SAE Technical Paper*. SAE International.

Teng, H., Regner, G., and Cowland, C. (2007b). Waste heat recovery of heavy-duty diesel engines by organic rankine cycle part ii: Working fluids for whr-orc. In *SAE Technical Paper*. SAE International.

Ternel, C., Leduc, P., and Duparchy, A. (2011). Apparatus for controlling a working fluid with a low freezing point flowing through a closed cycle operating according to a rankine cycle and method using such an apparatus. EP Patent App. EP20,110,290,052.

Thome, J. R. (2010). *Wolverine Tube Inc Engineering Data Book III*. Heat Transfer Databook. Wolverine Tube Inc.

Thompson, I., Spence, S., and McCartan, C. (2009). A review of turbocompounding and the current state of the art. pages 1–10. Paper 101219.

Tona, P., Peralez, J., and Sciarretta, A. (2012). Supervision and control prototyping for an engine exhaust gas heat recovery system based on a steam rankine cycle. In *Advanced Intelligent Mechatronics (AIM), 2012 IEEE/ASME International Conference on*, pages 695–701.

Vaja, I. (2009). *Definition of an object oriented library for the dynamic simulation of advanced energy systems: Methodologies, Tools and Applications to Combined ICE-ORC Power Plants*. PhD thesis, University of Parma.

Wang, T., Zhang, Y., Peng, Z., and Shu, G. (2011). A review of researches on thermal exhaust heat recovery with rankine cycle. *Renewable and Sustainable Energy Reviews*, 15(6):2862 – 2871.

Willems, F., Kupper, F., and Cloudt, R. (2012). Integrated powertrain control for optimal co2-nox tradeoff in an euro-vi diesel engine with waste heat recovery system. In *American Control Conference (ACC), 2012*, pages 1296–1301.

Zhang, J., Zhang, W., Hou, G., and Fang, F. (2012a). Dynamic modeling and multivariable control of organic rankine cycles in waste heat utilizing processes. *Computers & Mathematics with Applications*, 64(5):908 – 921. Advanced Technologies in Computer, Consumer and Control.

Zhang, J., Zhou, Y., Gao, S., and Hou, G. (2012b). Constrained predictive control based on state space model of organic rankine cycle system for waste heat recovery. In *24th Chinese Control and Decision Conference (CCDC), 2012*, pages 230–234.

Zhang, J., Zhou, Y., Li, Y., Hou, G., and Fang, F. (2013). Generalized predictive control applied in waste heat recovery power plants. *Applied Energy*, 102:320 – 326. Special Issue on Advances in sustainable biofuel production and use - XIX International Symposium on Alcohol Fuels - ISAF.

Ziegler, J. G. and Nichols, N. B. (1942). Optimum settings for automatic controllers. *Transactions of ASME*, 64:759–768.

Appendix

Appendix A

Test rig

Every experimental tests carried out during this PhD and presented among this thesis have been performed on a dedicated rig built during the PhD.
Figure A.1 presents the working fluid pump used on the experimental setup (in blue on the picture). It is an industrial pump made of 3 axial pistons coupled to a variable speed electric motor. A membrane is fitted on the pump exhaust port to reduce pressure pulsation. This component is used only for development purpose and is way too big to be implemented on a vehicle.
In the tested tailpipe boiler, a thermal shield is housing the boiler to avoid radiation for that latter to tubes and other components.
The test rig was fully instrumented. Pressure and temperature sensors were mounted at each components interface (inlet and outlet). For sake of reproducibility and security two pairs of P/T sensors have been installed at the expansion machine inlet. An electric dynamometer is used to brake the expansion machine and measure the torque produced by that one.

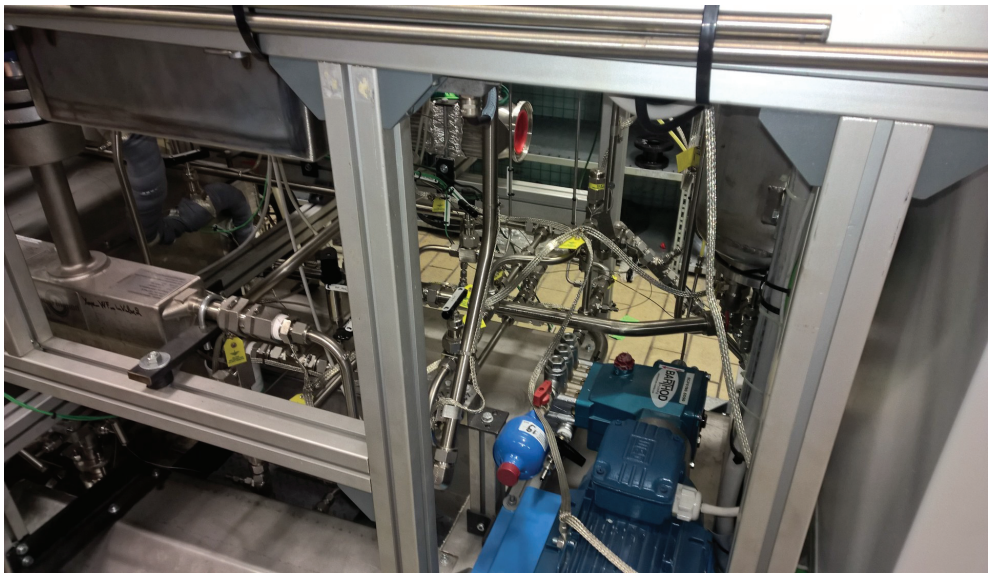


Figure A.1 – Working fluid pump

Appendix B

Experimental test

Some other experimental results are shown in this section.
First of all, the controller shown in section 5.4 is tested on steady state operating points where the engine map is partly screened. Figure B.1 shows the working fluid superheat at the expansion machine inlet. It can be noticed that this quantity is really well controlled over the tested engine operating map (SP is 25°C). The associated manipulated variable, namely the working fluid mass flow rate, is shown in Figure B.2. This quantity is controlled in order to achieve the superheat objective by acting on a fluid distributor at the pump outlet since the pump was delivering too high flow rate even at low speed.

One interesting quantity to look at is the working fluid temperature at the expansion machine

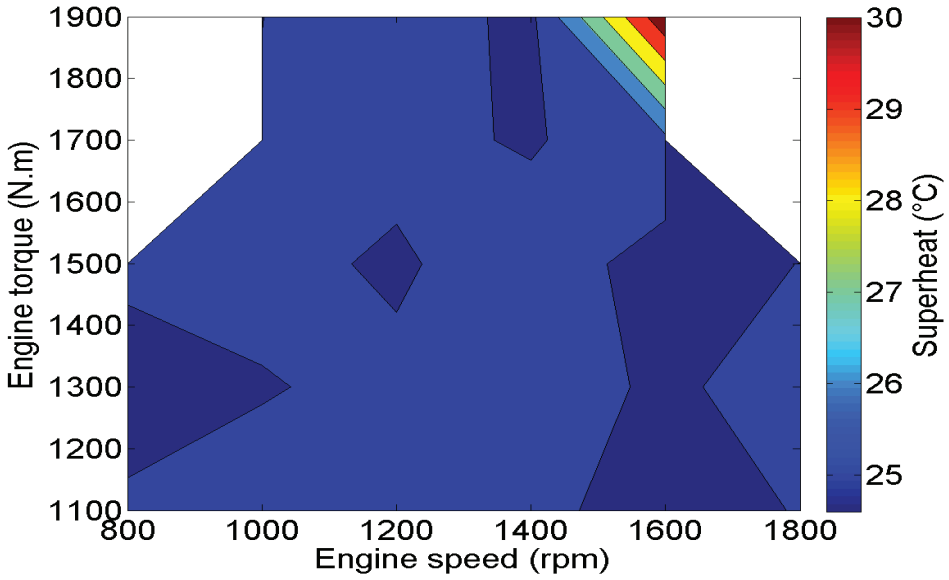


Figure B.1 – Steady state experimental tests: working fluid superheat at expansion machine inlet

inlet. The pressure resulting from the fluid conditions at the expansion machine inlet and the speed of that latter, the temperature is adjusted to answer the control objective. The temperature is reaching 230°C at high engine load that could cause premature working fluid degradation. It seems that ethanol degrades over 220°C and this should be taken into account when generating set point. Reliable and high performance controller are required to achieve this objective.
Figure B.4 is presenting the working fluid to exhaust gas heat flow rate ratio (H_R). This one is

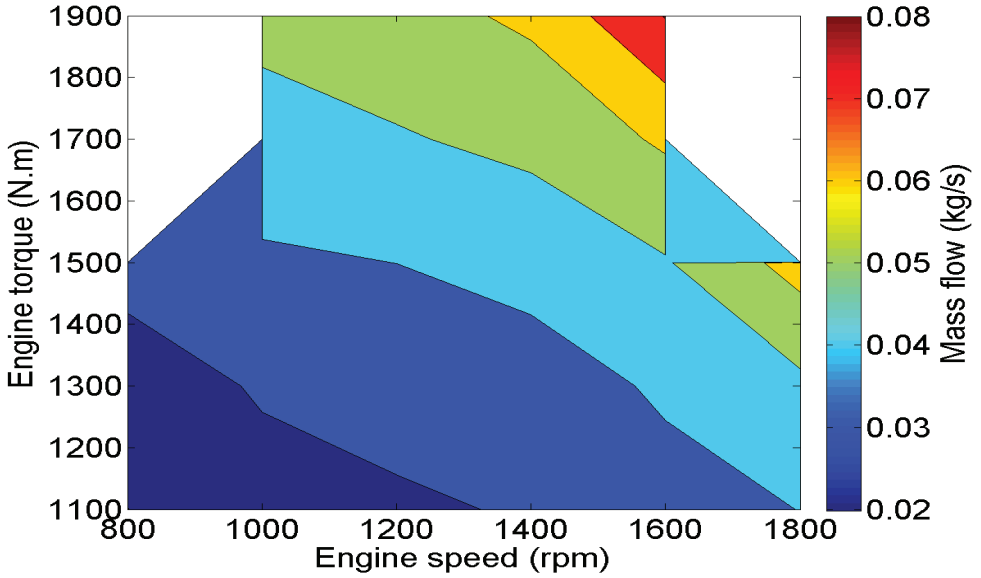


Figure B.2 – Steady state experimental tests: working fluid mass flow rate

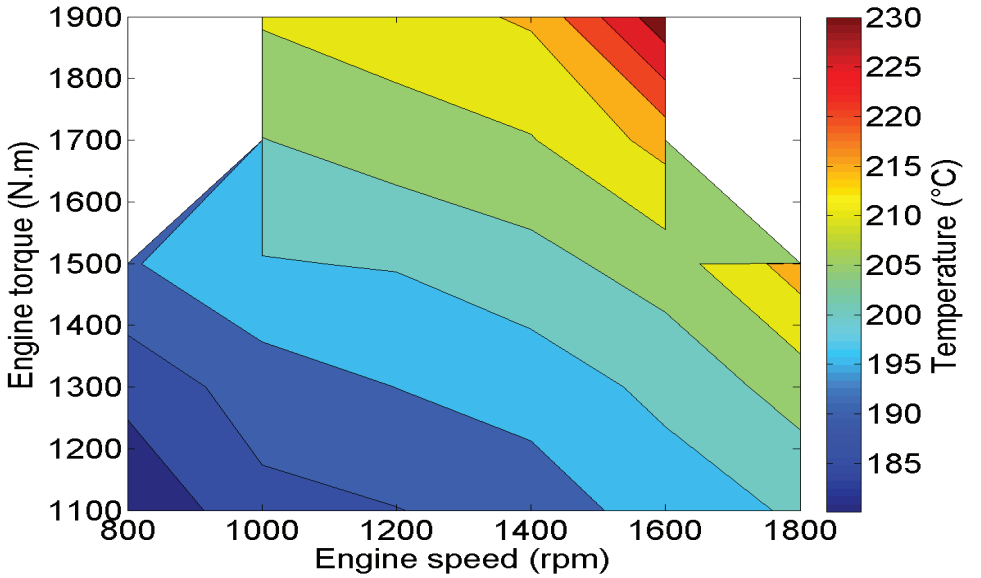


Figure B.3 – Steady state experimental tests: working fluid temperature at expansion machine inlet

defined as:

$$H_R = \frac{\dot{Q}_f}{\dot{Q}_{exh}} = \frac{\dot{m}_f \Delta h_{f_{in-out,evap}}}{\dot{m}_{exh} c_{p_{exh}} \Delta T_{exh_{in-out,evap}}} \tag{B.1}$$

It can be noticed that this evaporator loses a part of the heat contained in the exhaust gas to the ambient. Insulation could be beneficial to increase the heat transferred to the working fluid and then the power generated by the expansion machine. However, insulation will result into an increase in working fluid mass flow rate and therefore in evaporating pressure. This means that the working fluid temperature will be even higher than the temperature shown in Figure B.3 and the risk of fluid degradation will be higher. It shows that the degradation temperature of the working fluid should be considered in the design phase of the system and particularly on the expansion machine design.

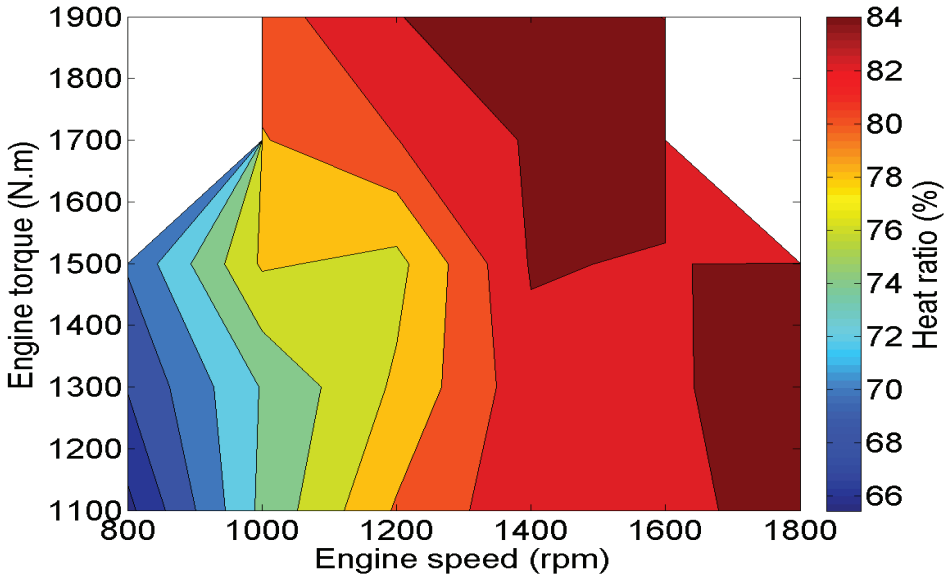


Figure B.4 – Steady state experimental tests: heat flow rate ratio over the tailpipe evaporator

Appendix C

MMPC: β_i expression

$$\beta_{1,k} = \sum_{i=1}^{N}\left[\beta_{1,k}^{'}+\beta_{1,k}^{''}+\beta_{1,k}^{'''}+\beta_{1,k}^{''''}\right]-2w_u u_{k-1}t_p, \tag{C.1}$$

$$\beta_{1,k}^{'} = -G_i\,\tau_i\,{w_{i,k}}^2\,y_{p,k}\left(e^{\frac{L_i}{\tau_i}}+2\,e^{-\frac{t_p}{\tau_i}}-e^{\frac{L_i-2\,t_p}{\tau_i}}-2\right) \tag{C.2}$$

$$\beta_{1,k}^{''} = -{G_i}^2\,\tau_i\,u(t_{k-\lambda_i-1})\,{w_{i,k}}^2\,e^{-\frac{2\,t_p}{\tau_i}}\left(e^{\frac{\Delta L_i}{\tau_i}}-1\right)\left(e^{\frac{t_p}{\tau_i}}-1\right)\left(e^{\frac{L_i}{\tau_i}}-2\,e^{\frac{t_p}{\tau_i}}+e^{\frac{L_i+t_p}{\tau_i}}\right) \tag{C.3}$$

$$\begin{aligned}\beta_{1,k}^{'''} = &\sum_{j=1}^{\lambda_i}{G_i}^2\,\tau_i\,u(t_{k-j})\,{w_{i,k}}^2\,e^{\frac{\Delta L_i-t_p-j\,T_s+\lambda_i\,T_s}{\tau_i}}\left(e^{\frac{T_s}{\tau_i}}-1\right)\left(e^{\frac{L_i-t_p}{\tau_i}}-2\right)\ldots\\ &-{G_i}^2\,\tau_i\,u(t_{k-j})\,{w_{i,k}}^2\,e^{\frac{\Delta L_i-j\,T_s+\lambda_i\,T_s}{\tau_i}}\left(e^{\frac{L_i}{\tau_i}}-2\right)\left(e^{\frac{T_s}{\tau_i}}-1\right)\end{aligned} \tag{C.4}$$

$$\beta_{1,k}^{''''} = 2\,G_i\,w_{i,k}\left(e_k-y^{SP}\right)\left(t_p+\tau_i\,e^{\frac{L_i-t_p}{\tau_i}}-\tau_i\,e^{\frac{L_i}{\tau_i}}\right) \tag{C.5}$$

$$\beta_{2,k} = \frac{{G_i}^2\,{w_{i,k}}^2\left(2\,t_p+4\,\tau_i\,e^{\frac{L_i-t_p}{\tau_i}}-\tau_i\,e^{\frac{2\,L_i-2\,t_p}{\tau_i}}-4\,\tau_i\,e^{\frac{L_i}{\tau_i}}+\tau_i\,e^{\frac{2\,L_i}{\tau_i}}\right)}{2}+w_u t_p \tag{C.6}$$

Appendix D

OMPC: $\hat{\beta}_i$ expression

$$\hat{\beta}_1 = \left[\beta'_{1,k} + \hat{\beta}''_{1,k} + \hat{\beta}'''_{1,k} + \hat{\beta}''''_{1,k}\right] - 2w_u u_{k-1} t_p, \tag{D.1}$$

$$\hat{\beta}'_{1,k} = -\hat{G}\,\hat{\tau}\,y_{p,k}\left(e^{\frac{\hat{L}}{\hat{\tau}}} + 2\,e^{-\frac{t_p}{\hat{\tau}}} - e^{\frac{\hat{L}-2\,t_p}{\hat{\tau}}} - 2\right) \tag{D.2}$$

$$\hat{\beta}''_{1,k} = -\hat{G}^2\,\hat{\tau}\,u(t_{k-\lambda-1})\,e^{-\frac{2\,t_p}{\hat{\tau}}}\left(e^{\frac{\Delta L}{\hat{\tau}}} - 1\right)\left(e^{\frac{t_p}{\hat{\tau}}} - 1\right)\left(e^{\frac{\hat{L}}{\hat{\tau}}} - 2\,e^{\frac{t_p}{\hat{\tau}}} + e^{\frac{\hat{L}+t_p}{\hat{\tau}}}\right) \tag{D.3}$$

$$\begin{aligned}\hat{\beta}'''_{1,k} = {} & \sum_{j=1}^{\lambda} \hat{G}^2\,\hat{\tau}\,u(t_{k-j})\,e^{\frac{\Delta L - t_p - j\,T_s + \lambda\,T_s}{\hat{\tau}}}\left(e^{\frac{T_s}{\hat{\tau}}} - 1\right)\left(e^{\frac{\hat{L}-t_p}{\hat{\tau}}} - 2\right)\ldots \\ & -\hat{G}^2\,\hat{\tau}\,u(t_{k-j})\,e^{\frac{\Delta L - j\,T_s + \lambda\,T_s}{\hat{\tau}}}\left(e^{\frac{\hat{L}}{\hat{\tau}}} - 2\right)\left(e^{\frac{T_s}{\hat{\tau}}} - 1\right)\end{aligned} \tag{D.4}$$

$$\hat{\beta}''''_{1,k} = 2\,\hat{G}\left(e_k - y^{SP}\right)\left(t_p + \hat{\tau}\,e^{\frac{\hat{L}-t_p}{\hat{\tau}}} - \hat{\tau}\,e^{\frac{\hat{L}}{\hat{\tau}}}\right) \tag{D.5}$$

$$\hat{\beta}_2 = \frac{\hat{G}^2\left(2\,t_p + 4\,\hat{\tau}\,e^{\frac{\hat{L}-t_p}{\hat{\tau}}} - \hat{\tau}\,e^{\frac{2\,\hat{L}-2\,t_p}{\hat{\tau}}} - 4\,\hat{\tau}\,e^{\frac{\hat{L}}{\hat{\tau}}} + \hat{\tau}\,e^{\frac{2\,\hat{L}}{\hat{\tau}}}\right)}{2} + w_u t_p \tag{D.6}$$